

# EXPERIMENTAL INVESTIGATIONS OF LOCALIZED CORROSION OF HIGH-LEVEL WASTE CONTAINER MATERIALS

*Prepared for*

**Nuclear Regulatory Commission  
Contract NRC-02-88-005**

*Prepared by*

**Center for Nuclear Waste Regulatory Analyses  
San Antonio, Texas**

**February 1993**

462.2 --- T199303020004  
Experimental Investigations  
of Localized Corrosion of  
High-Level Waste Container  
Materials-CNWRA 93-004



**EXPERIMENTAL INVESTIGATIONS OF  
LOCALIZED CORROSION OF  
HIGH-LEVEL WASTE CONTAINER MATERIALS**

*Prepared for*

**Nuclear Regulatory Commission  
Contract NRC-02-88-005**

*Prepared by*

**N. Sridhar  
G. A. Cragolino  
D. Dunn**

**Center for Nuclear Waste Regulatory Analyses  
San Antonio, Texas**

**February 1993**

## PREVIOUS REPORTS IN SERIES

Number	Name	Date Issued
20-3704-042-005-900	Progress Report of Activities and Recommendations in the Integrated Waste Package Experimental Program	June 1990
CNWRA 90-01Q	Report on Research Activities for the Quarter January 1 through March 31, 1990	May 1990
CNWRA 90-02Q	Report on Research Activities for the Quarter April 1 through June 30, 1990	August 1990
CNWRA 90-03Q	Report on Research Activities for the Quarter July 1 through September 30, 1990	November 1990
CNWRA 91-01A NUREG/CR-5817	Report on Research Activities for Calendar Year 1990	December 1991
CNWRA 91-004	A Review of Localized Corrosion of High-Level Nuclear Waste Container Materials — I	April 1991
CNWRA 91-01Q	Report on Research Activities for the Quarter January 1 through March 31, 1991	May 1991
CNWRA 91-008	Hydrogen Embrittlement of Candidate Container Materials	June 1991
CNWRA 91-02Q	Report on Research Activities for the Quarter April 1 through June 30, 1991	August 1991
CNWRA 91-03Q	Report on Research Activities for the Quarter July 1 through September 30, 1991	November 1991
CNWRA 91-01A	Report on Research Activities for Calendar Year 1991	February 1992
CNWRA 92-021	A Review of Stress Corrosion Cracking of High-Level Nuclear Waste Container Materials — I	August 1992
CNWRA 92-01S	NRC High-Level Radioactive Waste Research at CNWRA January 1 through June 30 1992	September 1992
CNWRA 93-004	Long-term Stability of High-Level Nuclear Waste Container Materials: I — Thermal Stability of Alloy 825	February 1993

## ABSTRACT

This report describes, as part of the Integrated Waste Package Experiments (IWPE) project, the experimental studies performed to date on localized corrosion of candidate container materials for the proposed high-level waste (HLW) repository at Yucca Mountain. The initial phase of the experimental study focuses on the effect of environmental factors on the localized corrosion resistance using short-term cyclic polarization tests. For the Fe-Ni-Cr-Mo alloys, chloride is found to be the main factor in lowering the resistance to pitting and crevice corrosion. For the copper-based alloys, bicarbonate in combination with chloride or sulfate is found to be necessary, along with lower temperatures, to cause localized corrosion. In the second phase of the study, the use of repassivation potential as a lower-bound parameter for long-term prediction of localized corrosion of the Fe-Ni-Cr-Mo alloys is examined. Electrochemical tests in simulated crevice solutions are conducted to provide input to modeling and to enable a mechanistic interpretation of repassivation. The effect of surface condition on corrosion behavior is also studied briefly. Based on these studies, further long-term studies are recommended, with a focus on alloy 825.

# CONTENTS

Section		Page
1	EXECUTIVE SUMMARY .....	1-1
2	INTRODUCTION .....	2-1
3	MATERIALS AND ENVIRONMENTS .....	3-1
3.1	CANDIDATE CONTAINER MATERIALS AND DESIGNS .....	3-1
3.2	CHARACTERIZATION OF ALLOYS TESTED .....	3-1
3.3	ENVIRONMENTAL CONSIDERATIONS .....	3-3
4	LOCALIZED CORROSION OF Fe-Ni-Cr-Mo ALLOYS — EFFECT OF ENVIRONMENTAL FACTORS .....	4-1
4.1	EXPERIMENTAL APPROACH .....	4-1
4.2	EFFECT OF ENVIRONMENTAL FACTORS IN GROUNDWATER ON LOCALIZED CORROSION RESISTANCE .....	4-2
4.2.1	Factorial Experiments .....	4-2
4.2.2	Additional Experiments on Environmental Effects .....	4-5
4.3	ELECTROCHEMICAL RESPONSE TO SIMULATED CREVICE SOLUTIONS .....	4-9
4.4	EFFECTS OF CHLORIDE AND pH ON LOCALIZED CORROSION .....	4-15
4.5	THE EFFECTS OF SURFACE CHROMIUM-DEPLETION .....	4-17
5	REPASSIVATION POTENTIAL AS A LONG-TERM PREDICTION TOOL FOR AUSTENITIC ALLOYS .....	5-1
5.1	INTRODUCTION .....	5-1
5.2	EXPERIMENTAL PROCEDURES .....	5-2
5.2.1	Specimens and Solutions .....	5-2
5.2.2	Test Cell .....	5-2
5.2.3	Electrochemical Measurements .....	5-4
5.2.4	Post-Test Analyses .....	5-5
5.3	RESULTS OF REPASSIVATION POTENTIAL MEASUREMENTS .....	5-5
5.4	REPASSIVATION TIME .....	5-8
5.5	MECHANISTIC MODELING OF REPASSIVATION .....	5-9
5.5.1	Potential-Drop Mechanism .....	5-10
5.5.2	Solution-Change Mechanism .....	5-11
6	LOCALIZED CORROSION OF COPPER-BASED ALLOYS .....	6-1
6.1	INTRODUCTION .....	6-1
6.2	RESULTS OF FACTORIAL EXPERIMENTS .....	6-2
6.3	EFFECT OF BICARBONATE CONCENTRATION .....	6-4
6.4	POTENTIOSTATIC STUDIES .....	6-8

## CONTENTS (cont'd)

Section	Page
7	SUMMARY AND RECOMMENDATIONS . . . . . 7-1
7.1	SUMMARY OF CURRENT INVESTIGATIONS . . . . . 7-1
7.1.1	Austenitic Alloys . . . . . 7-1
7.1.2	Copper Based Alloys . . . . . 7-2
7.2	RECOMMENDATIONS FOR FURTHER STUDIES . . . . . 7-3
8	REFERENCES . . . . . 8-1
APPENDIX A: CHARACTERIZATION OF PLATES OF ALLOYS TESTED IN THE IWPE PROGRAM	
APPENDIX B: SOLUTION PREPARATION FOR LOCALIZED CORROSION EXPERIMENTS	
APPENDIX C: CYCLIC POLARIZATION EXPERIMENTS ON THE AUSTENITIC ALLOYS — DATA TABLES	
APPENDIX D: RESULTS OF CYCLIC POLARIZATION EXPERIMENTS ON COPPER-BASED ALLOYS	

## FIGURES

Figure		Page
3-1	Schematic illustration of annealing and descaling operations resulting in Cr-depletion on austenitic alloy surfaces . . . . .	3-2
3-2	Chromium content of mill-finished and polished alloy surfaces . . . . .	3-2
3-3	Effect of Cr-depletion on corrosion rate in boiling 50% $H_2SO_4$ + 42 g/l $Fe_2(SO_4)_3$ . Tests were conducted for 120 hours for alloy 825 and types 304L and 316L stainless steels and 24 hours for alloy C-22. . . . .	3-3
3-4	Concentration changes in J-13 water during reaction with crushed tuff at 100°C. Solutions taken at various times are from independent tests. (Abraham, Jain, and Soo, 1986) . . . . .	3-7
3-5	Concentration changes in 10X J-13 water during reaction with crushed tuff at 100°C. (Abraham, Jain, and Soo, 1986) . . . . .	3-7
4-1	Experimental apparatus used for cyclic polarization experiments showing the glass cell along with the condenser and trap. The Model 273 potentiostat and the computer for data acquisition are also shown. . . . .	4-2
4-2	Effect of nitrate on localized corrosion in a 1000 ppm $Cl^-$ solution at 95°C . . . . .	4-6
4-3	Effect of sulfate on localized corrosion in a 1000 ppm $Cl^-$ solution at 95°C . . . . .	4-6
4-4	Effect of bicarbonate on localized corrosion in a 1000 ppm $Cl^-$ solution at 95°C. . . . .	4-8
4-5	Cyclic polarization curves for alloy 825 in simulated crevice solutions at various pH values (measured at room temperature). Scan rate: 0.167 mV/sec. Solutions were deaerated with argon. Specimens were polished to 600-grit and partially immersed. . . . .	4-10
4-6	Cyclic polarization curves for type 304L stainless steel in simulated crevice solutions at various pH values (measured at room temperature). Scan rate: 0.167 mV/sec. Solutions were deaerated with argon. Specimens were polished to 600-grit and partially immersed. . . . .	4-12
4-7	Effects of pH and $Cl^-$ on corrosion potential of alloy 825 in reducing environments. Temperature: 95°C. . . . .	4-16
4-8	Effect of pH and $Cl^-$ on pitting and repassivation potentials of alloy 825 . . . . .	4-16
4-9	Specimen used to study the effect of surface Cr-depletion in alloy 825 using cyclic polarization test. The specimen is connected to the electrochemical equipment in the same manner as the cylindrical specimens in ASTM G-61. . . . .	4-19
4-10	Cyclic polarization curves of Cr-depleted and polished surfaces of alloy 825 in a 6 ppm $Cl^-$ solution at 95°C. Scan rate: 0.167 mV/sec. . . . .	4-19
4-11	Cyclic polarization curves of Cr-depleted and polished surfaces of alloy 825 in a 1000 ppm $Cl^-$ solution at 95°C. Scan rate: 0.167 mV/sec. . . . .	4-20
4-12	Repeated cyclic polarization curves of Cr-depleted surfaces of alloy 825 in a 1000 ppm $Cl^-$ solution at 95°C indicating the behavior of a progressively increasing Cr content. Scan rate: 0.167 mV/sec. . . . .	4-20

## FIGURES (cont'd)

Figure		Page
5-1	Schematic illustration of the approach used for long-term life prediction of container materials under localized corrosion conditions . . . . .	5-1
5-2	Schematic diagram of the cell and electrochemical testing system for the repassivation experiments . . . . .	5-3
5-3	Overall view of the cell, multi-channel potentiostat, and data acquisition system for repassivation experiments . . . . .	5-5
5-4	Schematic profiles of applied potential versus time used for various repassivation experiments. The fast-scan technique is shown in (b), while the slow-scan techniques are shown in (a), (c), and (d). . . . .	5-6
5-5	Actual potential and current density versus time plots for a specimen of type 316L stainless steel . . . . .	5-7
5-6	Effect of applied charge on repassivation potential for pitting of type 316L stainless steel in 1000 ppm Cl <sup>-</sup> solution at 95°C . . . . .	5-8
5-7	Effect of applied charge on repassivation potential for pitting of alloy 825 in 1000 ppm Cl <sup>-</sup> solution at 95°C . . . . .	5-9
5-8	The effect of applied potential on repassivation time of alloy 825 in a 1000 ppm Cl <sup>-</sup> solution at 95°C. Open circles: pits grown for 7 hours; closed circles: pits grown for 12 hours. . . . .	5-10
5-9	Dependence of E <sub>rp</sub> on Cl <sup>-</sup> concentration under slow-scan, potential staircase, and cyclic polarization techniques . . . . .	5-12
6-1	Effect of chloride and sulfate on breakdown and repassivation potentials for alloy CDA-715 in a 8500 ppm bicarbonate solution at 30°C . . . . .	6-3
6-2	Effect of bicarbonate concentration on breakdown and repassivation potentials of CDA-715. Solutions contained: 1000 ppm Cl <sup>-</sup> , 1000 ppm SO <sub>4</sub> <sup>2-</sup> , 10 ppm NO <sub>3</sub> <sup>-</sup> , 2 ppm F <sup>-</sup> . Temperature: 60°C. UC = Uniform Corrosion; LC = Localized Corrosion. . . . .	6-4
6-3	Effect of temperature on breakdown and repassivation potentials of CDA-715. Solutions contained: 8500 ppm HCO <sub>3</sub> <sup>-</sup> , 1000 ppm Cl <sup>-</sup> , 1000 ppm SO <sub>4</sub> <sup>2-</sup> , 10 ppm NO <sub>3</sub> <sup>-</sup> , 2 ppm F <sup>-</sup> . . . . .	6-5
6-4	Potential-pH equilibrium diagram for copper in the system: Cu-Cl <sup>-</sup> -SO <sub>3</sub> -CO <sub>2</sub> -H <sub>2</sub> O at 25°C. Solutions containing 22 ppm Cl <sup>-</sup> , 229 ppm CO <sub>2</sub> , and 46 ppm SO <sub>3</sub> . (Pourbaix, 1974). . . . .	6-6
6-5	Cyclic polarization curves of CDA-102 and CDA-715 in borate buffer solution at pH = 8.6 and temperature of 25°C. Scan rate: 0.167 mV/sec. Solutions were deaerated with argon. . . . .	6-7
6-6	Cyclic polarization curves on CDA-102 and CDA-715 in a solution containing 85 ppm bicarbonate at 30°C. Solutions were deaerated with argon. . . . .	6-7
6-7	Effect of Cl <sup>-</sup> or SO <sub>4</sub> <sup>2-</sup> addition on the anodic current density of CDA-102 under potentiostatic condition at 25°C. Base solution: 8500 ppm HCO <sub>3</sub> <sup>-</sup> , 6 ppm Cl <sup>-</sup> , 20 ppm SO <sub>4</sub> <sup>2-</sup> , 10 ppm NO <sub>3</sub> <sup>-</sup> , 2 ppm F <sup>-</sup> . . . . .	6-8

## FIGURES (cont'd)

Figure		Page
6-8	Effect of $\text{Cl}^-$ or $\text{SO}_4^{2-}$ addition on the anodic current density of CDA-715 under potentiostatic condition at $95^\circ\text{C}$ . Base solution: 8500 ppm $\text{HCO}_3^-$ , 6 ppm $\text{Cl}^-$ , 20 ppm $\text{SO}_4^{2-}$ , 10 ppm $\text{NO}_3^-$ , 2 ppm $\text{F}^-$ . . . . .	6-10

# TABLES

Table		Page
3-1	Chemical composition ranges of J-13 well water (Glassley, 1990) . . . . .	3-4
3-2	Analysis of solutions from U-bend stress corrosion cracking tests in aerated J-13 water under $\gamma$ -irradiation. Fresh J-13 water was added at the end of each period. (Westerman et al., 1987) . . . . .	3-5
4-1	Depassivation pH of three alloys under various simulated crevice solutions and temperatures measured by cyclic polarization technique . . . . .	4-14
4-2	Effect of aeration of H <sub>2</sub> O <sub>2</sub> addition on open-circuit potentials (mV versus SCE) of alloy 825 and Pt simulated J-13 solutions at 95°C . . . . .	4-17

## ACKNOWLEDGMENTS

This report was prepared to document work performed by the Center for Nuclear Waste Regulatory Analyses (CNWRA) for the U.S. Nuclear Regulatory Commission (NRC) under Contract No. NRC-02-88-005. The activities reported herein were performed on behalf of the NRC Office of Nuclear Regulatory Research, Division of Regulatory Applications, Michael McNeil, Project Officer. The report is an independent product of the CNWRA and does not necessarily reflect the views or regulatory position of the NRC.

The authors acknowledge the assistance of Walter Machowski who conducted the bulk of the electrochemical tests reported herein. The authors also express their appreciation to Fred Lyle for conducting the initial phase of the study on the environmental effects, Robert Mason for his assistance in the statistical analyses, Harold Saldana and Ramsey Railsback for performing the microscopy, Donald Pile for conducting the tests in simulated crevice solutions, Steven Griffin for modification of the electrochemical software, and Robert Brient for assistance with the quality assurance procedures. Special thanks go to Wendell Peters and Ben Delgado for modifying the electronics and assembling the automated data acquisition systems. Appreciation is also due Bonnie Garcia and Curtis Gray for assistance in preparing this document.

# 1 EXECUTIVE SUMMARY

The U.S. Nuclear Regulatory Commission (NRC) regulation 10 CFR 60.113 requires waste packages to provide substantially complete containment of radionuclides for a minimum period of 300 to 1000 years. As stated in the associated Division of High-Level Waste Management (DHLWM) user need, the important parameters that affect long-term performance of waste package components and the applicability of short-term, laboratory test techniques to predict long-term performance must be understood. The goal of the Integrated Waste Package Experiments (IWPE) program is to provide a critical evaluation of the information available for long-term performance prediction by a suitable combination of literature surveys and critical experiments. To achieve its objectives, the IWPE program is divided into six tasks: Task 1—Corrosion; Task 2—Stress Corrosion Cracking; Task 3—Materials Thermal Stability; Task 4—Microbiologically Influenced Corrosion; Task 5—Other Degradation Modes; and Task 6—General Reporting. The results of experimental activities in Task 1 are reported here.

Characterization of the initial microstructures of the candidate alloys, types 304L and 316L stainless steels, alloy 825, CDA-102 (oxygen-free copper), CDA-715 (Cu-30%Ni), and CDA 613 (Cu-7%Al), and the Center for Nuclear Waste Regulatory Analyses (CNWRA) reference alloy, alloy C-22, is reported in Chapter 3. Surface analyses indicate that the Ni-based alloys, alloys 825 and C-22, exhibit significant chromium depletion on the surface in the as-received condition. Tests in standard American Society for Testing and Materials (ASTM) solutions, as well as electrochemical tests in simulated groundwater environments, result in higher corrosion of the depleted surfaces of these alloys compared to the surfaces without Cr depletion. This may be important in the eventual performance of container materials in the field. The environmental considerations near the waste package are reviewed in Chapter 3. The uncertainties in the environment resulting from the placement of a high thermal load in a partially saturated repository horizon are described.

The studies on the effects of environmental variables on the localized corrosion of alloy 825 are reported in Chapter 4. A two-level, full factorial design is used to examine the main effects and interactions of chloride, sulfate, nitrate, fluoride, and temperature. These four anions, together with bicarbonate, which is maintained at a constant concentration in all the tests, are the predominant species in J-13 well water, the reference water for the experimental work in the Yucca Mountain Project (YMP). Additionally, the effects of chloride, nitrate, nitrite, silicate, magnesium, and bicarbonate concentration, and temperature are examined in greater detail. Cyclic, potentiodynamic polarization tests are used to determine the susceptibility of the alloy to localized corrosion. It is found that the electrochemical parameters measured in these tests (pitting potential, repassivation potential, and the difference between them) are not accurate indicators of the extent of localized corrosion observed visually on alloys 825 and C-22. The use of only electrochemical parameters to judge pitting becomes less valid for more corrosion resistant alloys such as alloy C-22. Therefore, the visual observation of localized corrosion of the specimens with a low power stereoscope and a scanning electron microscope is expressed in terms of a rating number. This rating number is combined with the electrochemical parameters in an index, termed localized corrosion index (LCI), to quantify the extent of localized corrosion and the effect of the environmental factors. Unlike the case of alloy 825, a good correlation is found for type 316L stainless steel between electrochemical parameters characterizing localized corrosion (pitting potential, repassivation potential, and the difference between them) and visual observation of pitting/crevice corrosion. The LCI for type 316L stainless steel is found to be higher than that for alloy 825, indicating that the latter is more resistant to localized corrosion as a result of the higher Cr and Mo contents.

For the Fe-Ni-Cr-Mo alloys, chloride is the most detrimental factor in inducing localized corrosion. Nitrate is the most effective inhibitor of localized corrosion, exhibiting this effect at a lower concentration in the case of alloy 825 than type 316L stainless steel. Sulfate is a less effective inhibitor, whereas bicarbonate has a variable effect. It is also found that localized corrosion in alloy 825 in simulated J-13 water at 95°C occurs with increasing probability starting at a chloride concentration of about 20 ppm. The electrochemical parameters indicating localized corrosion are independent of temperature up to a chloride concentration of about 1000 ppm. Only at higher chloride concentrations (10,000 ppm) is a pronounced effect of temperature on the pitting and repassivation potentials of alloy 825 observed. The effects of other environmental species are examined separately including nitrite, silicon (added as metasilicate), hydrogen peroxide, oxygen, and magnesium. The natural potential under conditions simulating water radiolysis effects, by the addition of hydrogen peroxide, is sufficiently high to cause localized corrosion of alloy 825 in a 100 ppm chloride solution. Pits grown in high chloride solutions have large depth/diameter ratios, and crevice corrosion is frequently observed in conjunction with pitting. Experimental investigations in simulated crevice/pit solutions are shown to yield valuable kinetic data that can be used in the existing crevice corrosion model, TWITCH, to better define conditions for initiation and repassivation. The effects of surface Cr-depletion on the localized corrosion behavior of alloy 825 are also discussed.

The general approach to long-term life prediction of container materials under localized corrosion environments is pointed out in Chapter 5. Two of the parameters that are important in this approach are the initiation and repassivation potentials. The main focus of these experiments is on alloy 825, with a limited testing of types 304L and 316L stainless steels, and alloy C-22. The alloys are evaluated in 1000 ppm chloride solution which has been identified as a model solution in previous experiments. The salient result from these experiments is that a lower bound value of repassivation potential, that is essentially independent of the extent of pitting, can be obtained in these alloy/environment combinations. Additionally, it is shown that the fast scan potential staircase tests yielded a lower (more conservative) value of repassivation potential than the slow scan tests, which is explained on the basis of the dependence of repassivation time on potential. This finding, which must be further confirmed by long-term corrosion tests under controlled potentials, enables the use of short-term, accelerated tests to derive parameters for long-term predictions. The mechanistic aspects of initiation and repassivation, in the context of crevice corrosion, are outlined.

The effect of environmental factors on the localized corrosion of copper-based alloys is examined in Chapter 6. Unlike the case of Fe-Ni-Cr-Mo alloys, the electrochemical response of the copper-based alloys, CDA-102 (oxygen-free copper) and CDA-715 (Cu-30%Ni) to varying environmental compositions is more complex. Hysteresis in the potentiodynamic polarization curves, which has been used for the Fe-Ni-Cr-Mo alloys as a partial indicator of localized corrosion, is indicative of the extent of localized corrosion in only some solutions. In environments containing a bicarbonate concentration comparable to the nominal concentrations found in J-13 well water, active dissolution is the predominant mode of corrosion at 30°C, whereas a limited region of passivity is found at 95°C. On the other hand, both alloys exhibit an extended passive region in solutions containing a higher bicarbonate concentration (8500 ppm). At 30°C, CDA-102 and CDA-715 exhibit shallow, localized corrosion in the 8500 ppm bicarbonate solution that is enhanced by the addition of 1000 ppm chloride and/or sulfate. Localized corrosion of CDA-715 in solutions containing high concentrations of those anions is observed up to 80°C. A temperature increase to 95°C essentially eliminates localized corrosion and results in the formation of thick, dark films. Localized corrosion of CDA-102 and CDA-715 occurs in the form of shallow and wide pits, that become broader with time in potentiostatic tests. Bicarbonate is also found to play a role in increasing the active corrosion of copper, possibly by the formation of soluble cupric complexes. In

the absence of bicarbonate, but at the same pH maintained by a borate buffer, only passive corrosion is observed.

Both the list of container materials and designs are evolving (Short et al., 1991; McCright et al., 1991). Use of alternate materials such as alloy C-4 and Ti-grade 12 is being discussed along with alloy 825. Additionally, use of bimetallic construction (either metallurgically bonded or as loose lining) has been discussed, with carbon-steel as an outer, thick-walled container, and one of the above alloys as an inner lining. The copper-based alloys have received diminished consideration. Some of these changes can have a significant impact on the IWPE activities. However, from the point of view of localized corrosion, the methodologies established in the current IWPE program can still be utilized for the new materials and designs. For example, localized corrosion is important for both Ti and Fe-Ni-Cr-Mo alloys, and the use of repassivation potentials for long-term life prediction has been demonstrated for carbon steel, stainless steels, and Ti alloys (Okayama, et al., 1987a; Nakayama and Akashi, 1991; Fukuda and Akashi, 1992). The use of a thick outer steel container will change the corrosion potential of the inner, higher-alloy lining through galvanic effects as well as through a reduction of gamma radiolysis. However, the method of comparing the corrosion potential to the initiation and repassivation potentials for localized corrosion can still be utilized.

Long-term corrosion experiments at controlled potentials above and below the repassivation potentials are recommended in Chapter 7. It is also recommended that further experiments in analyzing the chemical conditions inside crevices be undertaken to check the validity of assumptions made in the model.

## 2 INTRODUCTION

The NRC regulation 10 CFR 60.113 requires waste packages to provide substantially complete containment of radionuclides for a minimum period of 300 to 1000 years. Arising from this requirement is the need for the U.S. Department of Energy (DOE) to demonstrate, through proper selection, design, testing, and analyses, the long-term performance of waste packages. In order to evaluate DOE's resolution of these technical issues, NRC must develop an understanding of the important factors that affect long-term performance of waste package materials and the limitations and applicability of various test methods used to demonstrate performance. The IWPE program at the CNWRA supports the NRC in attaining these objectives. The overall technical objectives of the IWPE Project are to

- Develop a good understanding of the information currently available on metal corrosion and on other metal degradation processes
- Assess the current status of YMP Waste Package Programs
- Conduct waste package experiments to scope and study the key parameters affecting long-term material performance
- Experimentally assess waste package materials and designs selected by the DOE and provide independent evaluation for reasonable assurance of long-term performance
- Support the Office of Nuclear Regulatory Research in addressing the needs of the DHLWM

One of the research needs identified by the DHLWM is the clarification of factors affecting the results of tests used to verify long-term performance of waste package components. Localized corrosion (pitting and crevice corrosion) is considered to be one of the most important degradation processes that affect the performance of HLW container materials. Hence, an objective of IWPE is to examine the applicability of parameters derived from short-term localized corrosion tests to long-term performance prediction. This objective is being addressed in Task 1 of the IWPE program.

In the U.S. geologic disposal program, two different types of waste package emplacement concepts are being considered: (i) vertical emplacement of a single-wall or double-wall container in a borehole with an air gap between the container and the borehole, and (ii) horizontal emplacement of a double-wall container surrounded by a suitable backfill in the drifts of the underground repository. The vertical emplacement of a thin, single-wall container, made of type 304L stainless steel, is the present reference design (Site Characterization Plan (SCP), 1988). It has also been proposed that high thermal loading be used to create a dry-out zone around the Engineered Barrier System (EBS) for thousands of years that will minimize corrosion and nongaseous radionuclide transport. The drying out process may create deposition of solids rich in Ca and Si (Beavers et al., 1992). However, backflow of the condensate through fractures intersecting the borehole may result in an aqueous environment around the container, as indicated by the results of some field heater tests (Patrick, 1986; Zimmerman et al., 1986; Ramirez, 1991). The rewetting of the dried solids can cause the formation of solutions rich in chloride and sulfate as shown experimentally by Beavers et al. (1992). Hence, a conservative approach in life prediction is to assume the presence of aqueous conditions surrounding the containers. Given the uncertainties in the type of waste package design that will be used by DOE, and the constitution of the environment that will

be encountered by the waste packages, it is important to establish, where possible, experimental methodologies that will apply to classes of materials rather than particular alloys and to investigate the effects of environmental factors over wide ranges. Furthermore, it is important to demonstrate that these experimental techniques can be used to derive long-term performance functions of the waste package materials. Both aspects, as they apply to the phenomena of localized corrosion, are addressed in this report. While a significant part of long-term performance prediction involves modeling, the present report focuses on the results of experimental investigations. The applicability of the results to modeling activities is pointed out where appropriate.

The report is organized in terms of two broad classes of materials: the Fe-Ni-Cr-Mo alloys and the copper-based alloys. However, because the Fe-Ni-Cr-Mo alloys, especially alloy 825, appear to be preferred currently by DOE and its contractors, more effort is devoted to these alloys.

## 3 MATERIALS AND ENVIRONMENTS

### 3.1 CANDIDATE CONTAINER MATERIALS AND DESIGNS

The DOE's list of container materials for high-level nuclear waste disposal has undergone many revisions over the last two decades, but has been confined to six alloys after about 1984 (McCright, 1988). These consist of the alloys based on a fully austenitic structure (face centered cubic lattice) that are in the Fe-Ni-Cr-Mo alloy family, and copper-based alloys including oxygen-free copper. Since late 1983, when the decision was made to locate the repository horizon in the unsaturated zone of the Yucca Mountain site, the container design has been essentially confined to a single-wall concept with a relatively thin wall (approximately 12 mm thick). The IWPE plan and activities have reflected these considerations. Additionally, the CNWRA proposed the addition of a seventh alloy, alloy C-22 (which is marketed under its proprietary name of Hastelloy® alloy C-22), as a reference material for comparison of localized corrosion data of the other DOE candidate container alloys. Many of the IWPE activities have focused on alloy 825 because it is considered to be one of the top candidates for container design. However, type 316L stainless steel and, to a lesser extent, type 304L stainless steel and alloy C-22 have also been studied. Among the copper-based alloys, importance was given to CDA-102 and CDA-715.

### 3.2 CHARACTERIZATION OF ALLOYS TESTED

The chemical compositions, mechanical properties, and microstructures of the specific heats that have been tested so far in the IWPE program are shown in Appendix A. Specimens from the as-received plates of the austenitic alloys were subjected to ASTM intergranular corrosion tests to ensure that they were heat-treated properly. The results indicated that they were of acceptable microstructure for further study (Cragolino and Sridhar, 1990a).

One important aspect of determining the field performance of austenitic alloys is the surface chemical composition. It has been shown that surface Cr-depletion of Ni-base alloys has an adverse effect on the stress corrosion cracking resistance in oil and gas production environments (Place et al., 1991). The origin of the Cr-depleted layer is explained schematically in Figure 3-1. Annealing the alloy in air results in a Cr-rich oxide scale beneath which is a Cr-depleted metallic region. There is a gradient in the concentration of Cr in this region, depending on the alloy (Fabis and Covino, 1986) and annealing conditions (Lee et al., 1991). During the descaling operation, the pickling acid removes the scale partly by dissolution of the scale, but mainly by dissolving the underlying Cr-depleted region and lifting the scale off (Covino, 1987; Grubb, 1991). However, the dissolution rate of the Cr-depleted region varies from alloy to alloy, and is not sufficiently high for the more corrosion resistant alloys to effect a complete removal of the depleted region. Thus, a residual Cr-depleted layer can be found on the finished product, especially in the more corrosion resistant alloys. Such a Cr-depletion, using scanning electron microscopy (SEM) energy dispersive x-ray (EDX) analysis, is shown for alloys 825 and C-22 in Figure 3-2. It can also be seen from this figure that types 304L and 316L stainless steels do not exhibit significant Cr-depletion, because the original Cr-depleted regions in these alloys have been dissolved completely by the descaling acids. These data represent an approximate analysis of Cr-depletion, because the EDX analysis is averaged over a finite volume of substrate.

As a result of Cr-depletion, the corrosion rate in an oxidizing acid environment (50% H<sub>2</sub>SO<sub>4</sub> + 42 g/l Fe<sub>2</sub>(SO<sub>4</sub>)<sub>3</sub>) of the mill-finished surface is higher than that of the polished surface (Figure 3-3). While this environment is far from anticipated in the repository, it is used as a standard quality control

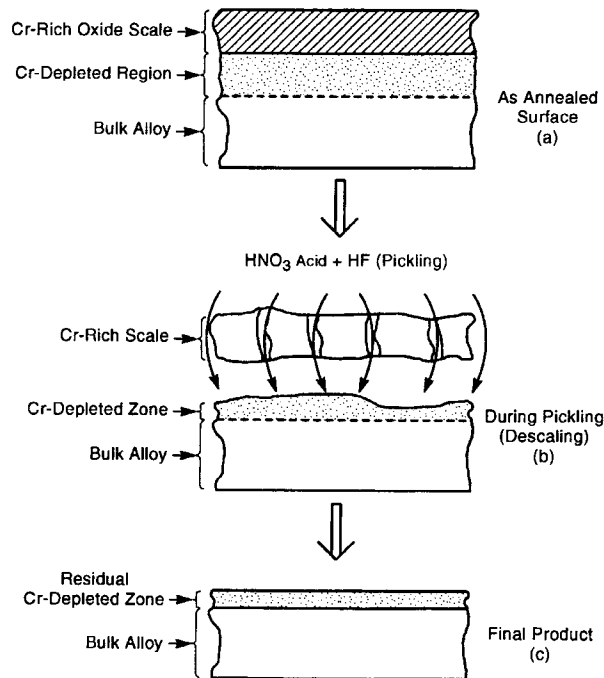


**Figure 3-1. Schematic illustration of annealing and descaling operations resulting in Cr-depletion on austenitic alloy surfaces**

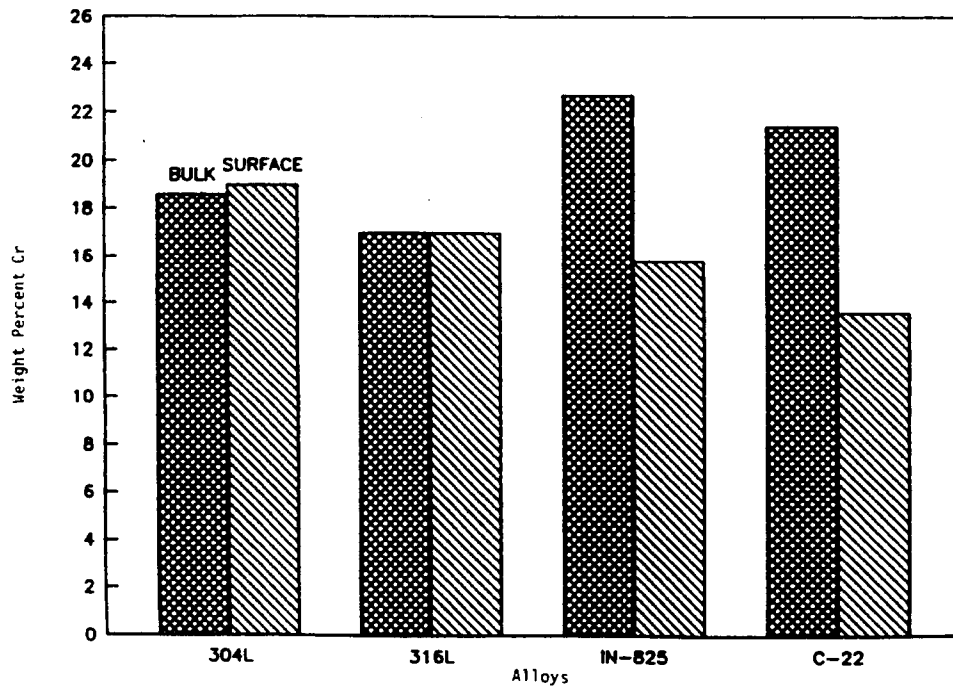


**Figure 3-2. Chromium content of mill-finished and polished alloy surfaces**

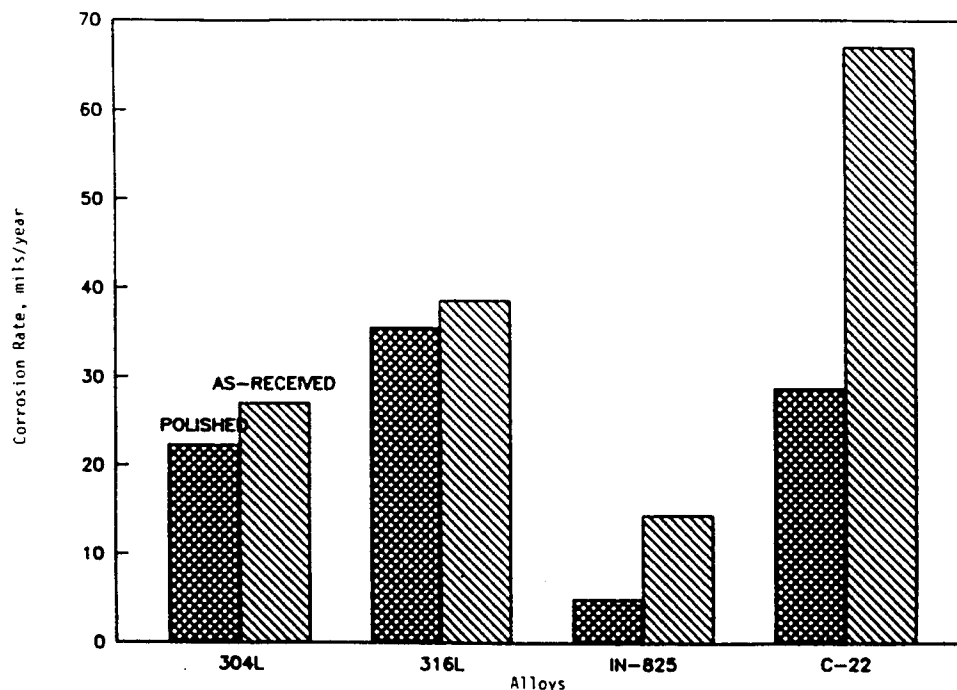


Figure 3-3. Effect of Cr-depletion on corrosion rate in boiling 50% $H_2SO_4$  + 42 g/l  $Fe_2(SO_4)_3$ . Tests were conducted for 120 hours for alloy 825 and types 304L and 316L stainless steels and 24 hours for alloy C-22.

test in the industry. The same test can be used as a quality control specification for the container material. The effects of Cr-depletion on waste container performance in simulated repository environments will be discussed in a later chapter.

### 3.3 ENVIRONMENTAL CONSIDERATIONS

It is well known that water extracted from the J-13 well, located in the saturated zone of the Yucca Mountain site, has been used as the reference groundwater for experimental studies (Glassley, 1986), assuming that its composition is close to that of the vadose water in the unsaturated zone in the Topopah Spring tuff. However, the J-13 well water has a range of composition for various species (Glassley, 1990). As shown in Table 3-1, J-13 water is a neutral pH water in which the prevailing ionic species are  $HCO_3^-$  and  $Na^+$ . Other anions, such as  $Cl^-$ ,  $F^-$ ,  $SO_4^{2-}$  and  $NO_3^-$ , are present at lower concentrations. The silicon content of the water, in the form of silicic acid, is relatively high. Waters from other wells in the vicinity of Yucca Mountain have similar chemical compositions, but differences in pH and ion concentration ratios are considered to be significant (Kerrisk, 1987).

Of greater importance to all localized corrosion processes is the evolution of the environmental composition as a result of the emplacement of the waste packages in the repository. These changes in the environmental composition can occur by the following processes:

- **Rock-water interactions over long periods of time and modified by the increase in temperature:** Modeling efforts in this area (Pabalan and Murphy, 1991) have shown that,

**Table 3-1. Chemical composition ranges of J-13 well water (Glassley, 1990)**

Species	mg/L	mMoles/L
Li <sup>+</sup>	0.04-0.17	0.006-0.024
Na <sup>+</sup>	42-50	1.83-2.17
K <sup>+</sup>	3.7-6.6	0.10-0.17
Mg <sup>2+</sup>	1.7-2.5	0.07-0.10
Ca <sup>2+</sup>	11.5-15.0	0.29-0.37
Sr <sup>2+</sup>	0.02-0.1	0.0002-0.001
Fe <sup>3+</sup>	<0.01-0.16	<0.0002-0.003
Al <sup>3+</sup>	0.008-0.11	0.0003-0.004
Si(SiO <sub>2</sub> )	26.6-31.9	0.95-1.14
NO <sub>3</sub> <sup>-</sup>	6.8-10.1	0.113-0.168
F <sup>-</sup>	1.7-2.7	0.029-0.135
Cl <sup>-</sup>	6.3-8.4	0.178-0.237
HCO <sub>3</sub> <sup>-</sup>	118-143	1.93-2.34
SO <sub>4</sub> <sup>2-</sup>	17-21	0.18-0.22
pH	—	6.8-8.3

as the temperature increases, the bicarbonate concentration will decrease due to CO<sub>2</sub> volatilization resulting in a concomitant increase in pH. In many of the reported stress corrosion cracking experiments, J-13 water conditioned by contact with crushed tuff at the test temperature has been used. It can be presumed, however, that the concentration should be extremely dependent on the mineralogical composition of the rock and the temperature and, also, unless equilibrium conditions were rapidly established, on the duration of the conditioning process and the volume ratio of the rock to the water. The evolution of J-13 water in contact with crushed tuff at 50°C and 90°C and under  $\gamma$ -irradiation is shown in Table 3-2 (Westerman et al., 1987). The autoclaves were continuously purged with air and were open to the atmosphere via 9 meters of outlet tubing. After each period of testing, as shown in the first column of Table 3-2, the solution was replaced with fresh J-13 water. Fresh rock was replaced after each test period up to 10 months and not thereafter. Although some of the changes in the concentration of species such as NO<sub>2</sub><sup>-</sup> and NO<sub>3</sub><sup>-</sup> may be the result of radiolysis, changes in the concentration of other species such as Cl<sup>-</sup>, HCO<sub>3</sub><sup>-</sup>, and SO<sub>4</sub><sup>2-</sup> are most probably due to interaction of the solution with rock and specimens. Unfortunately, no systematic variations in the concentrations of any species is discernible.

Table 3-2. Analysis of solutions from U-bend stress corrosion cracking tests in aerated J-13 water under  $\gamma$ -irradiation. Fresh J-13 water was added at the end of each period. (Westerman et al., 1987)

Time, Month	pH	Cond., $\mu\text{S/cm}$	Concentration, mg/L									
			F	Cl	NO <sub>2</sub>	NO <sub>3</sub>	HCO <sub>3</sub>	SO <sub>4</sub>	Ca	Na	Si	NH <sub>3</sub>
50°C Test												
3	7.7	780	2.2	51	5	42	190	100	42	110	25	—
5	7.3	5400	7.0	420	570	670	210	970	530	590	47	4.7
7	7.7	6800	7.2	470	680	770	180	1130	560	660	40	11
10	7.7	2520	2.5	119	106	201	142	802	278	218	37	2.0
16	7.8	1926	<0.1	110	24	189	100	510	140	200	26	0.4
24	8.1	2380	<0.1	37	37	323	34.3	806	210	275	37	0.03
25	8.1	1000	<0.1	25	<1	125	56.3	219	98	97	28	0.01
90°C Test												
3	9.2	1240	1.5	140	2	1	24	300	23	250	66	—
5	8.2	1085	0.6	14	11	23	65	88	44	27	28	1.4
7	8.0	8450	12	600	1700	110	230	1400	820	950	58	0.3
10	8.3	123	0.2	0.3	3	10	34	8	22	3	22	—
14	8.9	115	0.2	0.6	3	7	33	12	14	7	34	<0.1
23	9.0	601	<0.1	27	43	<1	47	138	18	101	28	0.04

The pH at the end of each period is higher than the initial pH of the J-13 water reported (7.1 - 7.6), which is consistent with the model predictions (Pabalan and Murphy, 1991). The  $\text{Cl}^-$  and  $\text{SO}_4^{2-}$  are generally much higher than found in the initial J-13 water that was used by the investigators. These results are corroborated by the measurement of high conductivity at the end of each period. The authors report that the measurements of high ionic concentrations are reproducible.

A further confirmation of the increase in concentration of ionic species due to rock-water interactions has been presented by Abraham et al. (1986). When synthetic J-13 water was heated in the presence of crushed tuff to boiling temperatures ( $100^\circ\text{C}$ ) under refluxing conditions, it was shown (Abraham et al., 1986) that the concentration of several anions and cations, such as  $\text{SO}_4^{2-}$ ,  $\text{NO}_3^-$ ,  $\text{Cl}^-$ ,  $\text{Na}^+$ ,  $\text{K}^+$  and  $\text{Ca}^{2+}$ , increases significantly with time (Figures 3-4 and 3-5). Detailed solution analyses were carried out after various time periods of testing. Interestingly, reaction of boiling distilled water with tuff produced an initial increase in  $\text{Cl}^-$  to about 160 ppm which, upon further treatment with new distilled water, decreased to a steady value of about 20 ppm, more than three times the 6 ppm concentration reported nominally for J-13 water.

In contrast to the above experiments, a review of rock-water interaction experiments performed at Lawrence Livermore National Laboratories (LLNL) (Knauss et al., 1985; Oversby, 1985; Glassley, 1986) indicated no significant changes from the initial J-13 values for chloride, fluoride, nitrate, and sulfate. These experiments were conducted as essentially closed systems. In the results reported by Oversby (1985), the pH increased to about 9 after 70 days at  $150^\circ\text{C}$ , whereas, a slight decrease in the dissolved bicarbonate content was observed. This was attributed to the gradual exsolution of  $\text{CO}_2$  from the solution through the pores in the polytetrafluoroethylene (PTFE) liner. Knauss et al. (1985) used an impermeable gold-bag, and, hence, did not observe any increase in pH during the course of their experiments. A slight decrease in the pH (measured at  $25^\circ\text{C}$ ) was noted and attributed to the precipitation of Ca and Mg carbonates which have retrograde solubility. The most significant compositional change was the dissolution of silicon from the tuff.

- **Changes due to occluded regions such as crevices:** It has been well established that concentration of anionic species such as chloride can increase greatly in regions such as crevices, while pH can decrease due to hydrolysis of cationic species such as  $\text{Fe}^{2+}$ ,  $\text{Cr}^{3+}$ , and  $\text{Ni}^{2+}$  (Turnbull, 1983; Alavi and Cottis, 1987; Luo et al., 1992). Additionally, highly reducing conditions may be created in occluded regions due to the rapid depletion of oxygen and slow rediffusion from the bulk. The radiolysis reactions in acidic reducing solutions may be significantly different from those in the bulk oxidizing solutions (Spinks and Woods, 1990).
- **Changes due to repeated/episodic evaporation and re-wetting of container:** This process is poorly understood and characterized. Experimental measurements of Beavers et al. (1992) have shown increases in anionic concentrations linearly proportional to the number of boil-down and refill cycles. However, the relationship of these procedures to scenarios in the repository is not clear. Westerman et al. (1987) performed boil-down tests in autoclaves at  $200^\circ\text{C}$  and 1000 psig with seven days in liquid and one day under "dry" conditions. The "dry" period was achieved by reducing the pressure. The reported concentration of chloride

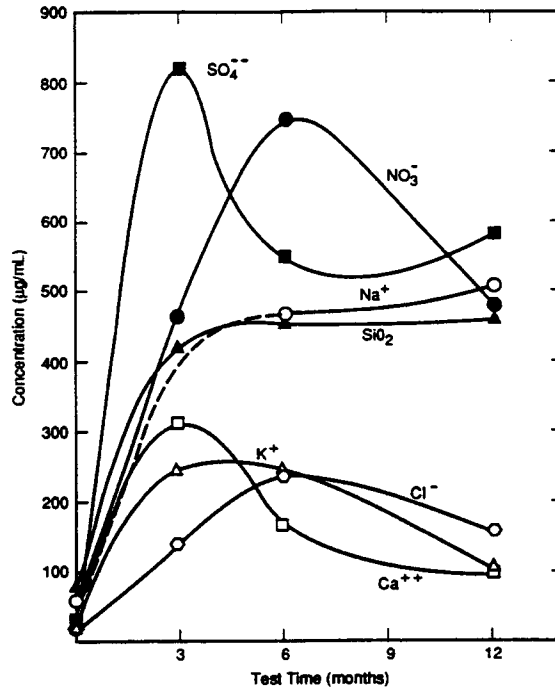


Figure 3-4. Concentration changes in J-13 water during reaction with crushed tuff at 100°C. Solutions taken at various times are from independent tests. (Abraham et al., 1986)

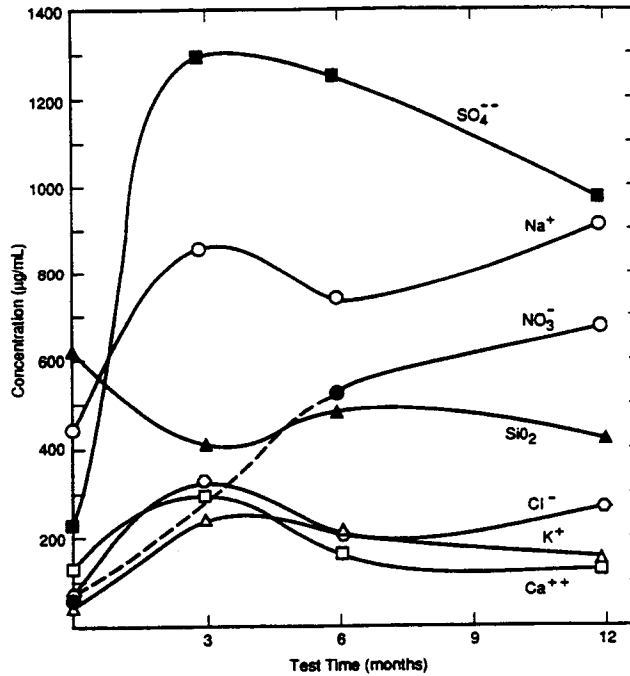


Figure 3-5. Concentration changes in 10X J-13 water during reaction with crushed tuff at 100°C. (Abraham et al., 1986)

and sulfate after 15 and 50 boil-down cycles were higher than initial values, but not high enough in proportion to the number of boil-down cycles if complete evaporation is assumed.

- **Changes due to radiolysis:** The gamma dose rate from spent fuel containers is expected to be as high as 0.1 Mrad/hr and, typically, about 0.01 Mrad/hr (Reed and van Konynenburg, 1991). The dose rate from glass waste is expected to be somewhat less, about 0.005 Mrad/hr (van Konynenburg, 1986). Some of the early field evidences of the effects of radiolysis on corrosion and stress corrosion cracking were observed in the Spent Fuel Test—Climax Program (Patrick, 1986). Corrosion of the carbon steel liners exposed to spent-fuel containers and cracking of Ni-Fe extensometer connecting rods were noted. In the latter case, laboratory simulation of stress corrosion cracking of Ni-Fe specimens in groundwater environments was achieved only upon addition of an oxidizing salt,  $\text{CuCl}_2$ . In addition to galvanic effects due to coupling with copper components, it is possible that radiolysis of the groundwater environment increased the concentration of oxidizing species, thus raising the corrosion potential high enough to cause corrosion and cracking.

Experimental investigations of chemical and electrochemical effects of  $\gamma$ -radiation have been reported by van Konynenburg (van Konynenburg, 1986; Glass et al., 1986; Kim and Oriani, 1987; Reed and van Konynenburg, 1990, 1991). Van Konynenburg (1986) interpreted the experimental results related to reaction of various types of glasses with water and water reacted with tuff. The major species present as a result of  $\gamma$ -radiation of water in contact with air were nitrite and nitrate. The ratio of nitrite to nitrate was dictated by the presence of catalytic surfaces such as tuff and ionic species in the water such as bicarbonate. In the absence of tuff rock and ionic species in water, the nitrite/nitrate ratio was close to 1. This is presumably due to the oxidation of nitrite to nitrate by the hydrogen peroxide that is formed in the water as a result of radiolysis. In the presence of catalysts that promote decomposition of hydrogen peroxide, the nitrite concentration increased. While the hydrogen peroxide concentration was not reported, van Konynenburg (1986) speculated that it would have been quite low. Reed and van Konynenburg (1990, 1991) reported that in moist-air system (at relative humidities of 15 percent at  $90^\circ\text{C}$ ), nitrites and nitrates were the main species as a result of radiolysis and copper specimens under these conditions formed hydrated cupric nitrates. In the 100 percent relative humidity environment, only  $\text{Cu}_2\text{O}$  and  $\text{CuO}$  were found on copper specimens. Irradiation experiments by Yunker (1990) on various copper alloys under 100 percent relative humidity conditions at  $95^\circ\text{C}$  have resulted in the formation of mainly  $\text{CuO}$ . Yunker reported estimated concentrations of  $\text{NO}_2^-$  in the gas phase of moist air mixtures exposed to irradiation but did not report any observation of nitrate corrosion products on copper specimens. Colloidal Fe(III) compounds, thought to be from the reaction of stainless steel vessels with the moist environment, have also been reported in these investigations (van Konynenburg, 1986). In situations where the aqueous phase is predominant (Glass et al., 1986) or where the aqueous phase is in contact with an inert gas such as argon (Kim and Oriani, 1987), formation of  $\text{H}_2\text{O}_2$  and  $\text{O}$  in the solution are more likely, although only indirect evidence for this has been provided. Unfortunately, the effect of radiolysis on environments within occluded regions such as crevices and cracks has not been studied systematically.

The foregoing discussion indicates that considerable uncertainty exists concerning the environment adjacent to the waste packages. Therefore, one of the early objectives of the IWPE was to explore the effects of key environmental factors, over a reasonably wide range, on localized corrosion.

In order to accomplish this objective at a reasonable level of effort, short-term electrochemical tests have to be used. Hence, a further objective of the IWPE program is to examine the utilization of the results of these short-term tests for long-term prediction.

## 4 LOCALIZED CORROSION OF Fe-Ni-Cr-Mo ALLOYS — EFFECT OF ENVIRONMENTAL FACTORS

### 4.1 EXPERIMENTAL APPROACH

These results have been reported in previous CNWRA reports (Cragolino and Sridhar, 1990b, 1991a, 1991b, 1991c, and 1992a; Sridhar et al., 1993b). Therefore, only the important conclusions from these studies are presented in this chapter. Additionally, the effect of surface Cr-depletion on the localized corrosion behavior is explored. Three types of solutions were used to study the effects of environmental factors:

- Simulated J-13 environments which contained various anionic species and a mixture of cationic species including  $\text{Na}^+$ ,  $\text{K}^+$ ,  $\text{Ca}^{2+}$ , and  $\text{Mg}^{2+}$ . Silica was not added to these solutions because of its slow solubility. These solutions will be referred to as SJ-13 water with appropriate modifiers related to the specific changes made (e.g., SJ-13 water + 300 ppm  $\text{Cl}^-$  refers to a simulated J-13 water whose total chloride concentration is 300 ppm).
- Factorial study environments which contained various anionic species, but where the cationic species were  $\text{Na}^+$  and  $\text{H}^+$ . The pH of these solutions was maintained at a relatively constant level by the addition of bicarbonate. These solutions will be referred to by their ionic concentrations (e.g., 1000 ppm  $\text{Cl}^-$  solution)
- Simulated crevice/pit solutions which contained various anionic concentrations and in which pH was altered by the addition of HCl. Again,  $\text{Na}^+$  was the only other cationic species. These solutions will be referred to by their ionic concentrations.

The preparation and analyses of these solutions are described in Appendix B. Further discussion of the chemical evolution of these environments during the tests can be found elsewhere (Pabalan and Murphy, 1991).

The cyclic, potentiodynamic polarization technique was used to study the localized corrosion behavior of these alloys. The test procedure is documented in CNWRA Technical Operating Procedure (TOP) 008 and is similar to that given in the ASTM Standard G-61. The test apparatus (Figure 4-1) consisted of a 5-port glass cell fitted with a water-cooled Allihn-type condenser and water trap to minimize air intrusion. Cylindrical specimens of 6.35 mm (0.25 in.) diameter, 19 mm to 48.64 mm (0.75 to 1.9 in.) length were used. These specimens were polished wet to a 600-grit finish on SiC paper. In most experiments, the specimens were fully immersed in the solution. In some experiments, they were partially immersed in the solution to avoid crevice corrosion in the gasket area where electrical connection is made to the specimens. As will be shown later, crevice corrosion is important in the low chloride solutions or at low temperatures which are marginal conditions for causing pitting. A long salt bridge-Luggin probe with a porous silica (vycor) tip was used so that the vycor tip was in the test solution and the other end was at room temperature. In experiments with dilute solutions such as the J-13 water, the electronic noise was high if a salt bridge with low chloride concentration (e.g., same concentration as the test solution) was used. This problem became especially acute for the EG&G Model 273 potentiostat which has a differential input. To avoid this problem, a more concentrated salt bridge solution, typically 0.5 M to saturated NaCl, was used. The liquid junction potential for the 0.5 M NaCl salt bridge solution

was 4.8 mV and was lower for the more concentrated solutions. The saturated calomel electrode (SCE) was used as the reference electrode in all the experiments. Platinum was used as a counter electrode in most of the experiments. In some cases, graphite was used. The solutions were continuously deaerated with high-purity argon. The corrosion potentials of the specimens and Pt were measured independently using a Keithley Model 614 electrometer. Polarization was performed using EG&G Models 273 and 173/276 potentiostats operated by Model 342C software. The resulting data were converted to ASCII files and stored as permanent records.

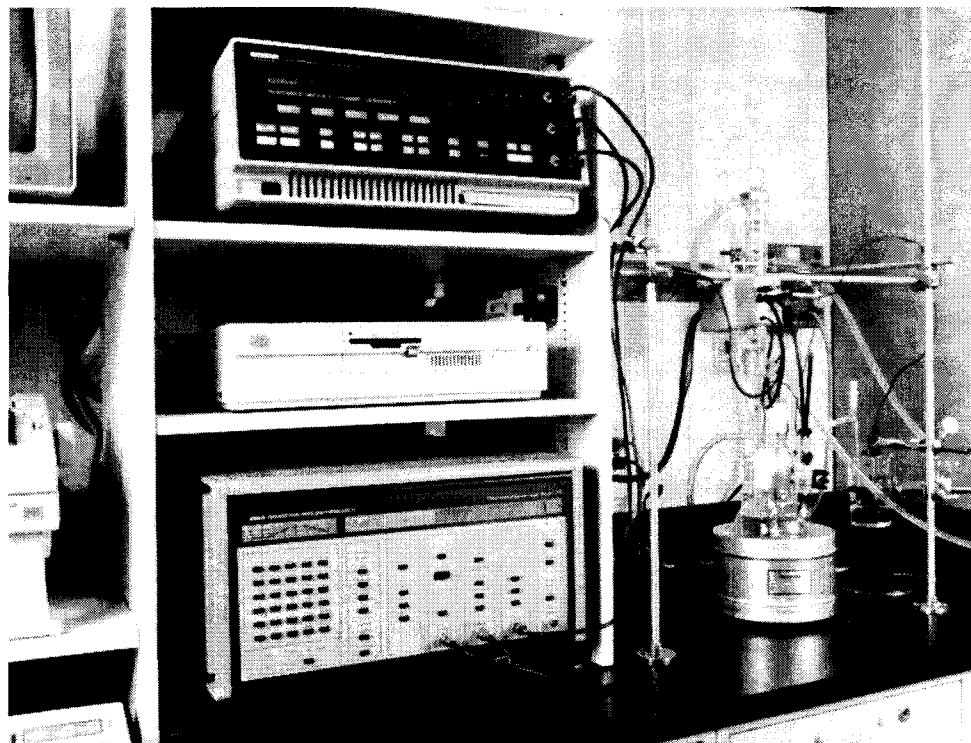


**Figure 4-1. Experimental apparatus used for cyclic polarization experiments showing the glass cell along with the condenser and trap. The Model 273 potentiostat and the computer for data acquisition are also shown.**

Post-test examination of the specimens was performed through a stereoscope at 70X magnification. Selected specimens were examined through a SEM and analyzed using EDX analysis.

## **4.2 EFFECT OF ENVIRONMENTAL FACTORS IN GROUNDWATER ON LOCALIZED CORROSION RESISTANCE**

### **4.2.1 Factorial Experiments**

A properly designed factorial experiment can reveal the effects of several variables and their interactions with a relatively modest expenditure of experimental effort. It is well known that several environmental factors, including temperature, can affect the localized corrosion behavior of a given alloy

(Szkłarska-Smialowska, 1986). However, a review of the literature (Cragolino and Sridhar, 1991e) indicated that few systematic studies of the localized corrosion behavior of stainless steels and Ni-base alloys existed in environments containing low concentrations of various anions such as those found in J-13 water. Beavers and Thompson (1988) were the first to use a fractional factorial matrix to study the effects of groundwater composition on localized corrosion behavior of candidate container materials. However, their design of the test matrix and the choice of measured parameters for analysis posed many disadvantages:

- Choice of a fractional factorial matrix meant that they could not investigate interactions between various environmental parameters.
- The assumption that the chosen factors were independent is not true for factors such as pH and bicarbonate concentration.
- The solubility of some species such as  $\text{SiO}_2$  is very low and time-dependent. Hence, analysis of results in terms of the effect of Si is questionable.
- The results were analyzed in terms of purely electrochemical parameters, although the authors acknowledged the lack of correlation between actual observation of localized corrosion and electrochemical parameters in some alloys.

The above mentioned limitations of the approach of Beavers and Thompson (1988) and Thompson et al. (1992) resulted in a low correlation coefficient. For example, the  $R^2$  value for the analysis of pitting potential ranged from 0.143 (for alloy 825) to 0.555 (for CDA-715). Hence, a further refinement of the factorial approach was attempted at the CNWRA. The approach was to use a full factorial design enabling an examination of interactions between all factors, limit the number of factors studied to those that have been found to be the most important in the literature, limit the study to the effect of anionic factors by using  $\text{Na}^+$  as the only cation, and use more realistic measures of localized corrosion.

The details of the factorial design have been elaborated elsewhere (Cragolino and Sridhar, 1991a) and will not be repeated here. More elaborate treatments of the subject of statistical experimental design can be found in Box et al. (1978) and Mason et al. (1989). For the factorial experiments performed over limited ranges of  $\text{Cl}^-$ ,  $\text{SO}_4^{2-}$ ,  $\text{NO}_3^-$ , and  $\text{F}^-$  concentrations and temperature, the relationship of localized corrosion to environmental factors have been derived using a LCI (Cragolino and Sridhar, 1990b, 1991f, 1992a). This LCI was devised specifically for alloys 825 and C-22, since the electrochemical behavior did not always correlate with visual observation of localized corrosion. This was especially true in low chloride environments where the alloy exhibited passivity up to potentials beyond the oxygen evolution regime. For types 304L and 316L stainless steels, there was a much better correlation between localized corrosion and electrochemical parameters. However, for consistency and for purposes of comparison, the LCI was modified to include the effects of lower pitting potential and the modified LCI was used for all alloys (Cragolino and Sridhar, 1991c). Since the original LCI is no longer used, the modified LCI will be referred to in this report as the LCI, defined as

$$LCI = \frac{(E_p - E_{rp}) \cdot 100}{E_p} \cdot \text{Visual Rating} \quad (4-1)$$

where,  $E_p$  is the pit initiation potential,  $E_{rp}$  is the repassivation potential, and visual rating is obtained by a combination of stereoscopic observation of pits at 70X and SEM-EDX analysis of corrosion products surrounding the pits (Cragolino and Sridhar, 1990b). Five broad classifications were created, and a rating number was assigned to each of these classifications. Details of the SEM examination were reported previously (Cragolino and Sridhar, 1991f). While these ratings have a certain element of subjectivity, it should be noted that a rating based only on the number of pits per unit area is insufficient to characterize the behavior, especially of alloy 825, since both the depth of pits and type of corrosion products associated with the pits varied. The most severe cases (Rating = 4) had not only deep pits but also crevice corrosion. There were no thick corrosion products deposited on the pits. Specimens of Rating = 3 also exhibited deep pits of a similar kind but did not show extensive crevice corrosion. The pits were found to have considerable undermining beneath the surface. SEM-EDX examination indicated that the corrosion products associated with these pits were rich in Cr and Mo. In some specimens, the pits were quite numerous but shallow and covered with a brown deposit. No crevice corrosion was observed in these specimens, which were given a rating of 2. SEM-EDX examination of these pits indicated that they were associated with corrosion products rich in Fe and low in Cr and Mo. Finally, in one specimen, the pits were found to be flat depressions surrounded by a brown corrosion product rich in Fe. This specimen was given a rating of 1 to distinguish it from the shallow but narrow pits of Rating 2. A rating of zero was assigned to specimens with no pitting or crevice corrosion as observed at 70X.

The results of the factorial experiments are tabulated in Appendix C (Tables C-2 through C-5). The results of the analysis of the full-factorial experiments using LCI as the measure of localized corrosion for type 316L stainless steel and alloy 825 are shown in Eqs. (4-2) and (4-3), respectively. The analysis considers the independent variables to be scaled on a -1 to +1 range, as shown in Eq. (4-4) where  $A$  is the actual value (in ppm or degrees C) of a given factor and  $X_A$  is the scaled value of the same factor. The factor effect is the contribution of any factor to LCI at its highest level (+1). The coefficients in Eqs. (4-2) and (4-3) are the factor effects divided by 2. The standard error and 95-percent confidence interval were calculated for each of the factor effects (Appendix C, Tables C-4 and C-5), and only those factors whose factor effects were greater than the 95-percent confidence interval are included in Eqs. (4-2) and (4-3).

$$(LCI)_{316L} = 364.12 + 320.2(X_{Cl}) \quad (4-2)$$

$$\begin{aligned} (LCI)_{825} = & 95.5 + 84.5(X_{Cl}) - 84.5(X_{NO_3}) - 87.0(X_{Cl} \cdot X_{NO_3}) \\ & - 10.2(X_F) + 9.4(X_T \cdot X_F) - 8.1(X_T \cdot X_{NO_3}) \\ & - 7.0(X_{Cl} \cdot X_T \cdot X_{NO_3}) \end{aligned} \quad (4-3)$$

$$X_A = \frac{2(A - A_{avg})}{(A_{max} - A_{min})} \quad (4-4)$$

Equation (4-2) indicates that, for type 316L stainless steel, the only factor of major importance is chloride, which promotes localized corrosion (positive coefficient). Nitrate and chloride-nitrate interaction have marginal impact on the LCI of type 316L, whereas all the other factors have no

significant effect. Temperature was not examined as a factor for this alloy. In contrast, for alloy 825, Eq. (4-3) indicates that chloride, fluoride, and nitrate are all significant; and the interactions of Cl-NO<sub>3</sub>, T-F, T-NO<sub>3</sub>, and Cl-T-NO<sub>3</sub> are also significant. The average value of LCI for type 316L stainless steel is higher than that of alloy 825, indicating that the latter is more resistant to localized corrosion. This is understandable because the Cr and Mo contents of alloy 825 are significantly higher than those of type 316L stainless steel. In contrast to the results of Thompson et al. (1992), the empirical Eqs. 4-2 and 4-3 exhibit R<sup>2</sup> values of 0.991 and 0.977, respectively, confirming that the choice of measured parameters and independent factors is crucial in factorial designs.

There are several limitations to the factorial experiments:

- The Eqs. 4-2 and 4-3 are valid only within the ranges of the factors studied. Thus, while nitrate did not have any effect on the LCI of type 316L stainless steel in the 10–1000 ppm range, it can inhibit localized corrosion at higher concentrations. Similarly, the lack of a temperature effect for alloy 825 in the factorial experiments is valid only within the 6–1000 ppm chloride concentration range. Temperature was found to decrease E<sub>p</sub> and E<sub>rp</sub> of alloy 825 in the 10,000 ppm chloride solution (Cragolino and Sridhar, 1991a).
- The linear relationship assumed is a reasonable approximation only within the range of concentrations studied. It is well known that E<sub>p</sub> decreases with the logarithm of chloride concentration (Szkłarska-Smiałowska, 1986).
- The parameter, LCI, while useful for the factorial analysis of the localized corrosion of alloy 825, is of limited value in long-term prediction.

The ranges of concentrations of various anionic species assumed in the factorial experiments stemmed from prior studies by Abraham et al. (1986) on evaporative concentration of simulated J-13 water. However, even higher concentrations of some species may be possible, as discussed in Chapter 3. Hence, further experiments, using cyclic polarization technique, were conducted to determine the effects of chloride, sulfate, nitrate, and pH. The effect of chloride concentration and pH will be discussed in Section 4.4.

#### 4.2.2 Additional Experiments on Environmental Effects

The results of additional experiments with alloy 825 and type 316L stainless steel are shown in Tables C-6 and C-7, respectively. The effects of various anions on localized corrosion are discussed in the following sections. The effects of chloride concentration and pH will be discussed separately due to their importance in simulated crevice solution experiments. The effect of temperature will be discussed in the context of the effect of chloride concentration.

**Effect of Nitrate and Nitrite.** The inhibiting effect of nitrate for alloy 825 and type 316L stainless steel is compared in Figure 4-2. A lower concentration of nitrate is required to inhibit localized corrosion of alloy 825 completely. This can be rationalized by the higher chromium content of the alloy in comparison to type 316L stainless steel. It can also be seen from Table C-6 that nitrite has a similar inhibiting capacity to nitrate for alloy 825. Both nitrate and nitrite are anticipated under conditions of radiolysis of air + steam mixtures (Van Konynenburg, 1986), although the concentrations that will be attained are uncertain. Furthermore, since radiolysis plays an important role in the early time period

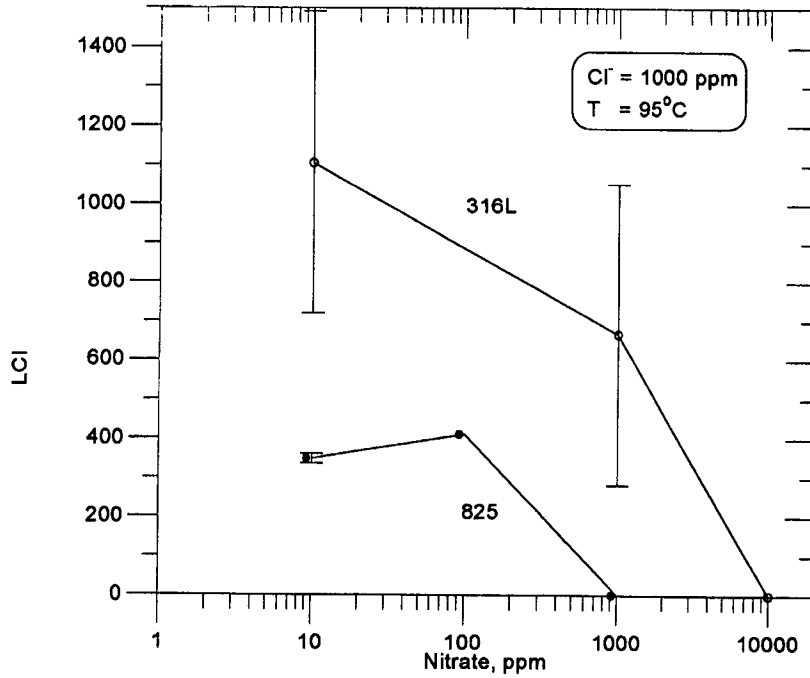


Figure 4-2. Effect of nitrate on localized corrosion in a 1000 ppm Cl<sup>-</sup> solution at 95°C

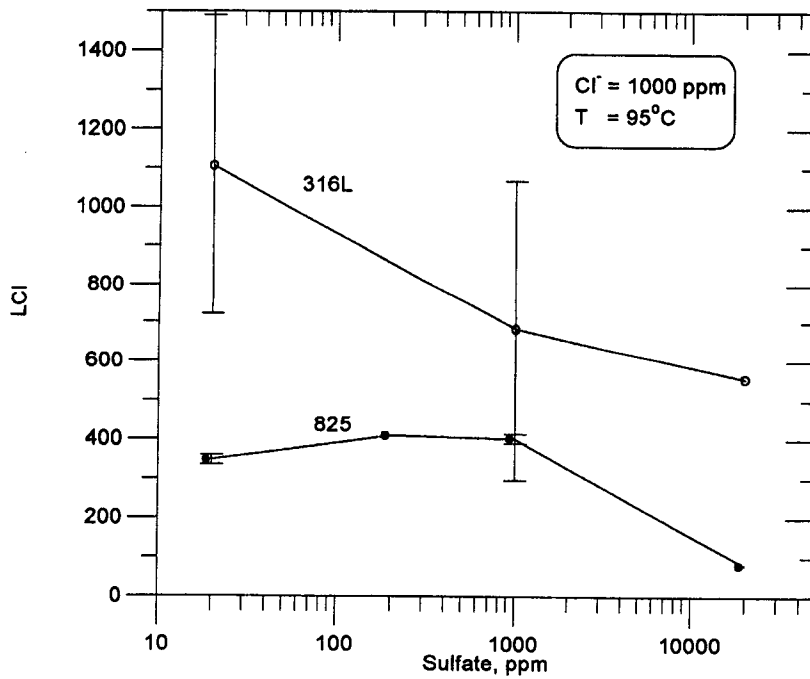


Figure 4-3. Effect of sulfate on localized corrosion in a 1000 ppm Cl<sup>-</sup> solution at 95°C

when the environment is anticipated to be dry and the proposed double-wall container may lessen the impact of radiolysis, the effects of nitrate and nitrate may not be significant for performance prediction.

**Effect of Sulfate.** While sulfate inhibits localized corrosion of alloy 825 more efficiently than of type 316L stainless steel (Figure 4-3), it is not as effective an inhibitor as nitrate. It is interesting to note that sulfate elevates the pit initiation potential, especially for type 316L stainless steel, but does not affect the repassivation potential significantly. The effect of sulfate on pit initiation potential of type 316L stainless steel is consistent with the literature on a variety of stainless steels (Rosenfeld and Danilov, 1967; Leckie and Uhlig, 1966; Bogaerts and Van Haute, 1985). From the present data and the literature, it appears that the anticipated concentrations of sulfate and sulfate to chloride ratio in the repository environment are not sufficient to affect localized corrosion of these alloys significantly.

**Mechanisms of Inhibition by Nitrate and Sulfate.** Nitrate and sulfate are believed to inhibit localized corrosion by competitive adsorption and displacement of chloride ions on the passive film (Leckie and Uhlig, 1966; Rosenfeld and Danilov, 1967; Brookes and Graham, 1989), although the fundamental mechanism for pitting was addressed differently by these investigators. An alternative mechanism for the inhibitive action of sulfate was proposed by Galvele (1976), who assumed that pit initiation occurs by chemical changes in pit embryos (nuclei) that are present prior to initiation of the macroscopic pits and that local accumulation of sulfate in pit nuclei occurs in preference to chloride by competitive electromigration. The fundamental mechanism of the inhibitive action of sulfate was not explained. Galvele (1981) explained the inhibitive effect of nitrate by suggesting that nitrate reduction to nitrogen occurs in the pit nuclei resulting in the consumption of  $H^+$ , which in turn results in a lesser tendency for the local environment to depassivate the alloy. It is interesting to note that the inhibiting effect of nitrate depends on when it is added. This is shown in Table C-6, where in one experiment nitrate was added before significant pitting occurred ( $592 \text{ mV}_{SCE}$ ) and inhibited subsequent localized corrosion to a large extent. On the other hand, when nitrate was added upon reversing the scan ( $979 \text{ mV}_{SCE}$ ), no inhibition was noted, possibly because considerable chloride accumulation had already occurred in the pits.

**Effect of Bicarbonate.** Bicarbonate additions beyond 85 ppm decreased the localized corrosion tendency of type 316L stainless steel, as shown in Figure 4-4. In contrast, bicarbonate additions resulted in a slight increase in the localized corrosion tendency of alloy 825. The inhibiting effect of bicarbonate for type 316L stainless steel is consistent with literature findings (Bogaerts and Van Haute, 1985; Jallerat et al., 1984). For example, Jallerat et al. (1984) showed that the concentration of bicarbonate required to inhibit localized corrosion in 316L stainless steel is related to chloride concentration by

$$\text{Log}(Cl^-) = 0.23 + 2.02 \text{ Log} (HCO_3^-) \quad (4-5)$$

In this relationship, for a chloride concentration of 1000 ppm (0.028 M), 8000 ppm bicarbonate is required for complete inhibition. While the present results are consistent with literature, some differences exist. Bogaerts and Van Haute (1985) did not perform cyclic polarization tests and relied only on increase in pit initiation potential as a measure of inhibition. Jallerat et al. (1984) performed cyclic polarization experiments, but did not report repassivation potentials or visual observations. Hence, in neither of these cases can true pit inhibition (complete lack of pitting) be established. Nevertheless, from these studies, it appears that bicarbonate, within the ranges of concentrations assumed to occur in the repository environment, does not play a significant role in localized corrosion.

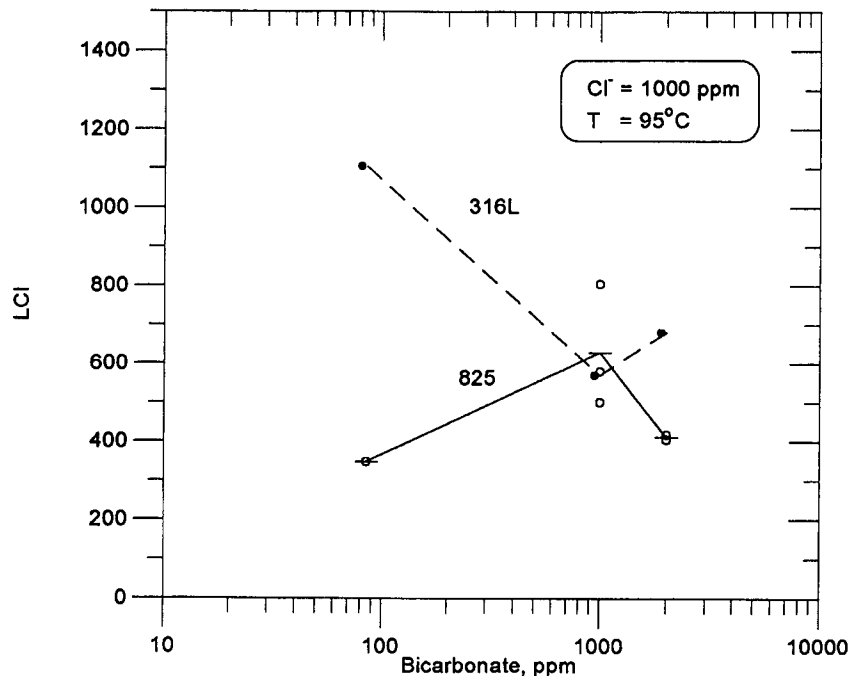


**Figure 4-4. Effect of bicarbonate on localized corrosion in a 1000 ppm Cl solution at 95°C.**

**Effect of Silicon.** The natural J-13 water has Si as one of the major components. The Si has, in the past formulations of simulated J-13 water, been added as  $\text{SiO}_2 \cdot n\text{H}_2\text{O}$ . However, because of its low solubility, unknown water of hydration, and slow dissolution rate, addition of silicic acid results in time-varying concentration of Si in the solution (Pabalan, 1989). Because of this, Si was excluded from the factorial experiments. However, the effect of dissolved Si on localized corrosion was studied subsequently by adding sodium metasilicate to simulated J-13 solutions of different chloride concentrations. The simulated J-13 solutions were prepared as described in Appendix B. Two chloride concentrations were examined: 6 ppm and 300 ppm. To each of these solutions, 0.0232 g/l of sodium metasilicate was added. Duplicate, cyclic polarization tests were conducted on alloy 825. The results are shown in Table C-6.

It can be seen from Table C-6 that Si, added as metasilicate, does not have a significant effect on localized corrosion of alloy 825 in simulated J-13 well water containing 6 and 300 ppm chloride.

**Effect of  $\text{Mg}^{2+}$ .** Since the natural J-13 water has significant concentrations of Mg and this cation has been found by Thompson et al. (1992) to be one of the important species promoting localized corrosion, its effect was studied by adding  $\text{MgCl}_2 \cdot 6\text{H}_2\text{O}$  instead of NaCl (0.347 g/l Mg) to a 1000 ppm Cl solution. The results are shown in Table C-6.

It can be seen that the addition of 348 ppm  $\text{Mg}^{2+}$  lowered the final pH due to hydrolysis of  $\text{Mg}^{2+}$ . Addition of  $\text{MgCl}_2$  lowered the pitting potential slightly (20–80 mV) and the repassivation potential by a greater extent (86–157 mV). This is in contrast with the results of Thompson et al. (1992)

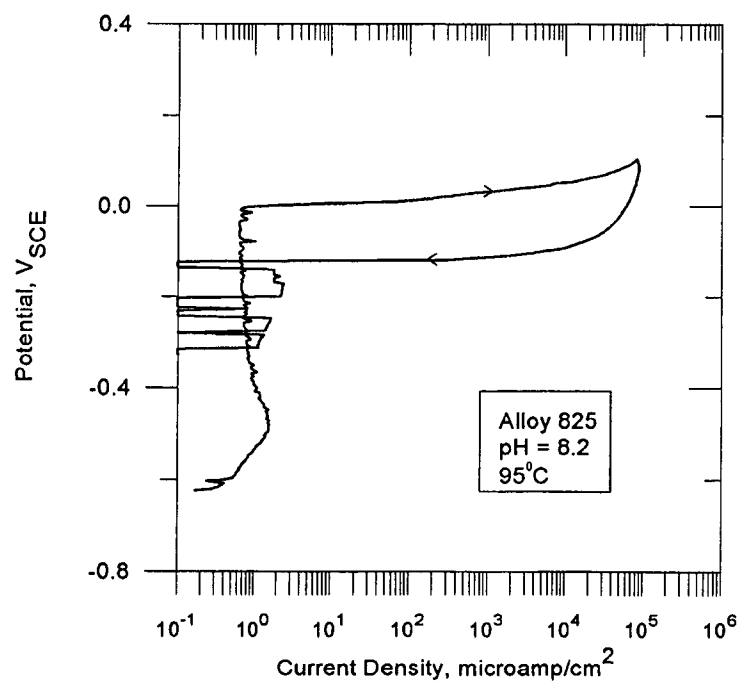
who found that addition of 20 ppm  $Mg^{2+}$  resulted in a decrease of both pitting and repassivation potentials by about 175 mV. Indeed, according to their analysis, Mg is the most dominant ionic species affecting localized corrosion of alloy 825 since its coefficient is higher than that of any other ionic species including chloride.

### 4.3 ELECTROCHEMICAL RESPONSE TO SIMULATED CREVICE SOLUTIONS

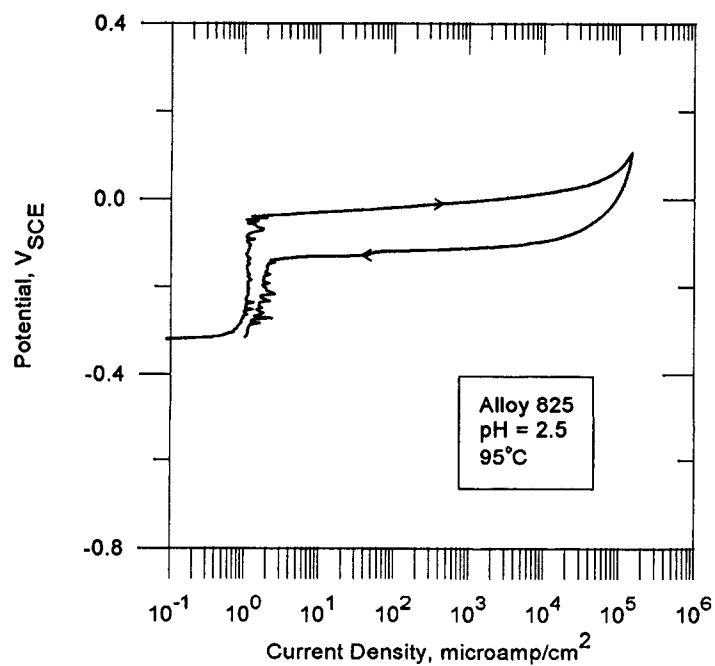
It is, by now, well established that solutions inside active pits or crevices of a variety of alloys are more acidic and high in anionic concentration than the bulk solution (Turnbull, 1983). There have also been many investigations of the electrochemical response of various alloys in simulated crevice/pit solutions (Tester and Isaacs, 1975; Crolet et al., 1976; Oldfield and Sutton, 1978b; Rosenfeld et al. 1978; Okayama et al., 1987b; Tsujikawa et al., 1987; Batista et al., 1988; Lott and Alkire, 1989; Hakkarainen, 1990). However, most of these investigators have examined the electrochemical response using potentiodynamic, galvanostatic, and potentiostatic techniques, but not cyclic polarization tests. Using cyclic polarization tests, the repassivation behavior in simulated crevice solutions can be obtained. Additionally, the lack of hysteresis is a good indicator of true depassivation.

For the tests in simulated crevice solutions, chloride concentrations ranging from 0.5 to 4 M were considered based on the predictions of various crevice-corrosion models (e.g., Walton and Kalandros, 1992) and experimental measurements (e.g., Luo et al., 1992). The effect of sulfate was studied by varying the sulfate and chloride concentrations such that the total ionic strength was approximately the same. All salts were added as sodium salts. The near-neutral solutions contained bicarbonate to an initial concentration of 85 ppm. The pH of the solutions was adjusted by using HCl, and, hence, the resultant concentration of chloride was higher depending on the pH. For the 4 M  $Cl^-$  solution with a pH of 0, the resulting concentration of  $Cl^-$  was 4.2 M. However, for the 0.5 M  $Cl^-$  solution, the addition of HCl to make the pH 0 resulted in a final  $Cl^-$  concentration of approximately 1.1 M. Therefore, future studies on the effect of pH at the low chloride concentrations should use alternate techniques, such as the ion-exchange method used by Okayama et al. (1987b).

Cyclic polarization experiments (ASTM G-61 standard practice) were conducted on cylindrical specimens (6.35 mm diameter  $\times$  19.1 mm long) on separate specimens in solutions of differing pH values. The specimens were wet-ground to 600-grit finish, degreased in acetone, rinsed and dried before each test. They were partially immersed in the solution during the test to avoid crevice corrosion in the gasket area. All solutions were purged with argon during the tests to simulate the reducing condition supposed to prevail in crevices. As explained in Appendix B, the final pH was attained quite quickly because of gas purging and heating and, hence, was assumed to be the pH of the solution in reporting the data. Unlike the case of the factorial experiments, the near-neutral solutions did not evolve in pH. The measured pH concurred reasonably well with the pH calculated using EQ/3 code. For the solutions which were acidified with HCl, the final and initial pH were not significantly different and the final pH is used in reporting the results. The exception to this are the tests performed at pH 3. In these cases, the final pH after polarization test increased to 8. Control tests in solutions with the same starting pH, but without the specimens or with unpolarized specimens, did not result in any change in pH. The main reason for the large increase in pH was found to be due to the overrun of the backward scan into the cathodic regime resulting in significant hydrogen evolution. In these cases, the starting pH was used for reporting the data. The results of these tests are shown in Tables C-8 and C-9 (Appendix C). Two examples of series of cyclic polarization curves for alloy 825 and type 304L stainless steel are shown in Figures 4-5 and 4-6, respectively.

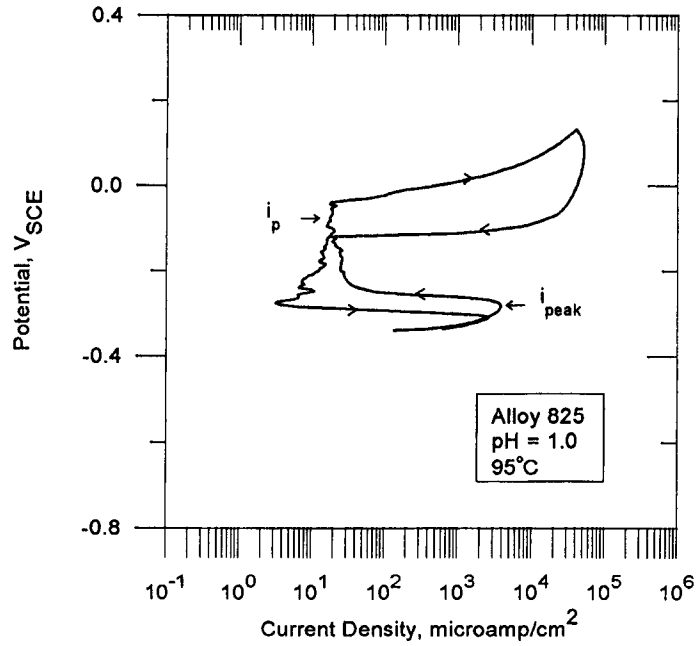


(a)

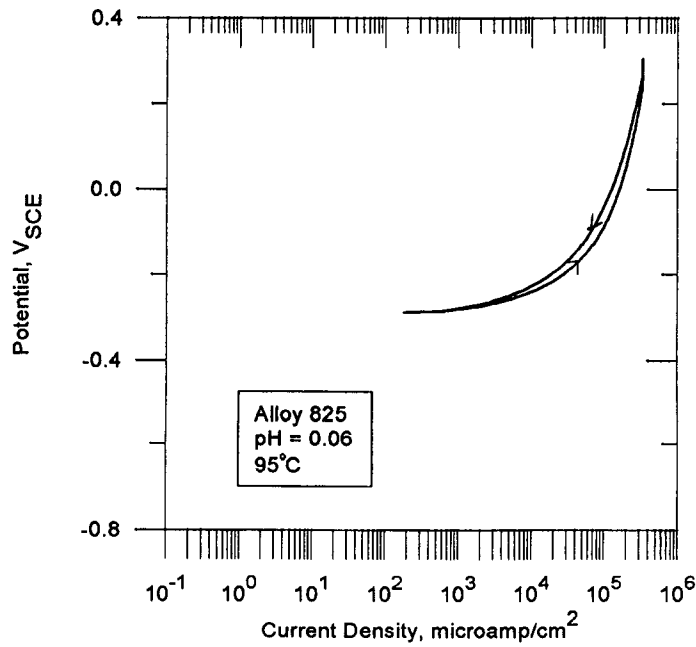


(b)

Figure 4-5. Cyclic polarization curves for alloy 825 in simulated crevice solutions at various pH values (measured at room temperature). Scan rate: 0.167 mV/sec. Solutions were deaerated with argon. Specimens were polished to 600-grit and partially immersed.

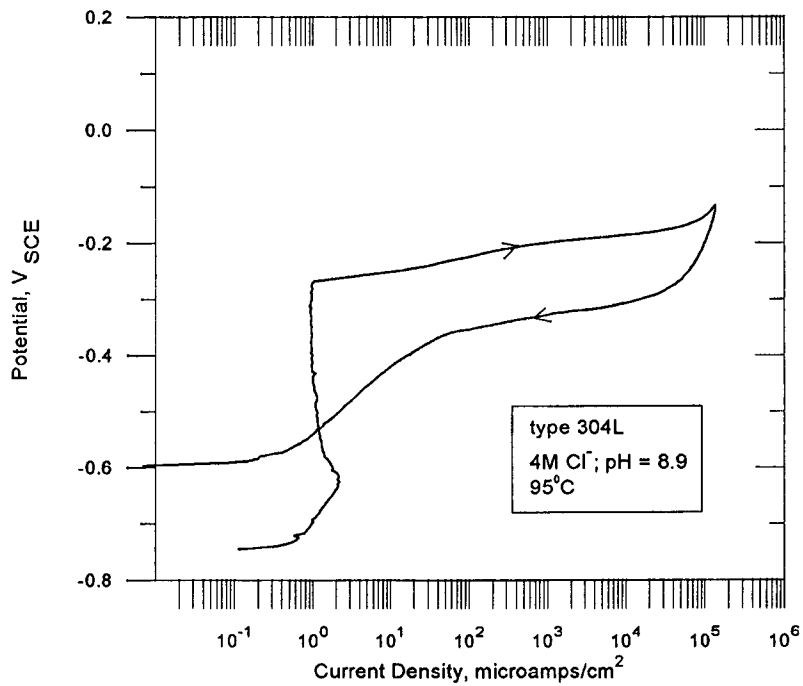


(c)

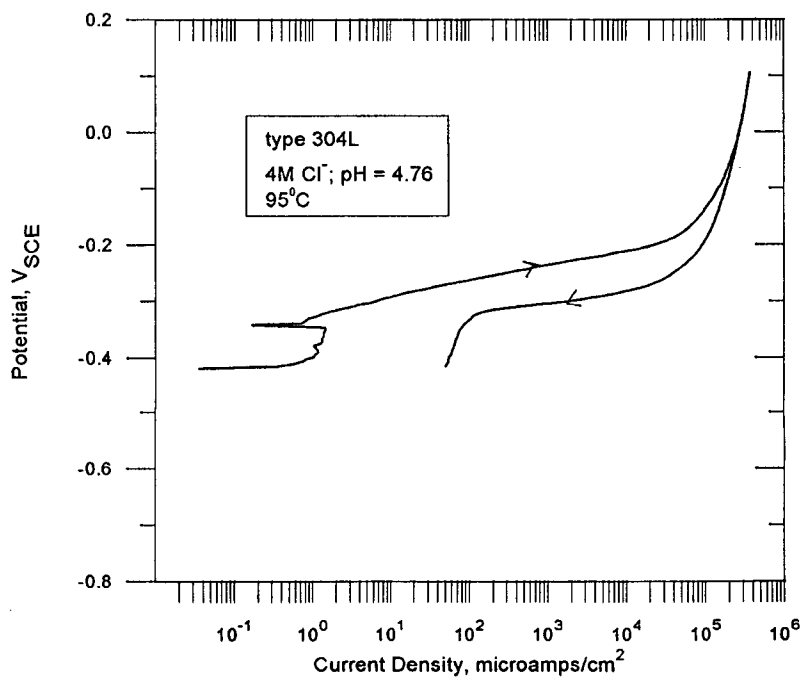


(d)

Figure 4-5. Cyclic polarization curves for alloy 825 in simulated crevice solutions at various pH values (measured at room temperature). Scan rate: 0.167 mV/sec. Solutions were deaerated with argon. Specimens were polished to 600-grit and partially immersed. (cont'd)

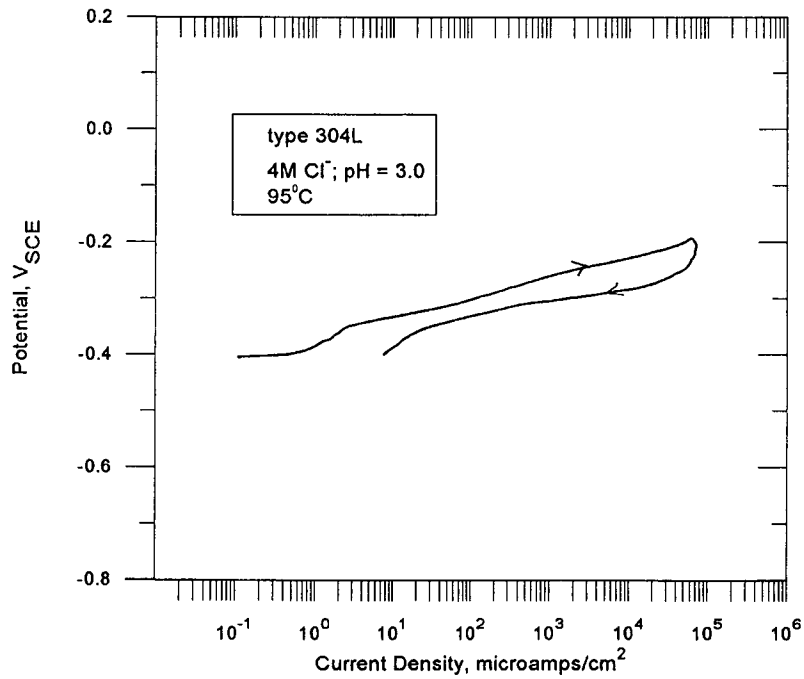


(a)

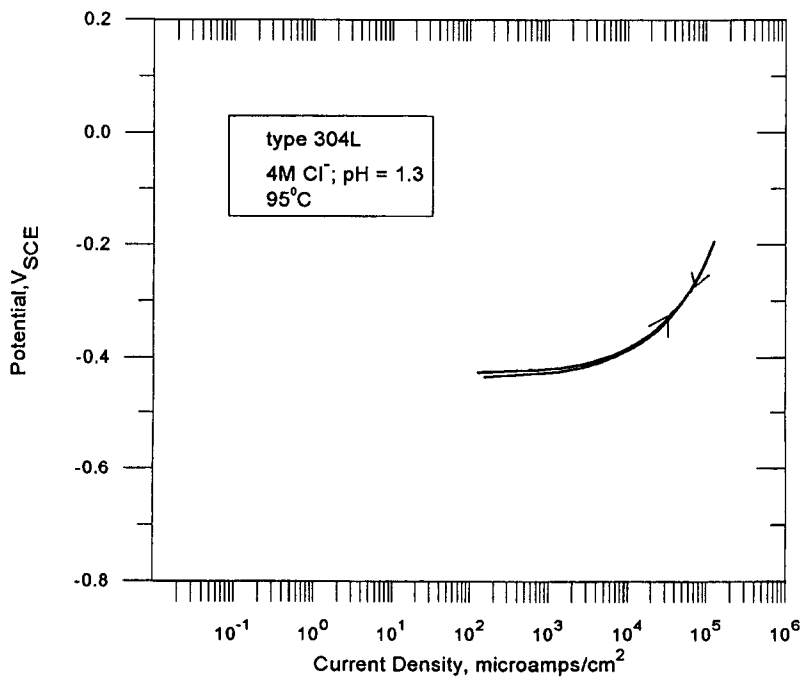


(b)

Figure 4-6. Cyclic polarization curves for type 304L stainless steel in simulated crevice solutions at various pH values (measured at room temperature). Scan rate: 0.167 mV/sec. Solutions were deaerated with argon. Specimens were polished to 600-grit and partially immersed.



(c)



(d)

Figure 4-6. Cyclic polarization curves for type 304L stainless steel in simulated crevice solutions at various pH values (measured at room temperature). Scan rate: 0.167 mV/sec. Solutions were deaerated with argon. Specimens were polished to 600-grit and partially immersed. (cont'd)

There was no crevice corrosion observed on any of these specimens because they were partially immersed in the solutions. As can be seen from Tables C-8 and C-9, the specimens exhibited passivity in solutions with pH below a certain value (Figures 4-5a through 4-5c, and 4-6a through 4-6c). In this regime of pH, ranging typically from 8 to 1, depending on the chloride concentration, the specimens pitted at potentials above a critical potential and the cyclic polarization curves exhibited significant hysteresis. Below a certain pH, which depended upon the alloy and to a lesser extent temperature, the alloys exhibited essentially an active behavior (Figures 4-5d and 4-6d). The pH at which a completely active behavior was observed is termed the depassivation pH,  $pH_D$ . Since the experiments were conducted at relatively large intervals of pH, no attempt is made to measure the  $pH_D$  exactly. The range of  $pH_D$  values is summarized in Table 4-1.

**Table 4-1. Depassivation pH of three alloys under various simulated crevice solutions and temperatures measured by cyclic polarization technique**

Alloy	Temperature °C	$pH_D$		
		4 M Chloride	0.5 M Chloride	3 M Chloride + 0.25 M Sulfate
Alloy 825	30	$-0.4 < pH < 0$	—	—
	95	$0.1 < pH < 1$	$0.09 < pH < 1$	$0.03 < pH < 1.1$
Type 316L Stainless Steel	30	—	—	—
	95	$pH < 1.10$	—	—
Type 304L Stainless Steel	30	$0.03 < pH < 1.1$	$0.11 < pH < 1.05$	—
	95	$1.3 < pH < 3$	$0.11 < pH < 1.09$	—

It must be emphasized that the pH values reported in Table 4-1 contain two sources of error: (i) they do not consider the liquid junction potentials arising between the reference electrode solution and the test solution which can be significant for concentrated solutions (Marcus, 1989), and (ii) they do not consider changes to the activity coefficient of  $Cl^-$  in highly concentrated solutions (Knauss et al., 1990). A third possible source of error, that of the measured pH being higher than the actual pH for a glass electrode in highly acidic solutions, is not significant over the range of pH used in these experiments (Bates, 1964).

The  $pH_D$  has been assumed by many investigators to be relatively independent of chloride concentration and temperature (e.g., Okayama et al. 1987). As shown in Table 4-1, the  $pH_D$  of alloy 825 is not dependent on the chloride and sulfate concentrations within the scatter in the data. However,  $pH_D$  decreases with a decrease in temperature. For type 304L stainless steel, the  $pH_D$  is dependent both on temperature and chloride concentration. The  $pH_D$  values for types 304L and 316L stainless steel in 4 M  $Cl^-$ , shown in Table 4-1, are similar to values reported by Okayama et al. (1987b), and slightly lower than those reported by Oldfield and Sutton (1978b). The results differ from the literature in the effect of temperature and chloride concentration on  $pH_D$ , possibly because of differences in test technique. For example, Okayama et al. (1987b) used open-circuit conditions to determine the pH at

which the corrosion potential fell sharply to active values. It must be assumed, from their data, that the deaeration of the solution was insufficient, since rather high corrosion potentials were observed at pH values above " $pH_D$ " while low corrosion potentials were observed at pH values below " $pH_D$ ". From Figure 4-5c, it can be seen that the high peak current density prior to complete depassivation may lead to a lowering of corrosion potential or an unstable corrosion potential, depending on the redox condition of the test. Conducting a cyclic polarization test, while more time-consuming, is a more reliable technique for determining depassivation. Oldfield and Sutton (1978b) conducted potentiodynamic tests (monotonic instead of cyclic) to determine depassivation pH. Below a pH of about 3, an anodic peak in the polarization curve prior to passivation was observed. By assuming a criterion of critical anodic peak for depassivation of  $10 \mu A/cm^2$ , they calculated the depassivation pH of type 316 stainless steel to be 1.65. The criterion of a critical anodic peak current density for determining depassivation pH suggests that alloy 825 has depassivated between pH values of 2.5 and 1, as shown in Figures 4-5b and 4-5c. However, the cyclic polarization tests show that pitting is still observed at pH 1 and completely active corrosion is not observed until the pH drops to about zero. Hence, it is not surprising that the depassivation pH arrived at by Oldfield and Sutton (1978b) for type 316 stainless steel is slightly higher than that reported in Table 4-1. Additionally, type 304L stainless steel does not exhibit an active peak at any pH value at  $95^\circ C$ , as shown in Figures 4-6a through 4-6c. In contrast, the hystereses in the cyclic polarization curves are more clear indicators of depassivation. As shown in Table C-9, more pronounced active-passive peaks are observed for type 304L stainless steel in lower chloride concentrations or lower temperatures. Similar behavior is also seen for type 316L stainless steel (Table C-10).

The approach for long-term prediction of crevice corrosion initiation is to use the TWITCH code (Walton and Kalandros, 1992) which requires the input criterion for depassivation,  $pH_D$ , obtained from short-term experiments. Generally, crevice corrosion is assumed to initiate when the pH of the solution inside the crevice attains a value corresponding to  $pH_D$  of the alloy (Oldfield and Sutton, 1978a; Sharland, 1992; Watson and Postlethwaite, 1990; Sridhar et al., 1991). The assumption that crevice corrosion initiates only after complete depassivation occurs is questionable. Other events that can trigger crevice corrosion prior to complete depassivation include: (i) pitting inside crevices, (ii) the increase in active peak current density (Figure 4-5c) resulting in active dissolution, especially if potential drop in the crevice is such that the potential moves from the passive region of the polarization curve to the active peak (Pickering, 1990), (iii) the increase in passive current density accelerating dissolution inside crevices, and, hence, the rate of change of solution chemistry, and (iv) the dissolution of MnS inclusions resulting in an acidic solution containing sulfur species that lead to destabilization of passive film (Lott and Alkire, 1989).

#### 4.4 EFFECTS OF CHLORIDE AND pH ON LOCALIZED CORROSION

Chloride and pH, along with temperature, are treated separately from other environmental factors because of their importance to localized corrosion processes. The results from all the cyclic polarization experiments are summarized in Figures 4-7 and 4-8. The corrosion potential in reducing environments, which is the condition prevailing in crevices or pits, is relatively independent of  $Cl^-$ , but increases with a decrease in pH (Figure 4-7). The corrosion potential under these conditions is determined by the combination of anodic dissolution and hydrogen evolution reaction. The addition of oxidizing agents such as oxygen and hydrogen peroxide increases the corrosion potential. In a separate set of experiments, open-circuit potentials were measured on alloy 825 and Pt immersed in simulated J-13 water containing 6 ppm and 1000 ppm chloride at  $95^\circ C$ . The purpose of these tests was to determine the effect of redox species such as of oxygen present in the natural environment and  $H_2O_2$  created as a

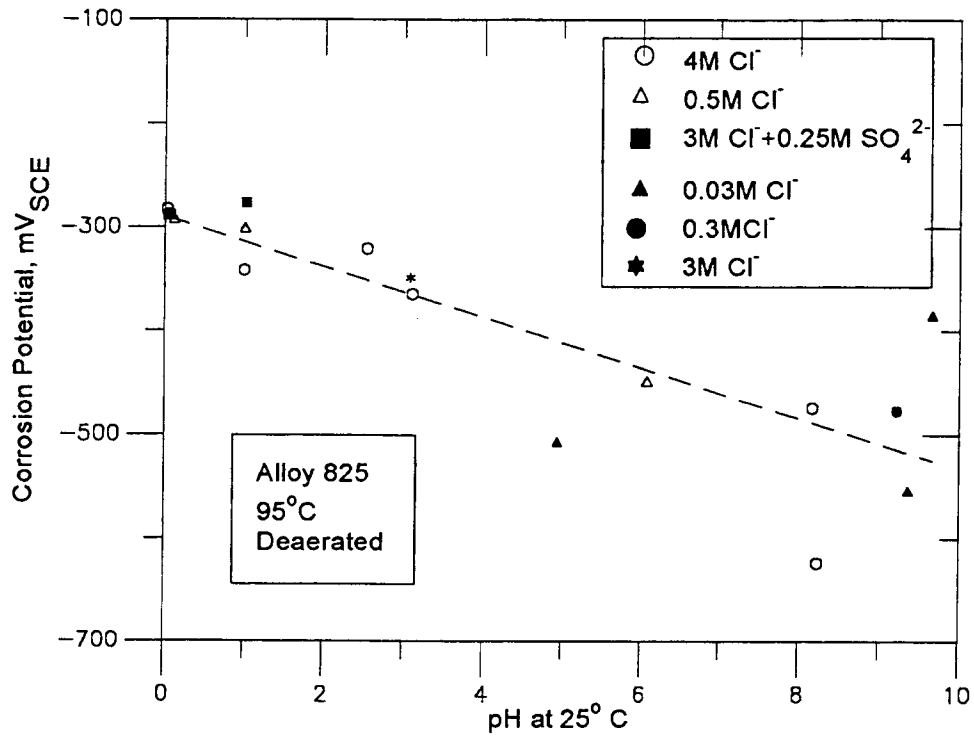


Figure 4-7. Effects of pH and Cl<sup>-</sup> on corrosion potential of alloy 825 in reducing environments. Temperature: 95°C.

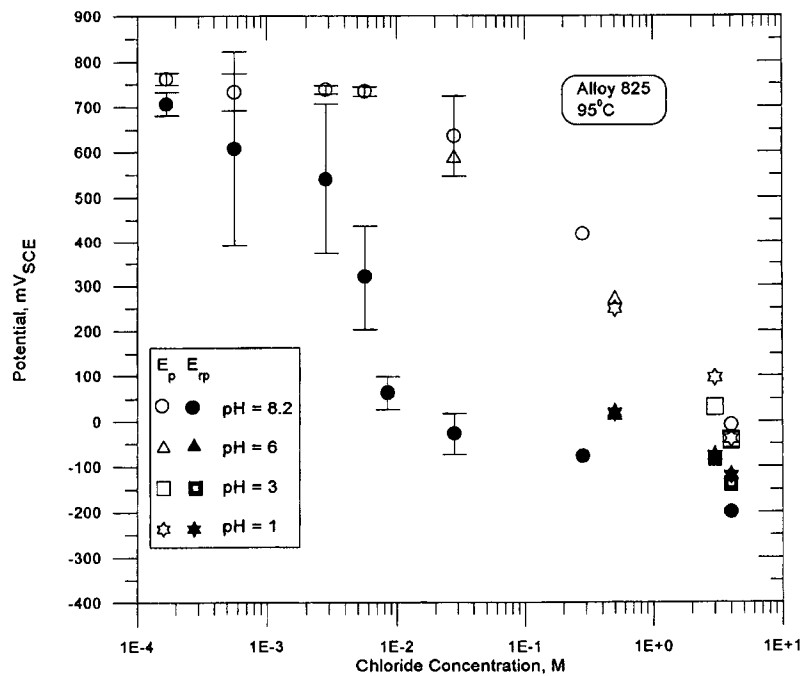


Figure 4-8. Effect of pH and Cl<sup>-</sup> on pitting and repassivation potentials of alloy 825

result of radiolysis. The solutions were aerated using bottled air.  $H_2O_2$  was added such that the concentration in the solution increased in steps of 0.1 mM.

The summary of results are shown in Table 4-2. The open-circuit potentials of both alloy 825 and Pt in aerated solution containing 1000 ppm chloride attained steady values of -280 mV and +140 mV, respectively. Although the value observed for Pt is well below the equilibrium value, the potential measured on alloy 825 is even more irreversible. These open-circuit measurements are governed not only by charge-transfer conditions but also by transport limiting processes. Hence, the measurements deviate considerably from the thermodynamically expected values. In the case of deaerated environments, the potentials of both alloy 825 and Pt increased with the addition of peroxide, although the increase was more pronounced for alloy 825 than Pt (Table 4-2). The value of the potential for alloy 825 and Pt in the 0.5 mM  $H_2O_2$  solution is almost independent of the presence of dissolved oxygen, indicating that the reduction of  $H_2O_2$  is the controlling cathodic reduction on both metals.

**Table 4-2. Effect of aeration of  $H_2O_2$  addition on open-circuit potentials (mV versus SCE) of alloy 825 and Pt simulated J-13 solutions at 95°C**

Condition	Alloy 825		Platinum	
	6 ppm Cl	1000 ppm Cl	6 ppm Cl	1000 ppm Cl
Deaerated, Argon	-545	-525	-478	-448
Argon + 0.5 mM $H_2O_2$	+118	+108	+73	+59
Aerated	-298	-280	+170	+140
Aerated + 0.5 mM $H_2O_2$	+132	+106	+79	+53

The effects of  $Cl^-$  and pH on pitting and repassivation potentials measured by cyclic polarization experiments are shown in Figure 4-8.

It is generally accepted that the pitting potential is relatively unaffected by pH for a wide variety of alloys, but it decreases with an increase in chloride concentration and temperature (Szklańska-Smiałowska, 1986). The findings reported here are in agreement. It can also be seen that the repassivation potential measured by the cyclic polarization technique is relatively less dependent on chloride concentration than the pitting potential. Again, this is in general agreement with the literature (Rosenfeld et al., 1978; Azzeri et al., 1982). In Chapter 5, the effect of test technique on these environmental effects will be discussed in greater detail.

#### 4.5 THE EFFECTS OF SURFACE CHROMIUM-DEPLETION

Surface Cr-depletion, its presence in some alloys and its causes were discussed in Section 3.2. The effect of Cr-depletion in the near-surface region of alloy 825 on the localized corrosion behavior is discussed in this section. In order to examine the effects of Cr-depletion, a specimen with two surfaces

in the as-mill-finished condition was machined as shown in Figure 4-9. The other surfaces were wet-ground to 600-grit finish before testing. In the 6 ppm chloride solution, simulating J-13 water, the cyclic polarization behavior of the specimen with Cr-depleted surfaces is compared to the cyclic polarization curve generated previously on a fully machined and polished specimen without any Cr-depletion (Figure 4-10). It can be seen that the Cr-depleted surface exhibited higher passive current density, lower breakdown potential, greater hysteresis, and pitting upon visual examination at 70X after the test. In a 1000 ppm chloride solution, considerable general corrosion was observed on the Cr-depleted surfaces. This is indicated in Figure 4-11, where the Cr-depleted specimen showed a very low break down potential compared to a machined specimen, but without any significant hysteresis.

Three possible outcomes for the effects of Cr-depletion can be postulated:

- The Cr-depleted layer, which is less corrosion resistant as seen in Figure 4-11, can be corroded away relatively rapidly and uniformly by the environment exposing a fully corrosion resistant substrate. In this case, the Cr-depletion does not need to be considered for long-term prediction.
- The Cr-depleted layer is progressively corroded by the environment until a layer with a Cr content sufficiently high to resist uniform dissolution, but not resistant enough to initiation of pitting, is exposed. In this case, Cr-depleted material will initiate pitting which can then serve to create a micro-environment aggressive enough to continue pit growth even through undepleted substrate.
- The Cr-depleted layer is inside a crevice where the high general dissolution can induce faster micro-chemical changes and, hence, a faster crevice corrosion initiation. It must be noted that many of the crevice corrosion initiation models assume a potential-independent passive current density of relatively low magnitude which will be violated by the Cr-depleted layer.

The second postulated outcome can be verified by conducting repeated cyclic polarization tests on the same specimen until the Cr-depleted layer is corroded away. The pit initiation potential can then be measured in successive polarization cycles. This is shown in Figure 4-12 for specimens exposed to a 1000 ppm  $\text{Cl}^-$  solution. In the first cycle, essentially uniform corrosion is observed. In the next cycle, some pitting is observed with a relatively low pit initiation potential, although no significant hysteresis is observed in the polarization curve. A greater hysteresis is observed in the following cycle with a further increase in pitting potential. The polished specimen, without surface Cr-depletion, is also shown for comparison. It can also be seen that the repassivation potential for the third cycle is close to that of the polished specimen, indicating that it is relatively less sensitive to Cr-depletion than the pitting potential. The repeated cyclic polarization curves suggest that under certain conditions of repository environment, the container may initially corrode uniformly and then may begin pitting at lower potentials than anticipated by laboratory tests on polished specimens. For long-term prediction, the question is whether the repassivation potential measured on nondepleted specimens is conservative enough to include Cr-depleted specimens. Additionally, the effect of dry exposure of Cr-depleted surfaces on subsequent wet exposure is being examined in ongoing experiments.

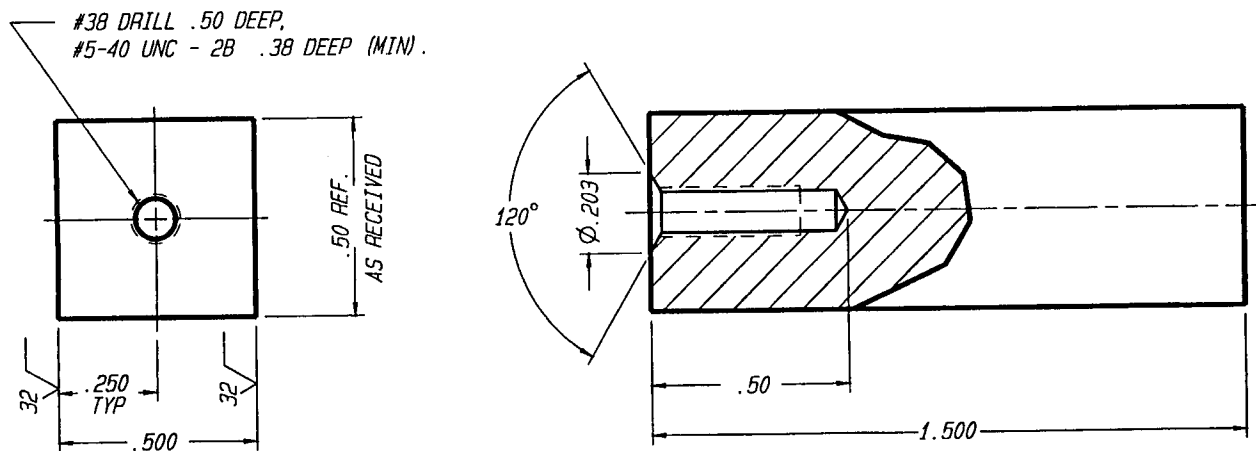


Figure 4-9. Specimen used to study the effect of surface Cr-depletion in alloy 825 using cyclic polarization test. The specimen is connected to the electrochemical equipment in the same manner as the cylindrical specimens in ASTM G-61.

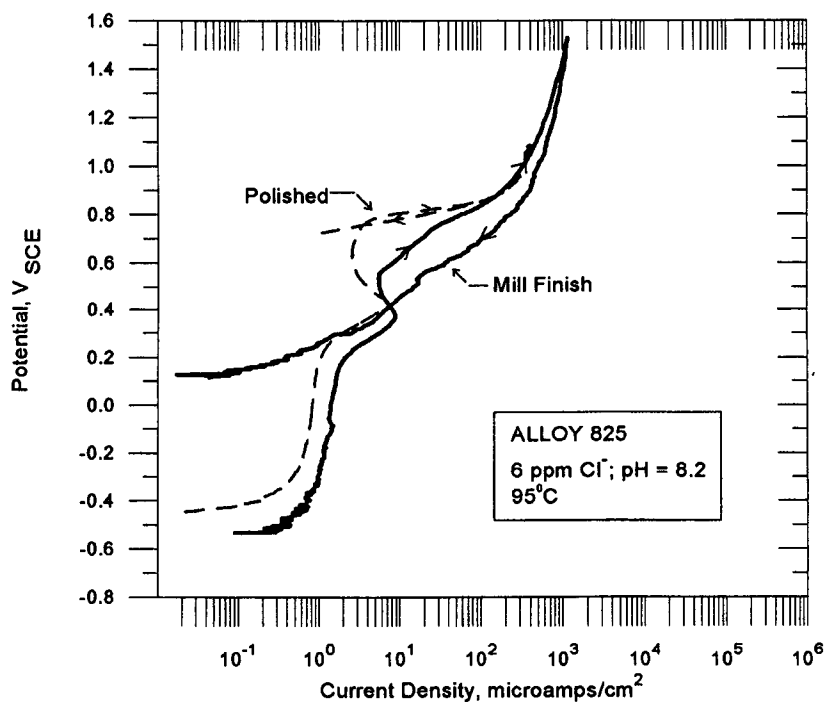


Figure 4-10. Cyclic polarization curves of Cr-depleted and polished surfaces of alloy 825 in a 6 ppm  $\text{Cl}^-$  solution at 95°C. Scan rate: 0.167 mV/sec.

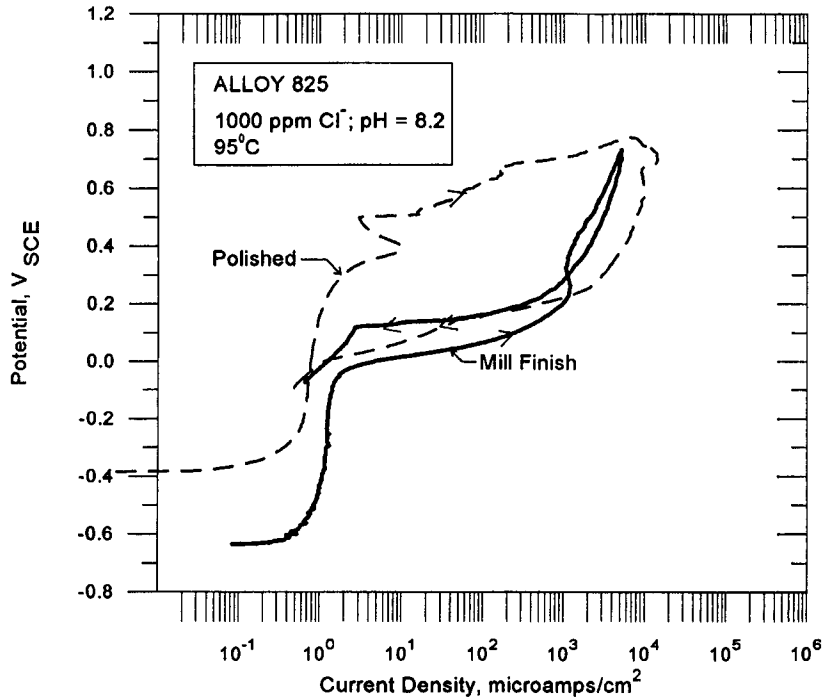


Figure 4-11. Cyclic polarization curves of Cr-depleted and polished surfaces of alloy 825 in a 1000 ppm  $\text{Cl}^-$  solution at 95°C. Scan rate: 0.167 mV/sec.

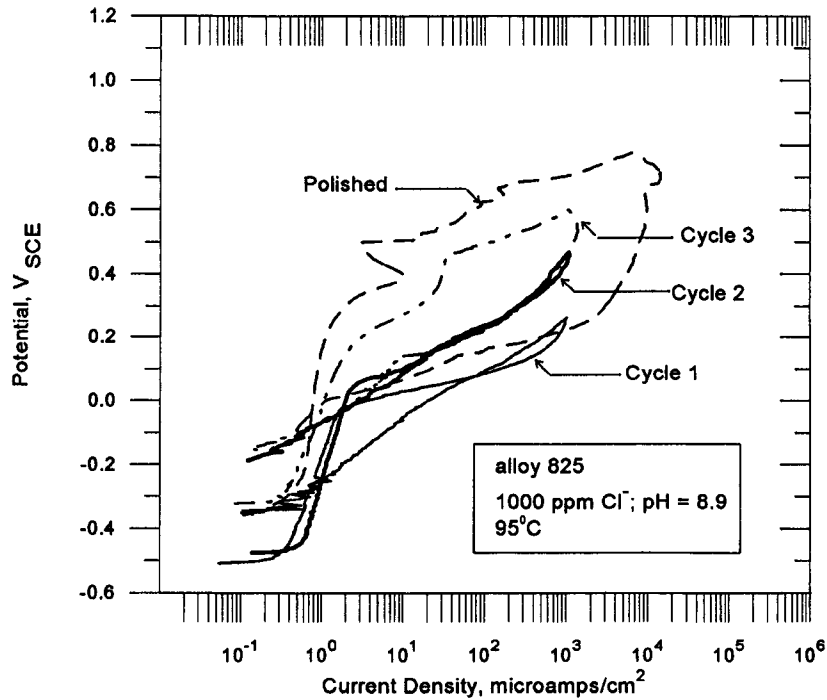


Figure 4-12. Repeated cyclic polarization curves of Cr-depleted surfaces of alloy 825 in a 1000 ppm  $\text{Cl}^-$  solution at 95°C indicating the behavior of a progressively increasing Cr content. Scan rate: 0.167 mV/sec.

# 5 REPASSIVATION POTENTIAL AS A LONG-TERM PREDICTION TOOL FOR AUSTENITIC ALLOYS

## 5.1 INTRODUCTION

In the previous section, cyclic polarization tests were used to study the effect of environmental factors on the localized corrosion behavior of Fe-Ni-Cr-Mo alloys. In this chapter, questions related to the use of parameters derived from these tests for long-term prediction are addressed. An approach to long-term life prediction of container materials under aqueous conditions assuming only corrosion-related failure modes is illustrated schematically in Figure 5-1. While the figure illustrates the approach for pitting, the same methodology can be used for crevice corrosion. As shown in Figure 5-1a, the corrosion potential of the container material, which is a mixed potential dictated by the kinetics of the anodic and cathodic reactions at the surface, exposed to the repository environment changes with time in response to factors such as radiolysis, temperature, and oxygen concentration (Macdonald and Urquidi-Macdonald, 1990). A simple increase in the corrosion potential to a constant upper limit is indicated in Figure 5-1a, although a more complex behavior may be observed in reality. Additionally, significant variation in the corrosion potential of containers may be expected, depending upon their location and thermal output.

It is also indicated in Figure 5-1a that, if the corrosion potential exceeds the pit-initiation potential,  $E_p$ , pits initiate and propagate into the container wall. If the corrosion potential drops below  $E_p$ , pits already initiated continue to grow, but no new pits initiate. Finally, if the corrosion potential

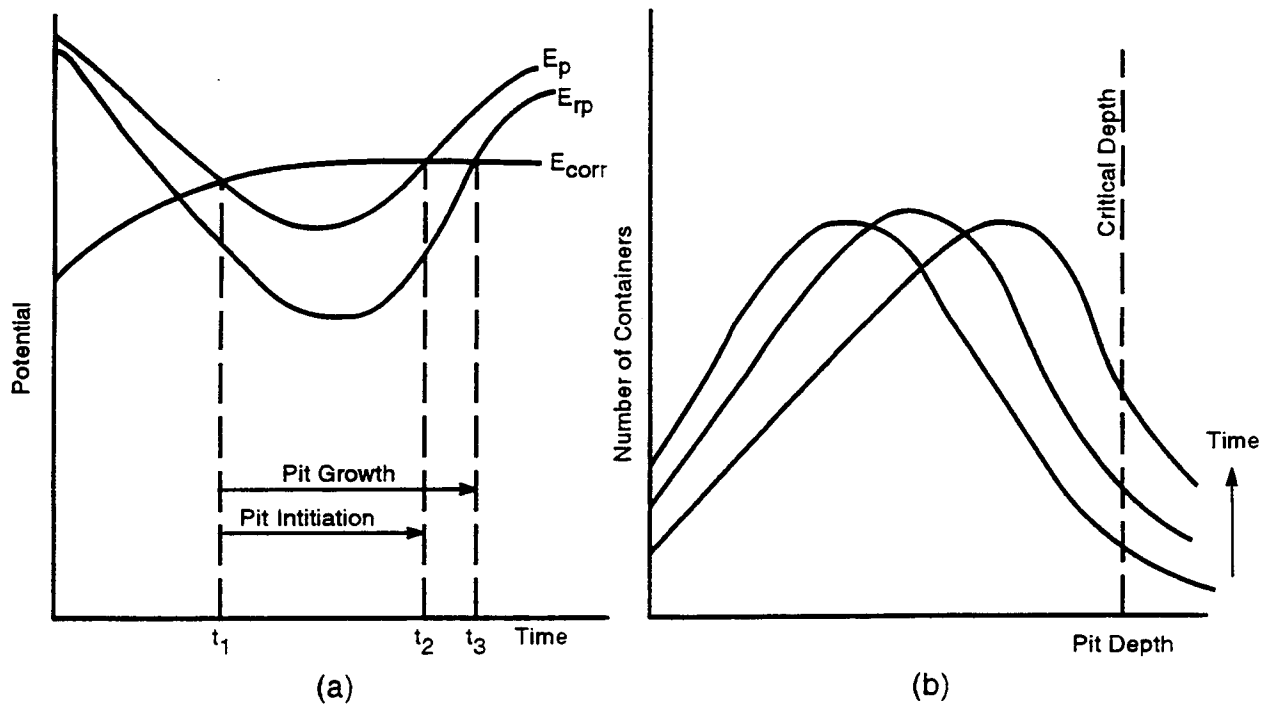


Figure 5-1. Schematic illustration of the approach used for long-term life prediction of container materials under localized corrosion conditions

drops below the repassivation potential,  $E_{rp}$ , all pits repassivate and cease to grow. After repassivation, the corrosion of the container continues in a uniform manner at a low rate determined by the passive current density. This concept of critical potentials has been well established in the literature for pitting and crevice corrosion (Szklaarska-Smialowska, 1986). Both  $E_p$  and  $E_{rp}$  are distributed values, and, hence, significant variability in the performance of various containers may be expected. The stochastic nature of localized corrosion and the variations in the corrosion potential of the containers in the repository can be taken into consideration by varying input parameters—for example, by a Monte-Carlo driver. The resulting distribution function of containers with pit depths exceeding a certain value for any given time period (Figure 5-1b), is termed a damage function (Macdonald and Urquidi-Macdonald, 1992). Containment can then be evaluated by comparing the fraction or number of containers with the deepest pits exceeding the critical pit depth at any given time period to a predetermined requirement. Although two potentials,  $E_p$  and  $E_{rp}$ , are defined, these two potentials may coincide to one critical potential in long-term exposure (Tsujikawa and Hisamatsu, 1984; Thompson and Syrett, 1992). Analogous parameters have been used to characterize the crevice-corrosion behavior of these alloys (Tsujikawa and Hisamatsu, 1984; Okayama et al., 1987a).

The current densities in an actively growing pit or crevice are quite high, on the order of 10 to 100 mA/cm<sup>2</sup> (100 to 1000 mm/year), whereas the anodic current density in the passive state ranges from 0.1 to 2.0  $\mu$ A/cm<sup>2</sup> ( $1 \times 10^{-3}$  to  $2 \times 10^{-2}$  mm/year). The latter would correspond to container lifetimes of approximately 12,500 to 625 years for a 12.5-mm-thick container, if failure is assumed to occur only when the container is penetrated completely. Two critical questions in the measurement and use of  $E_{rp}$  are its dependence on the extent of prior pit/crevice corrosion and its stability with respect to time of measurement.

## 5.2 EXPERIMENTAL PROCEDURES

### 5.2.1 Specimens and Solutions

This element of the test program focused on type 316L stainless steel and alloy 825. Limited tests were conducted on alloy C-22. Cylindrical specimens of these alloys (6.35 mm diameter  $\times$  48.5 mm long) were wet-ground to a 600-grit finish, rinsed in high-purity water, degreased with acetone, and dried before each test. The specimens were screwed onto a brass electrical contact, which was surrounded by a glass holder with a PTFE plug such that the brass did not come into contact with the test solution. The specimen assembly was partially immersed in the solution in order to avoid crevice corrosion at the specimen-PTFE interface. Post-test examination indicated that crevice corrosion did not occur in the specimens. The solution used was a model solution consisting of 85 ppm HCO<sub>3</sub><sup>-</sup>, 1000 ppm Cl<sup>-</sup>, 20 ppm SO<sub>4</sub><sup>2-</sup>, 10 ppm NO<sub>3</sub><sup>-</sup>, and 2 ppm F<sup>-</sup>, all added as Na salts. In two tests, the solution was augmented with SO<sub>4</sub><sup>2-</sup> to 1000 ppm. The initial pH of the solution at room temperature was approximately 8.0, while the final pH at room temperature was approximately 9.0. All tests were performed at  $95 \pm 2^\circ\text{C}$ .

### 5.2.2 Test Cell

The tests were conducted in a 1-liter reaction kettle (approximately 900 ml of solution), shown schematically in Figure 5-2, fitted with a fritted gas bubbler, platinum counter electrode, temperature probe, and a Luggin probe with a short salt bridge for the reference electrode. Nitrogen was bubbled at approximately 1 atmosphere pressure for 1 hour prior to the start and throughout the tests, the exit end going through a water trap to prevent back-diffusion of oxygen. A water-cooled condenser ensured that

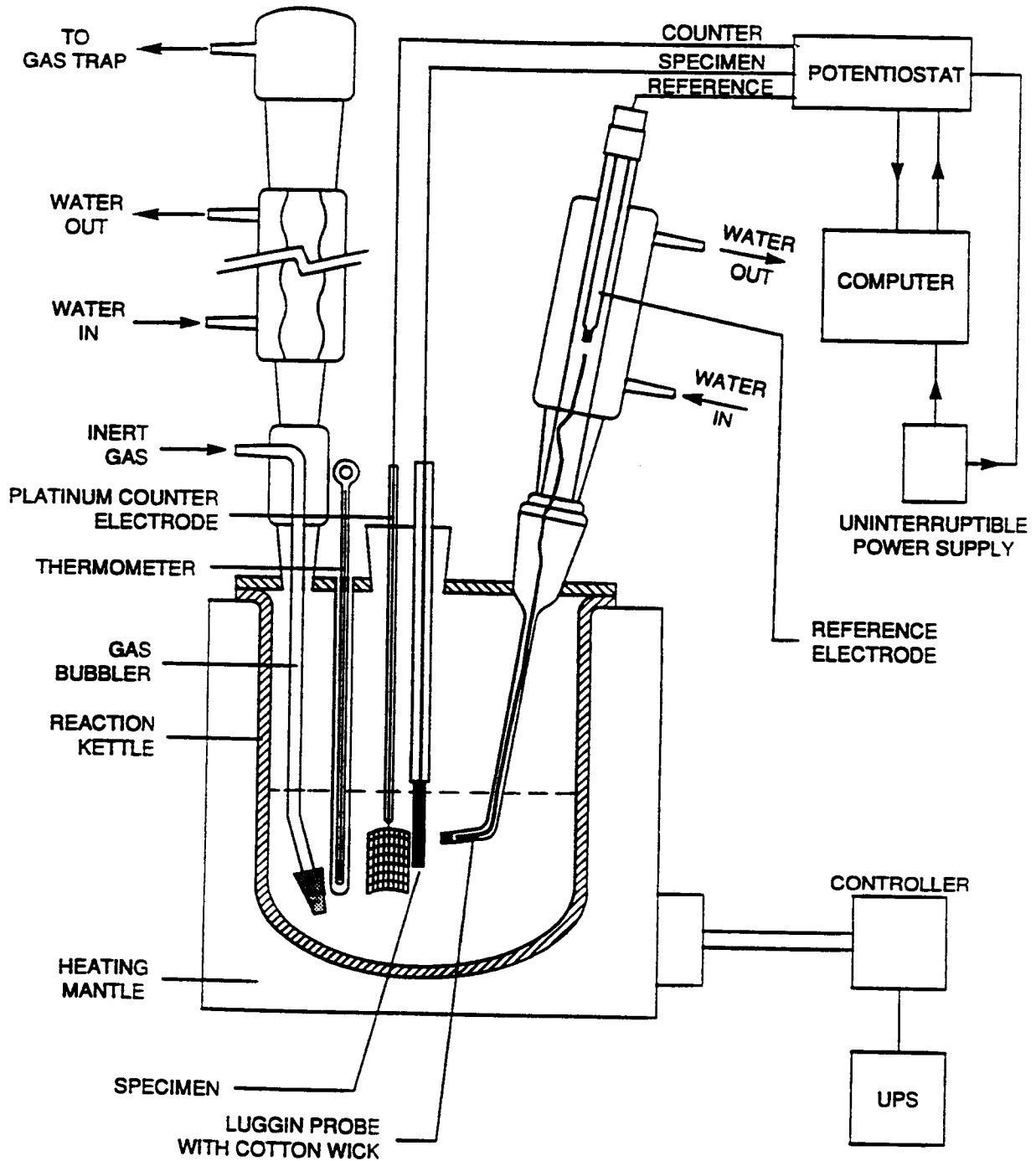


Figure 5-2. Schematic diagram of the cell and electrochemical testing system for the repassivation experiments

evaporative concentration of the solution did not take place. The Luggin probe had a porous silica tip to prevent drainage of the salt bridge solution. The salt bridge, which was filled with the test solution, was fitted with a water-cooled condenser. This ensured that the reference electrode tip was always at room temperature, which resulted in a reproducible thermal liquid junction potential and prevented the deterioration of the reference electrode at high temperatures. The SCE was used as the reference electrode in all the tests. A problem that was frequently encountered in the initial tests was the formation of air bubbles in the salt bridge. The discontinuity or poor electrical contact between the reference electrode and the test solution resulted in the generation of large noise signals in the measured current. A cotton wick, presoaked in the test solution, was introduced into the salt bridge (Figure 5-2) providing a continuous electrolyte path even in the presence of bubbles. The test vessel was sealed and heated to the desired temperature before introduction of the specimen.

### 5.2.3 Electrochemical Measurements

The electrochemical measurements were conducted using a potential staircase technique. A Electroynthesis Model 440 multi-channel potentiostat was used to control the potential. This was connected to a Strawberry Tree ACPC-16-16 16-channel, 16-bit analog-digital (A/D) converter and a ACAO 12-8 12-channel digital-analog converter (DAC) in a 386 computer. The resulting potential and currents were stored on a disk for later analyses. The resolution of the A/D was adjusted to 17 milliseconds per channel so that line noise was filtered out. The sampling rate was set at 10 Hz. The resolution of the A/D converter varies as a function of the selected voltage range. The software is capable of choosing the range automatically depending on the input value. Because the measured voltage was in the range of  $\pm 0.3$  V, the resolution of the measured voltage is approximately 0.25 mV. Since the current is converted to volts by a  $10\Omega$  resistor for measurement, the maximum resolution of current is approximately  $1.25 \times 10^{-7}$  A. The potential and current measurements were checked independently using a Keithley Model 614 electrometer and a Keithley Model 485 picoammeter. An overall view of the cells and the data acquisition system is shown in Figure 5-3.

The data acquisition and control were performed using Workbench® software. This is an icon-based programming environment capable of acquiring signals, performing arithmetic and logical operations on the signals, and controlling external instrumentation based on the results of the calculations. Four sets of experiments were performed. The typical experimental sequence is shown schematically in Figure 5-4. In the first set of experiments, the specimen was maintained at open-circuit potential for 1 hour [ $t_1$  in Figure 5-4(a)]; the potential was then increased to a predetermined value known to induce rapid initiation of pitting ( $t_2$ ) and maintained at this value to grow the pits (growth time =  $t_3 - t_2$ ). The measured currents were converted to current densities, integrated with respect to time to calculate charge density, and stored in a file. At the end of this period ( $t_3$ ), the potential was sequentially reduced by 10 mV, provided the measured minimum current density over a 3-minute period was greater than a threshold value of  $50 \mu\text{A}/\text{cm}^2$ . If the current density was less than this value, the potential was not reduced. The above step was repeated until the current density remained below  $50 \mu\text{A}/\text{cm}^2$  for at least 24 hours (greater than  $t_4$ ). The experiments were terminated typically after 24 hours, although some measurements were carried out for 220 hours. The potential at which the current density decreased to a value below  $50 \mu\text{A}/\text{cm}^2$  and remained at this value for at least 24 hours is referred to as the repassivation potential. In the second set of experiments [Figure 5-4(b)], the potential was reduced after time  $t_3$  in a rapid manner (within 0.5 seconds) to a lower potential such that the minimum current density during this period was less than  $50 \mu\text{A}/\text{cm}^2$ . In the third set of experiments [Figure 5-4(c)], the potential was reduced after  $t_3$  in 100 mV steps and maintained at each potential for 10 minutes. The same logic as above was followed for decreasing the potential. In the fourth set of experiments [Figure 5-4(d)], pits

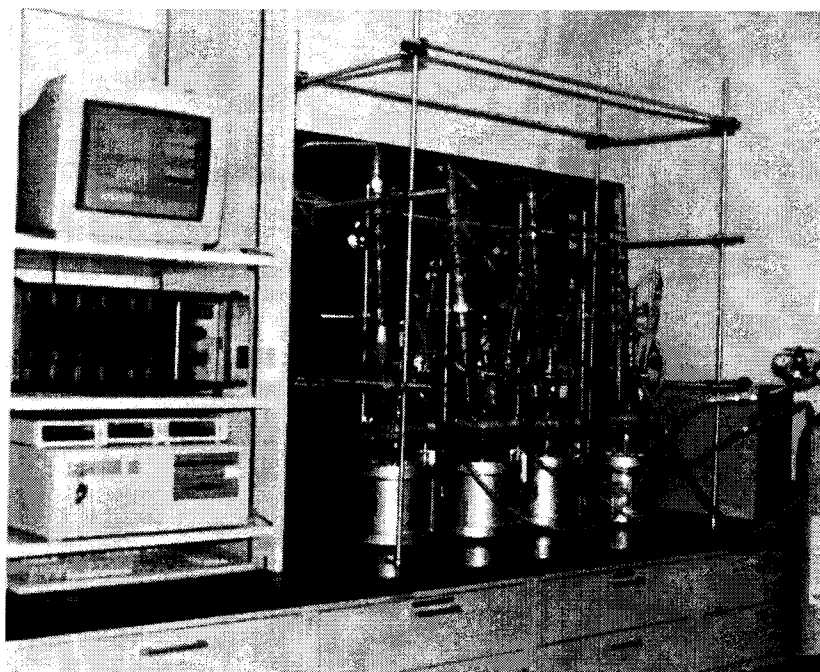


**Figure 5-3. Overall view of the cell, multi-channel potentiostat, and data acquisition system for repassivation experiments**

were initiated at a potential of  $600 \text{ mV}_{\text{SCE}}$  for alloy 825 and  $300 \text{ mV}_{\text{SCE}}$  for type 316L for 5 minutes after time period  $t_2$ , then decreased to 400 and 200  $\text{mV}_{\text{SCE}}$ , respectively, for a growth period, and at time  $t_4$ , potentials were stepped down according to the same logic scheme as before. A typical potential and current density versus time plot is shown in Figure 5-5.

#### **5.2.4 Post-Test Analyses**

The specimens were weighed at the beginning and end of each test and the weight loss computed as an independent verification of the electrochemical measurements. Weight loss was also calculated from the current density measurements and these values were in reasonable agreement (Cragolino and Sridhar, 1992b). The specimens were examined under the SEM to quantify the areal density of pits and cross-sectioned to quantify the pit depths under a metallographic microscope (Cragolino and Sridhar, 1992b).

### **5.3 RESULTS OF REPASSIVATION POTENTIAL MEASUREMENTS**

The effect of charge density on repassivation potentials for type 316L stainless steel and alloy 825 at  $95^\circ\text{C}$  is shown in Figures 5-6 and 5-7, respectively. The fast-scan data refer to the technique illustrated in Figure 5-4(b), while the slow scan data refer to a composite of data using the other three techniques. The open squares in Figure 5-6 represent data acquired using the technique shown in Figure 5-4(c). In both alloys, the fast-scan technique results in a lower repassivation potential by about 150 mV. This may be explained on the basis of the time required for repassivation. In the fast-scan technique, sufficient time is not given at the higher potentials for repassivation; hence, the downward

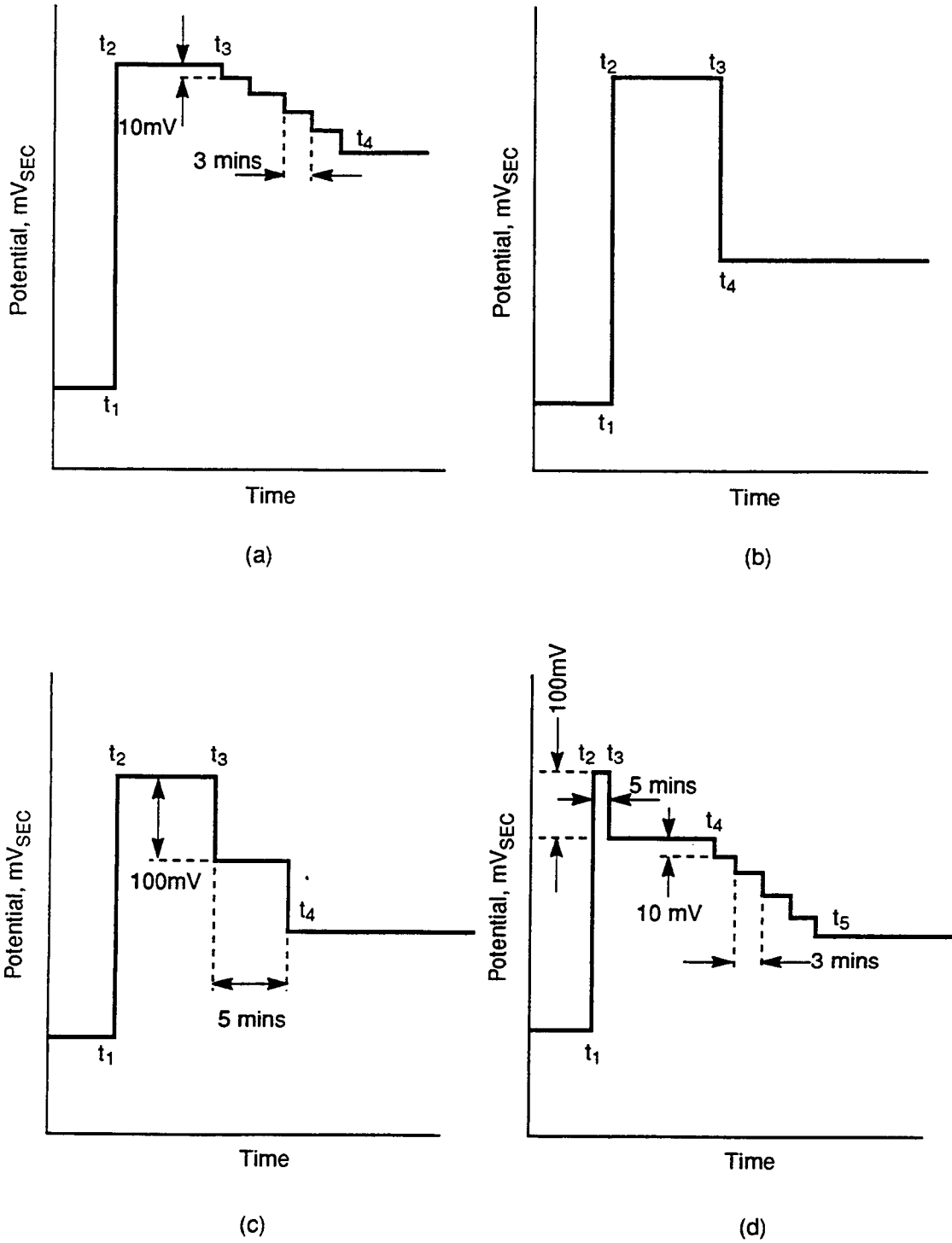


Figure 5-4. Schematic profiles of applied potential versus time used for various repassivation experiments. The fast-scan technique is shown in (b), while the slow-scan techniques are shown in (a), (c), and (d).

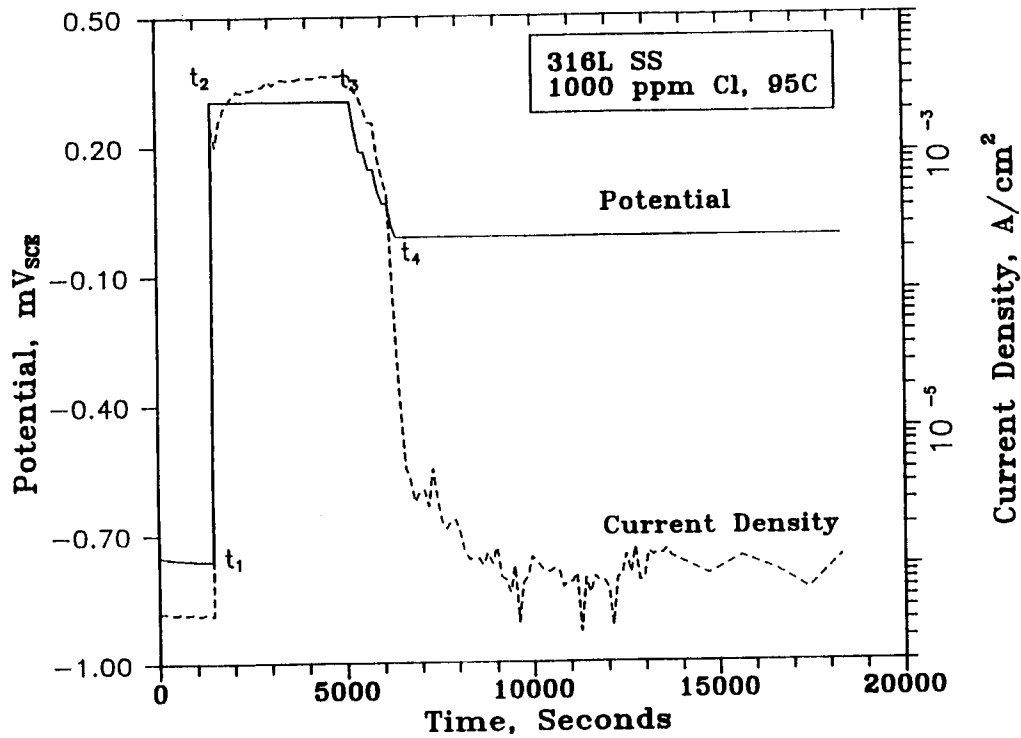


Figure 5-5. Actual potential and current density versus time plots for a specimen of type 316L stainless steel

potential scan overshoots the repassivation potential. If greater time is given at higher potentials, repassivation occurs at higher potentials. In one experiment, the technique shown in Figure 5-4(d) was used. After pit growth of type 316L stainless steel at  $300 \text{ mV}_{\text{SCE}}$  for 5 minutes, potential was decreased to  $100 \text{ mV}_{\text{SCE}}$  and held at that value. The current density decreased to  $1 \mu\text{A}/\text{cm}^2$  and stayed at that value for 69 hours. When the potential was increased to  $200 \text{ mV}_{\text{SCE}}$ , no current increase was observed, indicating that this was a repassivation potential by the definition of Starr et al. (1976).

The repassivation potential of  $-50 \text{ mV}_{\text{SCE}}$  for alloy 825 using the fast-scan technique is in the same range as the repassivation potential measured using the potentiodynamic technique reported before (Appendix C, Tables C-1 and C-2). Similarly, the repassivation potential for type 316L stainless steel using the fast-scan technique is closely approximated by that obtained using the potentiodynamic technique (Table C-3). This leads to the rather surprising conclusion that the slow back-scan technique does not always result in a conservative prediction since a more positive repassivation potential tends to suggest a more corrosion resistant alloy. Similar experiments on alloy C-22 using chloride concentration of 10,000 ppm failed to produce any pitting, but resulted in transpassive dissolution with the formation of gold colored film which turned dark after a few days at  $700 \text{ mV}_{\text{SCE}}$ . Hence, further experiments on this alloy were temporarily abandoned.

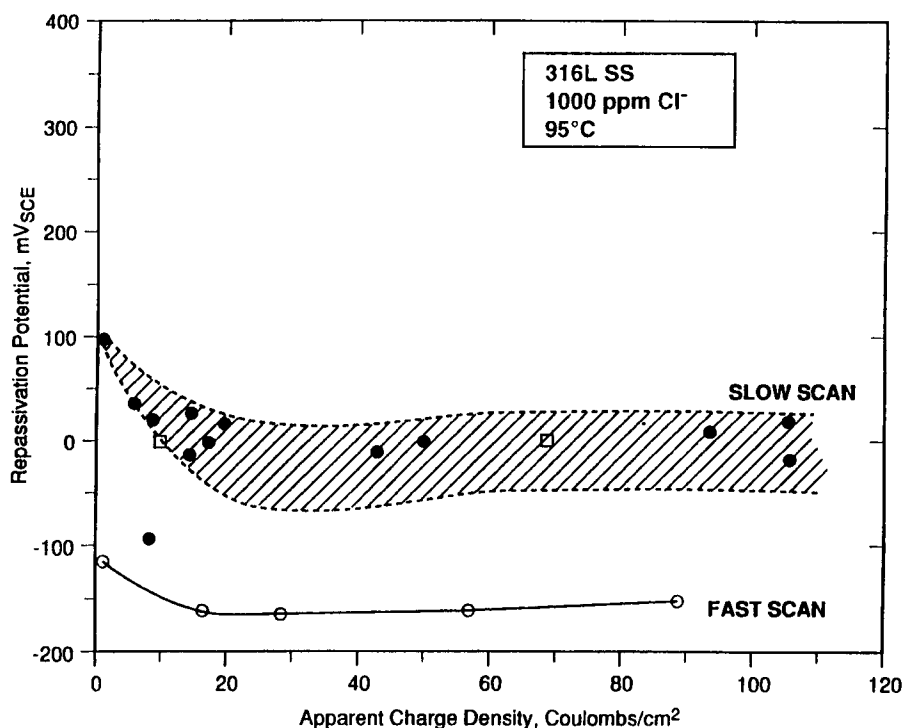


Figure 5-6. Effect of applied charge on repassivation potential for pitting of type 316L stainless steel in 1000 ppm  $\text{Cl}^-$  solution at  $95^\circ\text{C}$

- — Scan rates = 0.05–0.33 mV/sec.
- — Scan rate = 0.17 mV/sec.
- — Scan rate  $\approx$  700 mV/sec.

#### 5.4 REPASSIVATION TIME

Further experiments were conducted to determine the effect of potential on repassivation time. In these experiments, the pits were nucleated at 600 mV with respect to a SCE for 30 minutes and then grown at  $400 \text{ mV}_{\text{SCE}}$  for 6 and 12 hours. Repassivation time was measured by holding the potential at various values after the growth of pits and monitoring the time for the resulting current density to drop below  $50 \mu\text{A}/\text{cm}^2$ . The effect of potential upon repassivation time is shown in Figure 5-8. The open symbols represent the repassivation time data for the 6-hour growth time and a power-law fit through the data points is also shown.

Based on the data shown in Figure 5-8, the logarithm of the repassivation time (in seconds) can be represented as a linear function of logarithm of the repassivation potential (in millivolts) by Eq. 5-1.

$$\log_{10} t_{rp} = 30.14 \log_{10} (E_{rp}) - 63.86 \quad (5-1)$$

The regression coefficient for the relationship shown in Eq. 5-1 is  $R^2 = 0.8$ . The effect of potential on repassivation time is important in two respects:

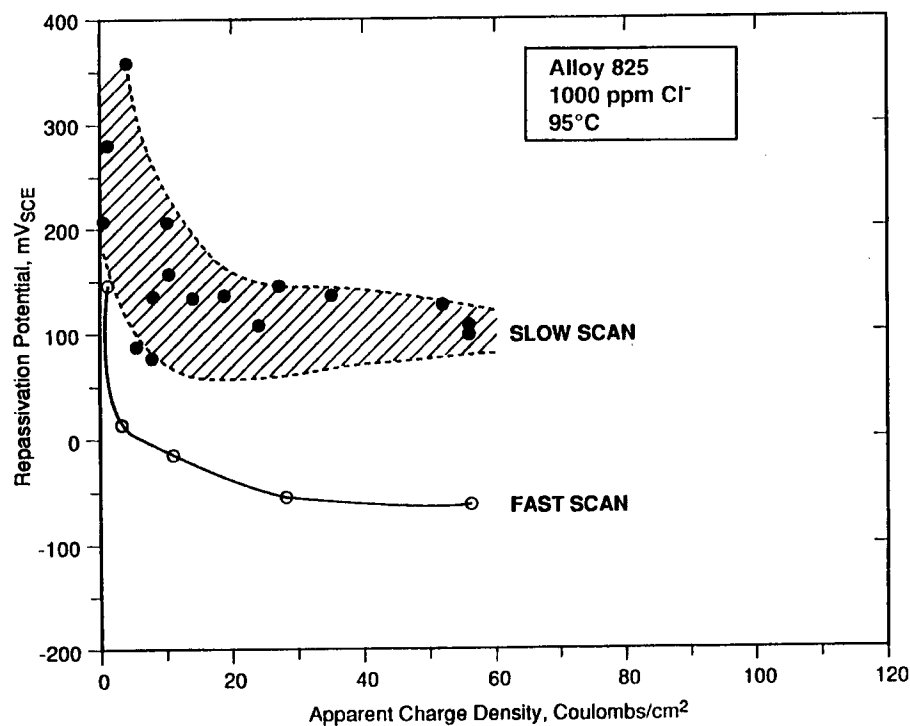


Figure 5-7. Effect of applied charge on repassivation potential for pitting of alloy 825 in 1000 ppm  $\text{Cl}^-$  solution at  $95^\circ\text{C}$

- — Scan rate = 0.05 mV/sec.
- — Scan rate  $\approx$  700 mV/sec.

- It explains the effect of potential scan rate on the measured repassivation time. The fast-scan techniques produce lower repassivation potentials than the slow-scan techniques. Since long-term predictions of container performance have to rely, at least at present, on measured repassivation potentials, it is important to know the effect of scanning technique.
- The observation that there is a potential-dependent repassivation time is important to mechanistic modeling of repassivation as will be discussed later. It is important to point out the limitations of Eq. 5-1. It predicts that there is a finite repassivation time, however long, even at potentials above the pit initiation potentials. This is counterintuitive since an upper limit to repassivation potential equal to the pit nucleation potential would be expected. For example, at  $200 \text{ mV}_{\text{SCE}}$ , repassivation was not observed even after a few days. It is also empirical and, hence, has to be justified by detailed modeling of the relevant processes. It can also be seen from Figure 5-8 that the pits grown for a longer time period show a higher repassivation time for the same potential.

## 5.5 MECHANISTIC MODELING OF REPASSIVATION

In the following discussion, the concept of repassivation is examined further, based on the experimental data acquired so far. While much of the data pertains to pitting, crevice corrosion and pitting are regarded equivalently, especially where repassivation is discussed.

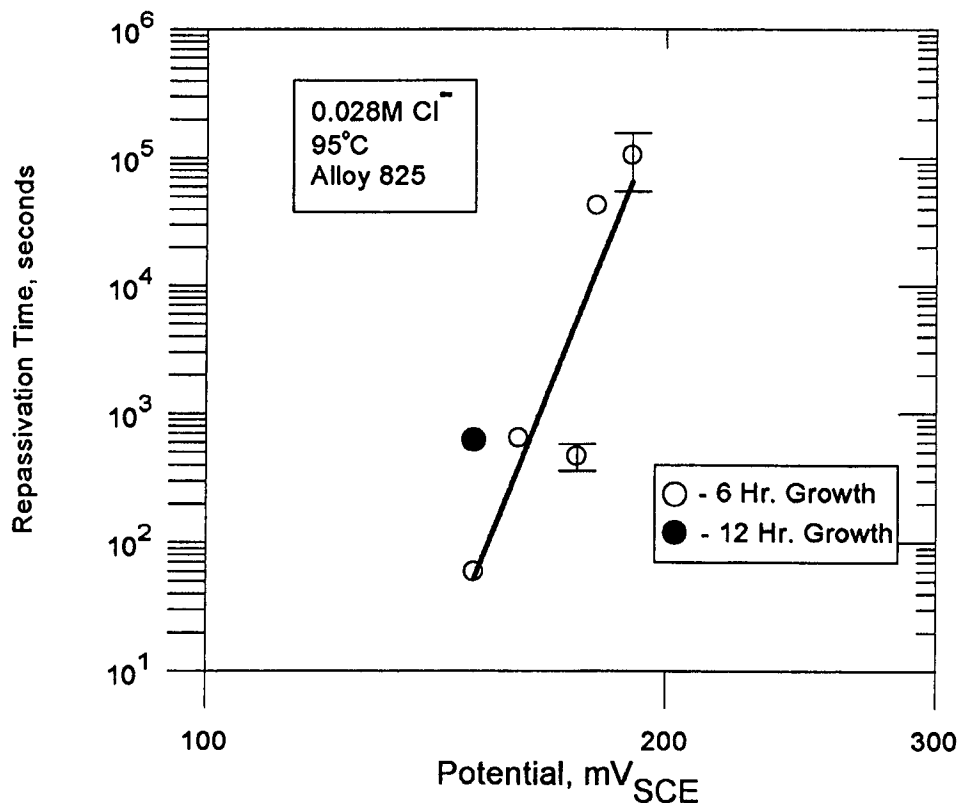


Figure 5-8. The effect of applied potential on repassivation time of alloy 825 in a 1000 ppm  $\text{Cl}^-$  solution at  $95^\circ\text{C}$ . Open circles: pits grown for 7 hours; closed circles: pits grown for 12 hours.

### 5.5.1 Potential-Drop Mechanism

The first mechanism involves changes in the potential inside the crevice as a result of changes in external potential (Newman, 1983; Newman and Franz, 1984; Rosenfeld et al., 1978). If it is assumed that crevice corrosion is initiated by complete depassivation and general dissolution in the crevice, then repassivation occurs when the internal potential is below the corrosion potential of the alloy in the crevice environment. The corrosion potential of alloy 825 in various simulated crevice solutions is relatively independent of chloride and sulfate concentration, but is dependent on pH as shown in Figure 4-7. The corrosion potentials of both passive and active conditions are represented in this figure. This indicates that the corrosion potential changes are primarily determined by the changes in the cathodic polarization curve related to hydrogen evolution and not the anodic polarization curve. The regression line from Figure 4-7 can be represented by

$$E_{corr} (mV_{SCE}) = -24.3pH - 290 \quad (5-2)$$

with an  $R^2 = 0.71$ . Assuming a crevice solution pH of 1, the internal potential has to be below  $-320 \text{ mV}_{SCE}$  to repassivate by this mechanism. The repassivation potential, under fast-scanning condition, for alloy 825 is  $-50 \text{ mV}_{SCE}$ , implying a potential drop of 270 mV in the crevice. This potential drop is possible (Hakkarainen, 1983), especially if a large anodic current density is present. Because an active crevice corrosion is being considered prior to repassivation, the pH assumed in the crevice is independent of prior crevice growth, being less than or equal to  $\text{pH}_D$ . Therefore, this mechanism predicts that the repassivation potential should be independent of prior pit growth. Because

the corrosion potential is independent of chloride concentration, this mechanism also predicts that repassivation potential should be relatively insensitive to bulk chloride concentration, at least as a first approximation.

### 5.5.2 Solution-Change Mechanism

The second mechanism involves changes in solution composition inside the crevice/pit as a result of changes in external potential (Tsujikawa et al., 1987; Strehblow, 1984). In the mechanism proposed by Tsujikawa et al. (1987), the chloride concentration and the pH inside an actively corroding crevice/pit are assumed to be related to each other through empirically-derived equations, and repassivation is assumed to occur when the chloride concentration decreases below a critical value. In the mechanism proposed by Strehblow (1984), a minimum chloride concentration in the pit/crevice is necessary to maintain a thin film of metallic chloride salt. The thin, salt film is considered to be necessary to maintain pit/crevice corrosion growth. Another approach is to consider the effect of chloride concentration on pitting inside a crevice or an actively growing pit. For a given external potential, corrected for ohmic potential drop, repassivation occurs when the chloride concentration inside the pit decreases below a critical value required to initiate new pits. Since the corrosion potential is relatively independent of chloride concentration (Figure 4-7), the effect of chloride is related to the change in pitting potential inside the crevice (Figure 4-8). This mechanism needs further exploration. While a rigorous treatment of the effect of external potential on chloride concentration is yet to be done, simpler models suggest that the chloride concentration in the crevice decreases when the external potential decreases. Other observations also support a transport-related mechanism. For example, Nakayama and Sasa (1976) observed that  $E_{rp}$  increased considerably upon ultrasonic agitation of the specimen, suggesting that increased transport of chlorides by agitation may have eased repassivation. The finite repassivation time observed in the CNWRA investigation (Figure 5-8), as well as in others (Strehblow, 1984), also suggest a transport-related mechanism.

The choice between the two types of mechanisms suggested above may be dictated by scan rate. At fast-scan rates, there is insufficient time for transport-related processes, and  $E_{rp}$  may be determined by potential drop considerations alone. At slow-scan rates or under potentiostatic conditions, transport processes become significant, and repassivation is observed at higher potentials. From the point of view of long-term prediction, a conservative, lower-bound parameter is desired, and the fast-scan rate technique seems adequate. This overall viewpoint of repassivation mechanism also has implications on the effect of environmental factors on repassivation potential. If potential-drop is the main parameter dictating repassivation under fast-scan techniques, then the repassivation potential ought to be relatively independent of bulk chloride concentration. On the other hand, if solution composition change is the important process dictating repassivation as in the slow-scan techniques, then the repassivation potential ought to depend on the bulk chloride concentration. The repassivation potentials derived from cyclic polarization technique and potential staircase technique are shown as functions of chloride concentration in Figure 5-9. The slope of the  $E_{rp}$  versus  $\log(\text{Cl}^-)$  curve for the potential staircase technique is  $-43.6$  mV/decade (Regression coefficient,  $R^2 = 0.98$ ) and that for the cyclic polarization technique is  $-33.8$  mV/decade (Regression coefficient,  $R^2 = 0.67$ ). While the cyclic polarization technique is not a fast-scan technique (scan rate:  $0.167$  mV/sec), it is faster than the potential staircase technique ( $0.056$  mV/sec) and shows a less steep dependence on chloride concentration. Much faster scan rates are being examined to investigate this point. From the point of view of long-term prediction and conservative use of parameters, the faster scan technique not only yields lower repassivation potentials, but also shows less sensitivity to environmental factors, at least pH and  $\text{Cl}^-$ .

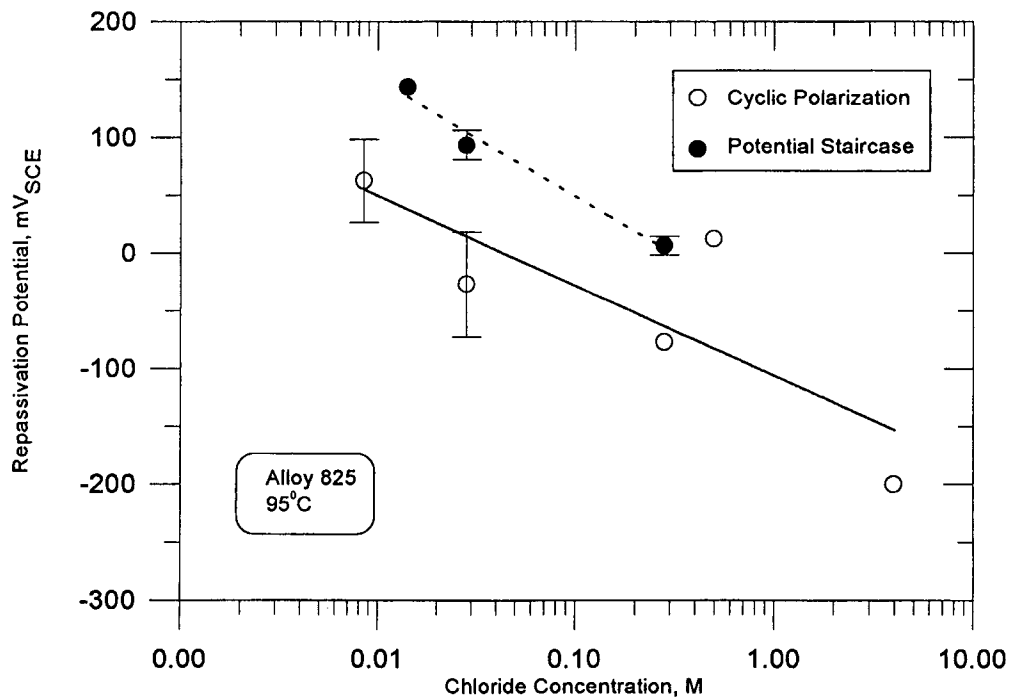


Figure 5-9. Dependence of  $E_{rp}$  on  $Cl^-$  concentration under slow-scan, potential staircase, and cyclic polarization techniques

## 6 LOCALIZED CORROSION OF COPPER-BASED ALLOYS

### 6.1 INTRODUCTION

Copper and its alloys are generally not believed to perform well in oxidizing environments such as that expected to be found at the Yucca Mountain repository horizon. Because of this, the current DOE container design concepts appear to de-emphasize Cu-based container materials. However, Cu-based alloys, especially oxygen-free copper (CDA-102) and Cu-30 weight percent Ni (CDA-715) are still being argued as viable choices (Peters and Kundig, 1991) because of their long history of usage, availability of geologic analogues, and the anticipated lack of susceptibility to localized corrosion under repository conditions. It is the last point that is examined in this chapter. Specifically, cyclic polarization tests are used to determine the combination of conditions that leads to localized corrosion of CDA-102 and CDA-715. Some potentiostatic experiments were also conducted to study the effect of longer-term exposure of these alloys to selected environments.

Unlike the case of Fe-Ni-Cr-Mo alloys, localized corrosion of Cu-base alloys can occur in a variety of forms depending on the environmental conditions: (i) Type-1 pitting, which occurs in hard waters at relatively low temperatures (Campbell, 1974); (ii) Type-2 pitting, which occurs in soft waters at relatively high temperatures (Mattsson and Fredriksson, 1968; Shalaby et al., 1989); (iii) crevice corrosion in alkaline, chloride environments (Efrid and Verink, 1977); (iv) localized corrosion in sulfide containing waters (Syrett and Wing, 1980); (v) horseshoe-type corrosion under turbulent flow conditions (Bianchi et al., 1978); and (vi) a new form of corrosion known as "ant-nest" corrosion, found mainly in air-conditioner tubes and supposed to be caused by organic acids (Notoya, 1990). It is difficult to predict the type of localized corrosion that will be observed on Cu-based alloys in the Yucca Mountain site repository environment based on the available literature on the environmental conditions. The groundwater compositions near the repository site are predominantly sodium-rich, the  $\text{Na}/(\text{Na} + \text{Ca} + \text{K})$  molar ratio ranging from 0.9 to 0.7 (Kerrisk, 1987). The calcium content of the J-13 well water, considered to be the reference water for DOE studies, is 0.5 mmoles/liter. Localized corrosion of copper-based alloys in these soft waters at 95°C would be expected to be of Type-2 nature. On the other hand, one can argue against the occurrence of Type-2 pitting because of the high  $\text{HCO}_3^-/\text{SO}_4^{2-}$  ratio (Mattsson and Fredriksson, 1968) and the absence of measurable iron and manganese (Campbell, 1974). A literature review of the localized corrosion behavior of copper and its alloys was conducted prior to the start of the experimental program (Cragolino and Sridhar, 1991e). This review, along with reviews conducted by LLNL (Farmer et al., 1988) indicated the following:

- The concentration of bicarbonate and the ratios of  $\text{HCO}_3^-/\text{Cl}^-$  and  $\text{HCO}_3^-/\text{SO}_4^{2-}$  are extremely important in causing localized corrosion.
- Higher temperature generally leads to lower susceptibility to localized corrosion. The effect of temperature on localized corrosion needs to be examined systematically.
- Localized corrosion in copper, because of its relatively weak passivity, tends to spread laterally rather than penetrate deeply as a narrow pit.
- While much investigation has been done on copper in a variety of groundwaters, very little systematic investigation of the combined effects of environmental factors affecting localized corrosion has been carried out. For example, the statistically designed experiments reported

by Thompson et al. (1992), while being a good first attempt at defining the individual roles of various environmental factors on the localized corrosion of CDA-102 and CDA-715, do not yield any information on the interactive effects of these environmental factors. There is a greater paucity of experimental data on the behavior of Cu-Ni alloy in groundwater environments at high temperatures.

In order to evaluate the interactive effects of the environmental factors and temperature, the experimental program reported here used a full-factorial statistical matrix. Four factors were considered in order to keep the number of experiments manageable:  $\text{HCO}_3^-$ ,  $\text{Cl}^-$ ,  $\text{SO}_4^{2-}$ , and temperature. These experiments were augmented by experiments at intermediate concentrations of  $\text{HCO}_3^-$  and temperature. Selected potentiostatic experiments were conducted to study the kinetics of breakdown and repassivation due to changes in  $\text{Cl}^-$  and  $\text{SO}_4^{2-}$  concentrations.

The four factors were chosen to include the nominal chemistry of J-13 water and to cover a reasonably wide range: bicarbonate (85-8500 ppm), chloride (6-1000 ppm), sulfate (20-1000 ppm), and temperature (30-95°C). All the solutions were prepared with constant concentrations of nitrate (10 ppm) and fluoride (2 ppm). The compositions of the two alloys examined and their microstructures are shown in Appendix A. Specimens were cut from 0.5-inch plates and tested in the as-received metallurgical condition. They were examined at the end of the test under a low-magnification stereoscope and a SEM. In the potentiodynamic polarization tests, the potential at which the current increased rapidly was not always associated with localized corrosion, and the pits were much shallower than those observed in Fe-Ni-Cr-Mo alloys. Hence, the corresponding potential has been termed breakdown potential,  $E_b$ , rather than pitting potential,  $E_p$ . The potential at which the reverse scan intersected the forward scan is called repassivation potential,  $E_{rp}$ , although, as will be indicated later, this potential does not always represent the repassivation process observed in the Fe-Ni-Cr-Mo alloys.

## 6.2 RESULTS OF FACTORIAL EXPERIMENTS

The results of these experiments are tabulated in Appendix D. A detailed discussion of these results can be found in a previous report (Cragolino and Sridhar, 1992a) and a paper (Sridhar and Cragolino, 1992). The salient points will be described below:

- The dependence of localized corrosion of copper-based alloys on environmental parameters is much more complex than that of the austenitic alloys. Significant four factor interactions such as that between bicarbonate, temperature, chloride, and sulfate are observed, which makes prediction of performance more difficult.
- Both CDA-102 and CDA-715 exhibit active or passive behavior depending upon the bicarbonate concentration or temperature. In the case of active corrosion, the hysteresis in the polarization curves has no meaning in terms of localized corrosion since no localized corrosion occurred. Hence, quantitative statistical analysis of the factorial experiments is more difficult than in the case of the austenitic alloys. However, if the environment is confined to the high bicarbonate concentration, then the cyclic polarization curves can be interpreted in terms of the well known electrochemical parameters such as  $E_p$  (referred to here as  $E_b$ ) and  $E_{rp}$ .

- For the environments containing 8500 ppm  $\text{HCO}_3^-$ , pitting type corrosion was caused by the addition of either  $\text{Cl}^-$  or  $\text{SO}_4^{2-}$  or both. This is illustrated for CDA-715 in Figure 6-1. The localized corrosion was found only at  $\text{HCO}_3^-$  concentration above 2000 ppm as shown in Figure 6-2. This high a concentration of  $\text{HCO}_3^-$  is not anticipated in the repository. Indeed, a decrease in bicarbonate concentration is expected in the repository due to thermal effects (Pabalan and Murphy, 1991). In the low bicarbonate environments, chloride and sulfate enhanced the active corrosion.
- Even in the high bicarbonate containing environment, localized corrosion is observed only at temperatures below about  $80^\circ\text{C}$ . This is illustrated in Figure 6-3 where the  $E_b$  and  $E_{rp}$  are plotted as a function of temperature. Below  $80^\circ\text{C}$ , there was a considerable difference between the two parameters and localized corrosion was observed visually. Above  $80^\circ\text{C}$ , no localized corrosion was observed and the specimens were covered by a thin, black film, probably  $\text{CuO}$ .
- The localized corrosion of specimens exposed under potentiostatic condition to 8500 ppm  $\text{HCO}_3^- + 1000$  ppm  $\text{SO}_4^{2-}$ , and 8500 ppm  $\text{HCO}_3^- + 1000$  ppm  $\text{Cl}^-$  environment at room temperature was quite shallow and was always covered by a bluish-green corrosion product. Underneath this corrosion product was a white layer. Preliminary X-ray diffraction of the corrosion product that was scraped off the surface indicated peaks corresponding to

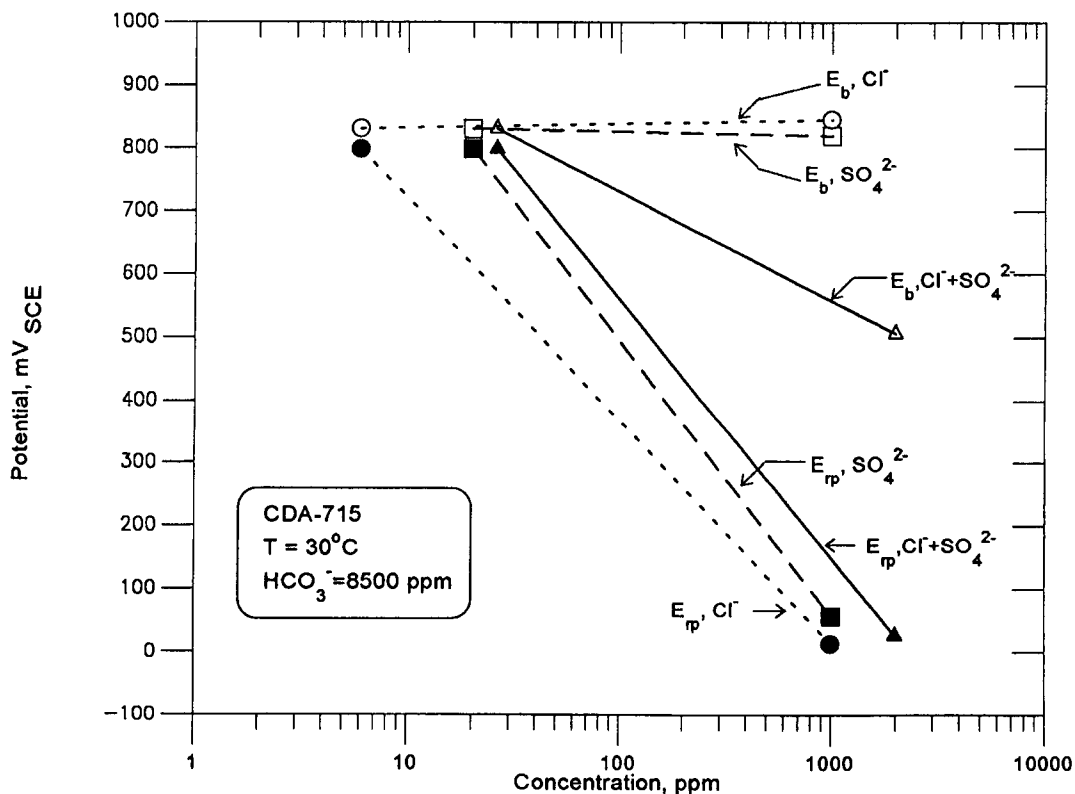


Figure 6-1. Effect of chloride and sulfate on breakdown and repassivation potentials for alloy CDA-715 in a 8500 ppm bicarbonate solution at  $30^\circ\text{C}$ . Open symbols: Breakdown potential,  $E_b$ ; Closed symbols: Repassivation potential,  $E_{rp}$

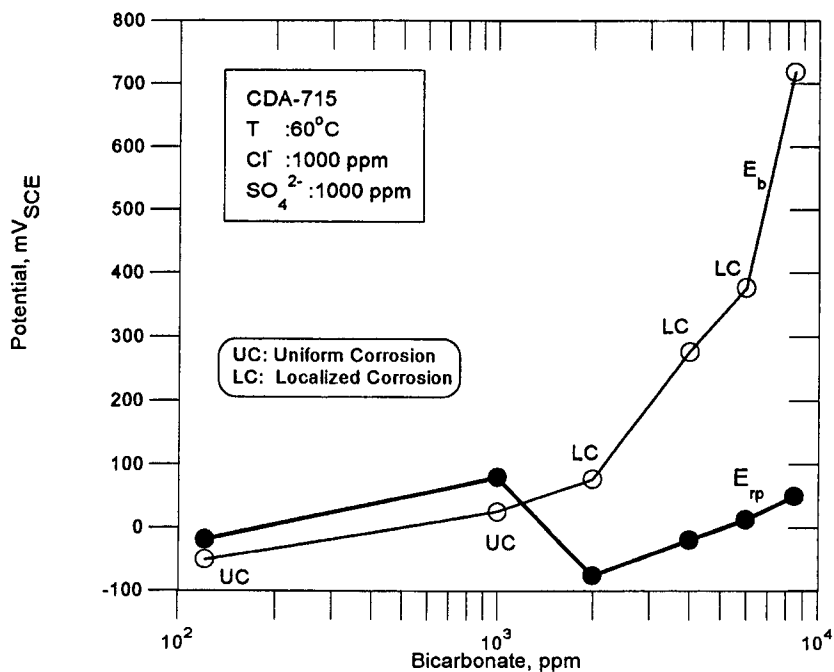


Figure 6-2. Effect of bicarbonate concentration on breakdown and repassivation potentials of CDA-715. Solutions contained: 1000 ppm  $\text{Cl}^-$ , 1000 ppm  $\text{SO}_4^{2-}$ , 10 ppm  $\text{NO}_3^-$ , 2 ppm  $\text{F}^-$ . Temperature: 60°C. UC = Uniform Corrosion; LC = Localized Corrosion.

- — Breakdown potential,  $E_b$
- — Repassivation potential,  $E_{rp}$

malachite and azurite (hydrated cupric carbonates), brochantite (hydrated cupric sulfate), cuprite ( $\text{Cu}_2\text{O}$ ), and atacamite (hydrated cupric chloride) (Table D-4).

### 6.3 EFFECT OF BICARBONATE CONCENTRATION

The potential - pH diagram (Figure 6-4) for copper in the system  $\text{Cu-HCO}_3^- - \text{Cl}^- - \text{SO}_4^{2-} - \text{H}_2\text{O}$  at 25°C (Pourbaix, 1974) suggests that at pH values in the range of 8 to 9, copper should form  $\text{Cu}_2\text{O}$  first as the potential is raised followed by malachite at higher potentials. At higher pH values, formation of cupric carbonate complexes and tenorite ( $\text{CuO}$ ) is indicated. The electrochemical response under potentiodynamic condition is somewhat different. Characterization of the electrochemical response of copper in mildly alkaline solutions ranging in pH from 8 to 11, such as borate buffer (pH = 8.2) and bicarbonate-carbonate solutions, has been performed by numerous investigators (Strehblow and Titze, 1980; De Chialvo et al., 1985; Perez Sanchez et al., 1990; Dong et al., 1992; Milosev et al., 1992; Drogowska et al., 1992; Tromans and Sun, 1992). These investigations have shown that polarization of copper in these solutions results in a passive behavior above a certain potential and that the passive film consists of an inner layer of  $\text{Cu}_2\text{O}$  and an outer layer of  $\text{Cu}(\text{OH})_2/\text{CuO}$  depending on the pH,  $\text{Cu}(\text{OH})_2$  being stable at more alkaline pH (Shoesmith et al., 1976). The cyclic polarization behavior of CDA-102 and CDA-715 in a borate buffer at pH = 8.6 (0.075 M  $\text{Na}_2\text{B}_4\text{O}_7$  + 0.15 M  $\text{H}_3\text{BO}_3$ ) is shown in Figure 6-5. The initial and final pH in this solution were within 0.1 pH unit. In both cases, a well-defined

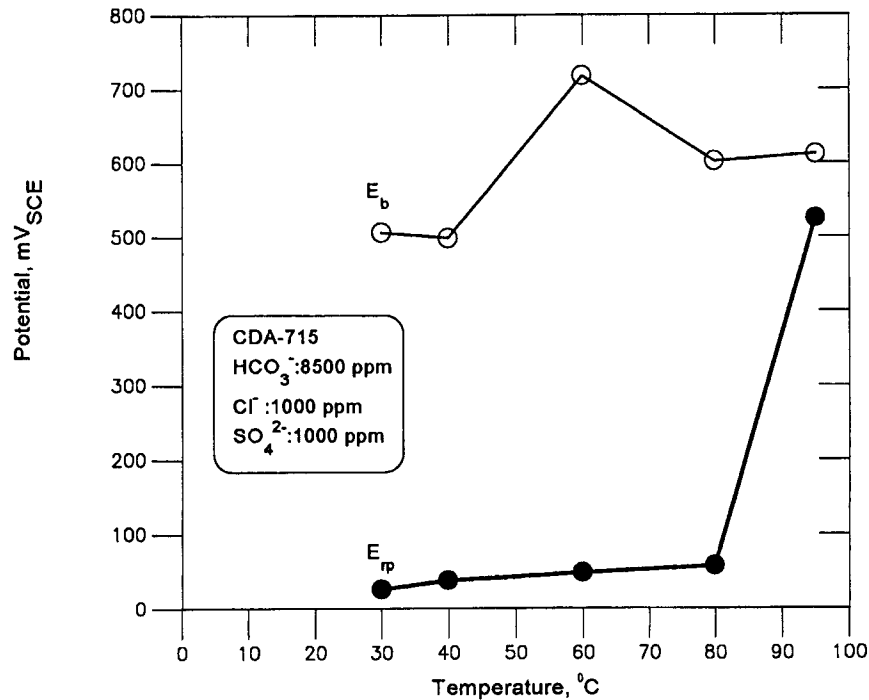


Figure 6-3. Effect of temperature on breakdown and repassivation potentials of CDA-715. Solutions contained: 8500 ppm  $\text{HCO}_3^-$ , 1000 ppm  $\text{Cl}^-$ , 1000 ppm  $\text{SO}_4^{2-}$ , 10 ppm  $\text{NO}_3^-$ , 2 ppm  $\text{F}^-$ .

- — Breakdown potential,  $E_b$
- — Repassivation potential,  $E_{rp}$

passive region is found. However, the passive regime is wider for CDA-715. In the case of CDA-102, the small deflection in the polarization curve at a potential of about  $-100 \text{ mV}_{\text{SCE}}$  has been reasonably well established to be due to  $\text{Cu}_2\text{O}$ . The formation of  $\text{Cu}_2\text{O}$  from Cu depends on the initial condition of the copper surface. Air exposure of the copper surface leads to a rapid formation of  $\text{Cu}_2\text{O}$  (Mayer and Muller, 1992) and subsequent polarization of this specimen will only indicate a weak current peak due to the cuprous oxide formation. The current peak at  $35 \text{ mV}_{\text{SCE}}$  is due to the formation of soluble cupric complexes followed by a passive region due to the formation of  $\text{CuO}$ . The current peak is considerably diminished for CDA-715 and the region of passivity is more extensive. The decrease in current peak may be due to transient effects of the enrichment of nickel at the surface. This may occur, for example, by preferential dissolution of copper in the active region. Presence of nickel enrichment in CDA-715 exposed to potential in this regime has been indicated by Auger spectroscopy (McGuire et al., 1978).

The polarization behavior of CDA-102 and CDA-715 at  $25^\circ\text{C}$  in an environment containing 85 ppm  $\text{HCO}_3^-$  is shown in Figure 6-6. A completely active corrosion is seen. This indicates that small concentrations of bicarbonate promote active dissolution, perhaps by the formation of soluble, cupric carbonate complexes. At higher concentrations of bicarbonate, passivity is introduced as discussed before. Interestingly, addition of bicarbonate to borate buffer solutions results in a passive behavior at all concentrations of bicarbonate, indicating that borate promotes passivity, perhaps by limiting the formation of soluble cupric complexes. Further investigation is necessary to establish whether the active

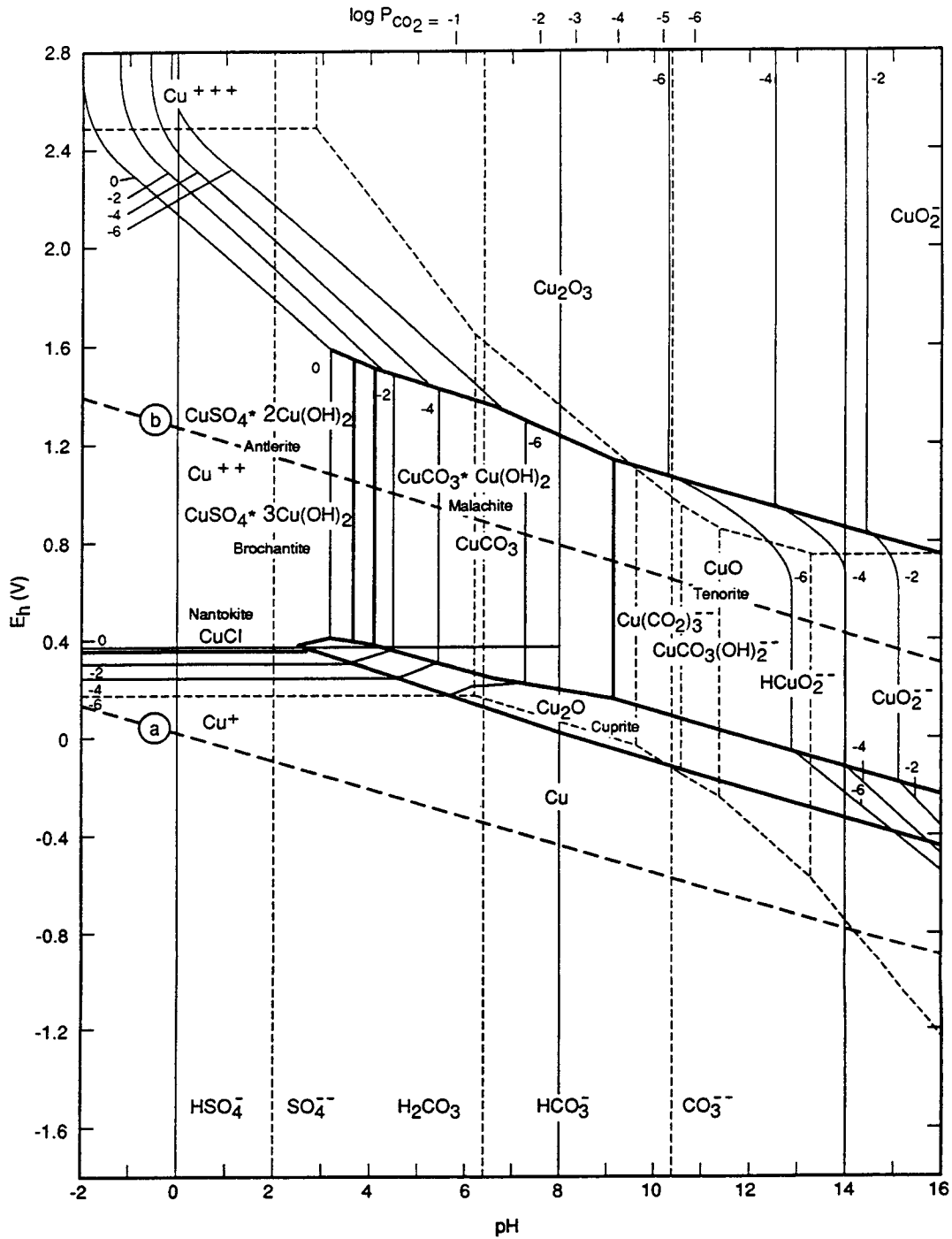


Figure 6-4. Potential-pH equilibrium diagram for copper in the system:  $\text{Cu-Cl}^- \text{-SO}_3 \text{-CO}_2 \text{-H}_2\text{O}$  at  $25^\circ\text{C}$ . Solutions containing 22 ppm  $\text{Cl}^-$ , 229 ppm  $\text{CO}_2$ , and 46 ppm  $\text{SO}_3$  (Pourbaix, 1974).

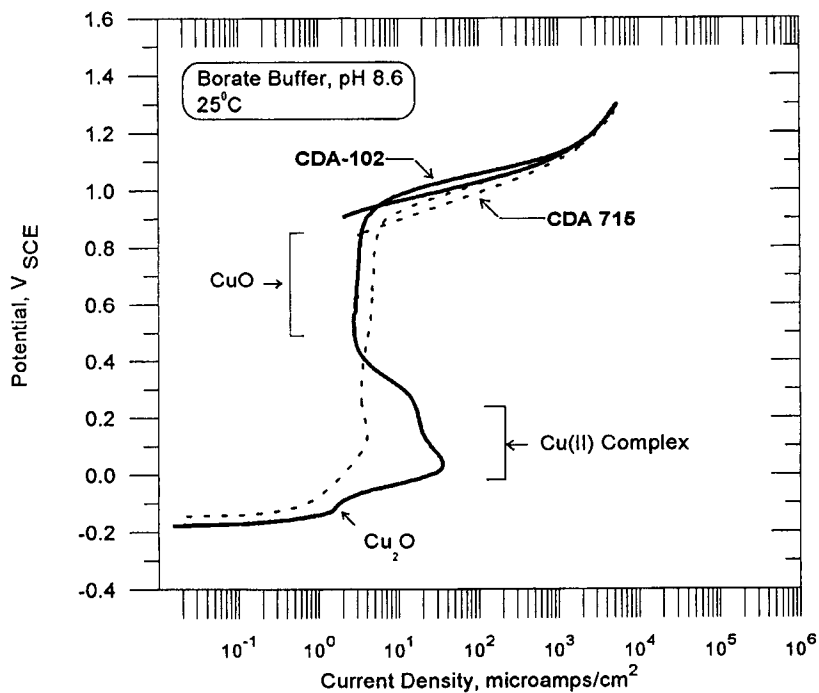


Figure 6-5. Cyclic polarization curves of CDA-102 and CDA-715 in borate buffer solution at pH = 8.6 and temperature of 25°C. Scan rate: 0.167 mV/sec. Solutions were deaerated with argon.

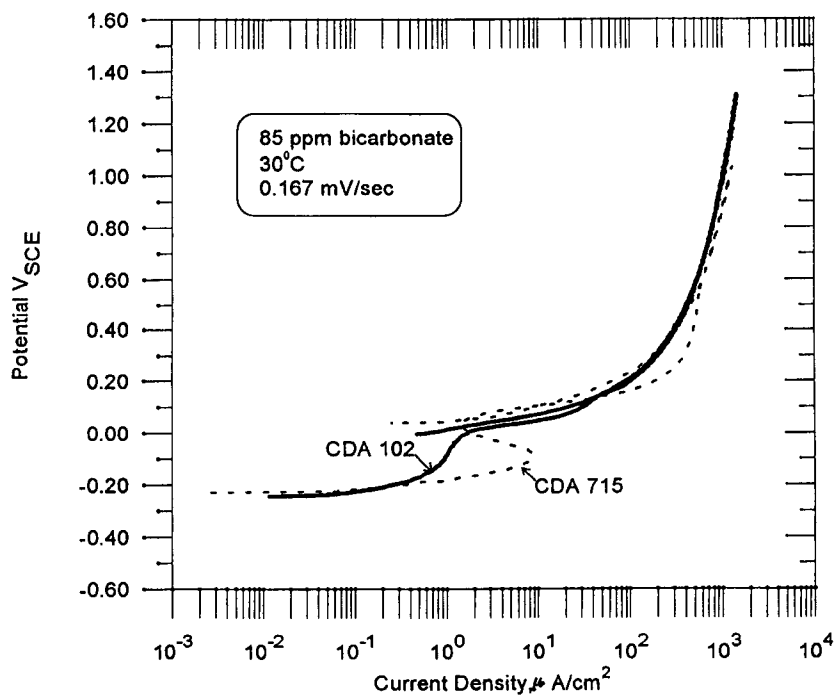


Figure 6-6. Cyclic polarization curves on CDA-102 and CDA-715 in a solution containing 85 ppm bicarbonate at 30°C. Solutions were deaerated with argon.

corrosion observed in short-term electrochemical tests is applicable to prediction of long-term behavior. The importance of long-term potentiostatic study over potentiodynamic studies for prediction of localized corrosion of copper has been pointed out by Akkaya and Ambrose (1985). While the literature abounds with studies of passivation and localized corrosion of copper, most of the attention has been focused on relatively high concentration of bicarbonate (0.1 M and above). Of greater importance to performance in the repository is the effect of small concentrations of bicarbonate since the environment is expected to show a decrease in bicarbonate concentration due to exsolution of  $\text{CO}_2$  (Pabalan and Murphy, 1991).

## 6.4 POTENTIOSTATIC STUDIES

While the cyclic polarization studies identified the combinations of environmental conditions that can promote localized corrosion of copper alloys, it is important to determine the extent of localized corrosion under potentiostatic conditions over a longer period of time. Limited studies were undertaken in this area. The test apparatus is the same as that used to measure repassivation potential for the austenitic alloys in Chapter 5. However, instead of initiating pitting and measuring repassivation, specimens were held at constant potentials while the current was monitored. The specimens were maintained at a potential of  $500 \text{ mV}_{\text{SCE}}$  in a solution of  $8500 \text{ ppm HCO}_3^-$ ,  $6 \text{ ppm Cl}^-$ ,  $20 \text{ ppm SO}_4^{2-}$ ,  $10 \text{ ppm NO}_3^-$ ,  $2 \text{ ppm F}^-$ . After the current density decreased to a low value (typically  $1 \mu\text{A}/\text{cm}^2$ ), chloride or sulfate was added from a stock solution so that the resultant concentration was  $1000 \text{ ppm}$ . The changes in the current density were monitored as a function of time for at least 24 hours. The effect of  $\text{Cl}^-$  or  $\text{SO}_4^{2-}$  addition on the current density is shown for CDA-102 in Figure 6-7. A rapid increase in current density was noted as soon as  $\text{Cl}^-$  or  $\text{SO}_4^{2-}$  was added, followed by a slow decline. The

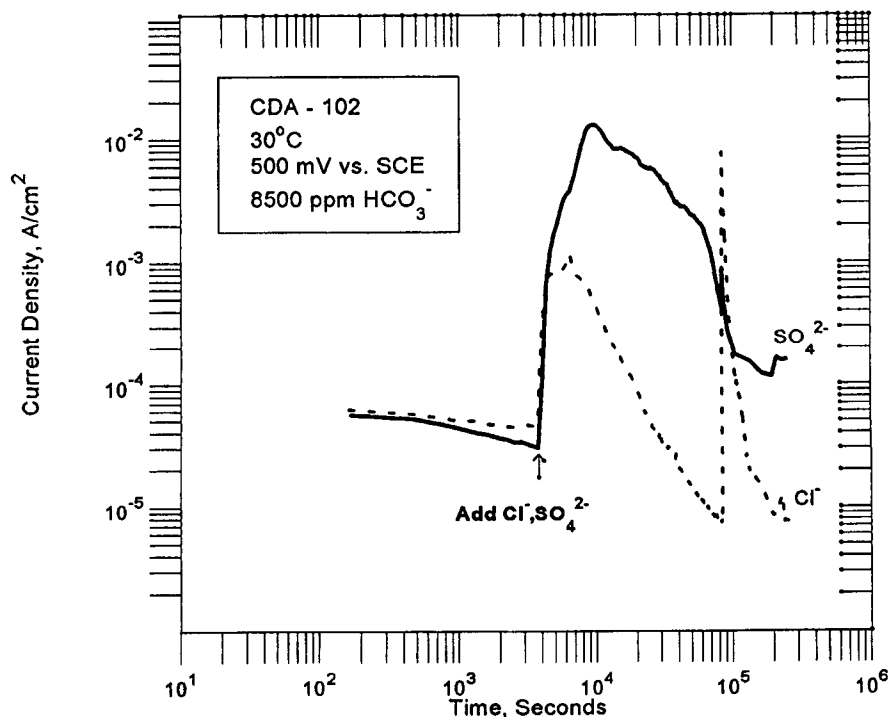


Figure 6-7. Effect of  $\text{Cl}^-$  or  $\text{SO}_4^{2-}$  addition on the anodic current density of CDA-102 under potentiostatic condition at  $25^\circ\text{C}$ . Base solution:  $8500 \text{ ppm HCO}_3^-$ ,  $6 \text{ ppm Cl}^-$ ,  $20 \text{ ppm SO}_4^{2-}$ ,  $10 \text{ ppm NO}_3^-$ ,  $2 \text{ ppm F}^-$ .

decrease in current density, which was more rapid for  $\text{Cl}^-$  solutions, was accompanied by a slow, lateral spreading of green corrosion products. The corrosion product formation was much heavier for the  $\text{SO}_4^{2-}$  solutions. After relatively long periods of time, short spikes in current density were noted, especially for the  $\text{Cl}^-$  solutions. This is probably related to the sloughing off of the corrosion products. Upon removal of the specimens, thick, green corrosion products overlaying red corrosion products were noted on these samples. The corrosion was uniform over the specimen surface. Somewhat similar behavior was noted, although to a much lesser extent, for CDA-715 at room temperature.

At  $95^\circ\text{C}$ , no consistent increase in current density was noted upon addition of  $\text{Cl}^-$  and  $\text{SO}_4^{2-}$  for either alloy. The current density remained at about  $1 \mu\text{A}/\text{cm}^2$  as shown in Figure 6-8 for CDA-715. The CDA-715 specimens retained their Ni-like color while the CDA-102 specimens exhibited a red to dark-brown coloration.

The contrast between the behavior at  $25^\circ\text{C}$  and  $95^\circ\text{C}$  is illustrated in Figure 6-8 for CDA-715. Although a sharp increase in current density is seen long after  $\text{SO}_4^{2-}$  was added, this current increase cannot be attributed to any localized corrosion event. Further experiments are necessary to verify this behavior.

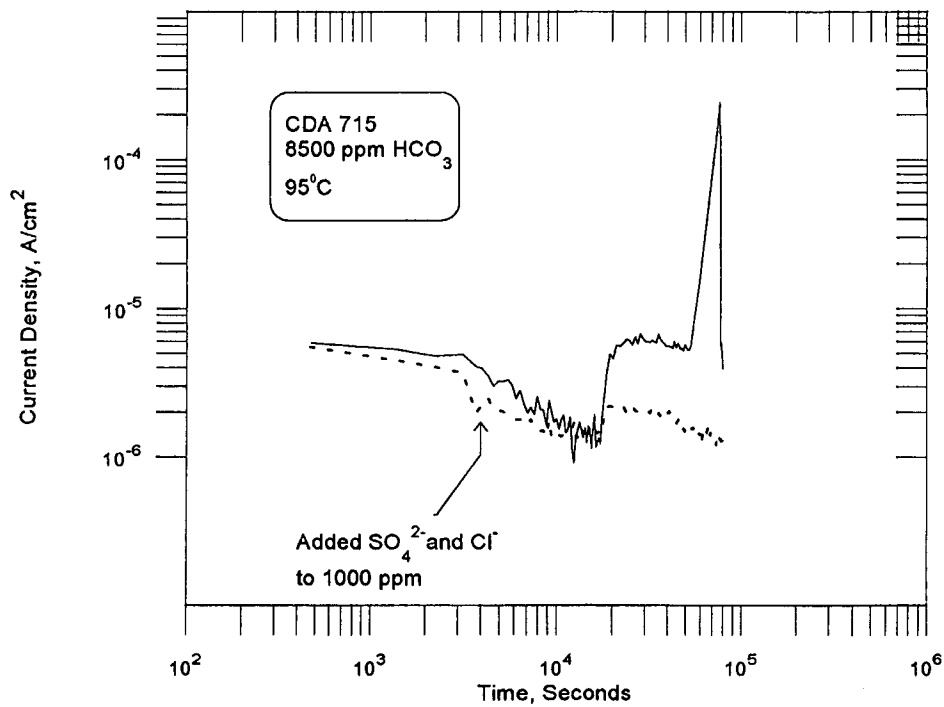


Figure 6-8. Effect of  $\text{Cl}^-$  or  $\text{SO}_4^{2-}$  addition on the anodic current density of CDA-715 under potentiostatic condition at  $95^\circ\text{C}$ . Base solution: 8500 ppm  $\text{HCO}_3^-$ , 6 ppm  $\text{Cl}^-$ , 20 ppm  $\text{SO}_4^{2-}$ , 10 ppm  $\text{NO}_3^-$ , 2 ppm  $\text{F}^-$ .

## 7 SUMMARY AND RECOMMENDATIONS

The corrosion of container materials is being examined in Task 1 of the IWPE program. In the context of NRC's role as a license reviewer, the objective of the CNWRA program is to assess test methodologies for various types of container materials and the applicability of the measured parameters for long-term performance prediction. The experimental investigation to date has concentrated on aqueous corrosion studies of the six DOE candidate alloys, three Fe-Ni-Cr-Mo alloys and three copper-based alloys, and the CNWRA reference material, with a focus on alloy 825. The fundamental approach in the study of localized corrosion has been to use short-term test techniques to delineate the effects of various environmental factors on localized corrosion, and then to examine the use of the parameters derived from short-term tests for their applicability to long-term prediction.

### 7.1 SUMMARY OF CURRENT INVESTIGATIONS

#### 7.1.1 Austenitic Alloys

Assuming the containers are exposed to aqueous environments, the interactive effects of environmental factors over limited ranges of concentrations and temperatures were investigated using a full-factorial test matrix and cyclic polarization test technique. The environmental factors have to be chosen carefully so that they are truly independent. Similarly, the measured parameter has to be chosen so that it is fully characteristic of localized corrosion. Otherwise, the factorial analysis results in a low correlation coefficient. The environmental factors examined were  $\text{Cl}^-$  (6-1000 ppm),  $\text{SO}_4^{2-}$  (20-1000 ppm),  $\text{NO}_3^-$  (10-1000 ppm),  $\text{F}^-$  (2-200 ppm), and temperature (60-95°C). For alloy 825, cyclic polarization curves did not always provide adequate information on the localized corrosion. This was especially true in rather benign environments where pitting did not initiate until high potentials were reached. Hence, a LCI was used which included visual information on the occurrence of localized corrosion. When LCI was used as the measured parameter, and when the environmental factors were chosen carefully, the correlation coefficient of the analysis was very high. Chloride was the most important accelerator of localized corrosion and nitrate was the most important inhibitor of localized corrosion. There was a strong interaction between chloride and nitrate. Temperature, sulfate, and fluoride did not affect localized corrosion significantly. For type 316L stainless steel, there was a good correlation between visual observation of localized corrosion and electrochemical parameters. Chloride was the only factor of importance in accelerating localized corrosion. Other factors are not important within the concentration ranges studied.

The factorial analyses are limited to the ranges of the environmental factors studied and linearity is assumed. Hence, additional experiments were conducted to define the true functional relationship between localized corrosion and chloride concentration. A logarithmic relationship was found between chloride concentration and pit initiation potential,  $E_p$  and repassivation potential,  $E_{rp}$ . The dependence of  $E_{rp}$  on chloride was not as steep as that of  $E_p$ . Other environmental parameters such as pH, bicarbonate, and silica did not have as much of an effect on these parameters as chloride. Presence of oxidizing agents such as  $\text{H}_2\text{O}_2$  increased the corrosion potential of alloy 825 such that it was above the  $E_{rp}$  when the chloride concentration was higher than 100 ppm. If these conditions are found to prevail in the proposed repository environment, alloy 825 may be marginal as a choice of container material.

The use of  $E_{rp}$  as a predictive parameter for localized corrosion was examined in detail. The extent of prior pit growth was not a factor in determining  $E_{rp}$  of alloy 825 and type 316L stainless steel, although it affects repassivation time. However, rate of backward potential scanning was important in determining  $E_{rp}$ . The fast scan technique yields a lower  $E_{rp}$ , which then represents a lower bound parameter for use in long-term prediction. The mechanistic aspects of  $E_{rp}$  were examined. It was found that the  $E_{rp}$  determined by fast scan technique is less sensitive to bulk chloride concentration than that determined by slow scan technique. Because the environment expected to contact the containers may range from distilled water to concentrated solutions, a less environment sensitive parameter such as  $E_{rp}$ , determined by cyclic polarization technique, is more useful for long-term prediction.

Surface chromium depletion has a profound effect on the corrosion behavior of alloy 825. Specimens with surface Cr-depletion exhibited pitting even in a 6 ppm chloride solution at 95°C. More importantly, high rates of uniform dissolution were noted at low potentials in the 1000 ppm chloride solutions. This high rate of uniform dissolution can affect crevice corrosion initiation. This must be investigated further.

Preliminary experiments with alloy C-22 suggest that this alloy is considerably more resistant to localized corrosion than alloy 825. The alloy could not be pitted even at high potentials in solutions with up to 10,000 ppm chloride concentration and 10,000 ppm sulfate concentration at 95°C. However, the cyclic polarization curves exhibited a hysteresis. Hence, the applicability of cyclic polarization test technique to determine  $E_{rp}$  for this type of alloy needs further examination.

### 7.1.2 Copper Based Alloys

The investigation focused on CDA-102 (oxygen-free copper) and CDA-715 (Cu-30 weight percent Ni). A full-factorial experimental design was used along with cyclic polarization technique to determine the combination of environmental factors leading to localized corrosion of CDA-102 and CDA-715. The environmental factors leading to localized corrosion of these alloys are considerably different from the austenitic alloys. The copper-based alloys are also much more complex in their response to environmental changes than the austenitic alloys. Localized corrosion was observed mainly in solutions containing concentrations of bicarbonate above 2000 ppm and at temperature below about 80°C. In one case, minor pitting was noted on CDA-102 in a 85 ppm bicarbonate solution at 95°C. However, the high temperature, 95°C, was beneficial because an adherent black film was formed on the surface and no localized corrosion was observed. The beneficial effect of temperature needs to be studied further. Both chloride and sulfate were detrimental to localized corrosion in the high bicarbonate containing solutions. There was an interaction between chloride and sulfate in reducing the  $E_p$ . Bicarbonate concentration, below about 2000 ppm, promoted active corrosion, perhaps by the formation of soluble cupric complexes.

The pits were shallow and tended to broaden with time. Under potentiostatic conditions, the current associated with pitting increased first as the pits formed, but subsequently decreased as the pits broadened and corrosion product build-up occurred on top of the pits. Periodic increases in current occurred as the corrosion products sloughed off the surface. However, at 95°C, no increase in current was observed as a uniform black film (believed to be CuO) formed on the surface.

Because of pit broadening with time and the general corrosion observed in low bicarbonate environment, the concept of repassivation potential cannot be applied to the copper-based alloys CDA-102 and CDA-715.

## 7.2 RECOMMENDATIONS FOR FURTHER STUDIES

Since any experiment, however long, is going to be of far shorter duration than the required lifetime of the container, performing immersion tests in environments closely resembling the anticipated environments of the repository will only serve to eliminate materials that fail quickly. One concept that is traditionally used in the corrosion field is the acceleration of the environmental conditions (e.g., increased concentration of chloride, increased temperature, or decreased pH). However, the extent of the acceleration is never certain unless it can be judged by field performance, and even then, only if the component fails in the field. Secondly, certain factors such as temperature may not always accelerate corrosion processes. For example, temperatures above a certain value have been shown to retard localized corrosion in steel and stainless steel by formation of a different type of surface film than at lower temperatures. The approach that has been used in the IWPE program is the use of critical potentials such as the repassivation potential. Repassivation potentials have been derived by the use of short-term tests ranging from a few hours to about 14 days. Current experiments have shown that the repassivation potentials derived from the fast-scan technique are lower-bound values and relatively insensitive to pH and chloride concentration. The concept of repassivation potential being the critical potential above which localized corrosion occurs has to be tested over longer periods of time. Based on the experience gained thus far, the following experiments, identified in the current IWPE plan, are recommended for the austenitic alloys:

- Perform long-term experiments, lasting from a few months to 5 years, in environments with different concentrations of chloride, under controlled potential conditions. The potentials should be controlled such that they are above and below the repassivation potentials. The chloride concentration can vary from 1000 ppm to 4 M. Intentional crevices should be included in some specimens. Additionally, some specimens should be tested under mill-finished surface condition to include Cr-depletion as a factor.
- Provide input data to mechanistic modeling of repassivation potential. Some of these data have already been generated by experiments in simulated crevice/pit solutions. Further experiments on measuring the chemical changes in the crevice upon changing external potential are needed to evaluate model predictions. The role of surface Cr-depletion in crevice corrosion needs to be examined further.
- Measure the parameters that determine the corrosion potentials under various anticipated conditions in the repository environment. This includes aeration and radiolytic generation of hydrogen peroxide.
- As mentioned before, alloy C-22 is much more resistant than alloy 825. Further experiments in determining the repassivation potential of this alloy must be performed. Alloy C-4, a possible alternative candidate that is being considered by DOE, is not as resistant to localized corrosion as alloy C-22 (Sridhar, 1987) because of its lower chromium and lack of tungsten as alloying elements.

- None of the tests conducted thus far considered heat-transfer effects and effects of periodic wet-dry cycles. Periodic dry cycles can alter container performance in two ways: (i) by concentrating salts and (ii) by aging of the passive film which alters the electronic properties of the film. The latter aspect can be studied by aging the specimens for various times in dry air and then measuring the critical potentials in an aqueous environment. Eventually, an integrated test considering all three factors must be performed.

Investigation of copper-based alloys has been put on abeyance because they have been de-emphasized by the DOE. However, as indicated in Chapter 6, the beneficial effect of high temperatures must be explored further. On the other hand, the effect of bicarbonate, when present in small concentrations, in promoting active corrosion needs further study under potentiostatic conditions.

## 8 REFERENCES

- Abraham, T., H. Jain, and P. Soo. 1986. *Stress Corrosion Cracking Tests on High-Level Waste Container Materials in Simulated Tuff Repository*. NUREG/CR-4619. Upton, NY: Brookhaven National Laboratories.
- Akkaya, M., and J.R. Ambrose. 1985. The effect of ammonium chloride and fluid velocity on the corrosion behavior of copper in sodium bicarbonate solutions. *Corrosion* 41(12):707-714.
- Alavi, A., and R.A. Cottis. 1987. The Determination of pH, Potential, and Chloride concentration in Corroding Crevices on 304 Stainless Steel and 7475 Aluminum Alloy. *Corrosion Science* 27(5):443-451.
- Azzzerri, N., F. Mancia, and A. Tamba. 1982. Electrochemical prediction of corrosion behavior of stainless steels in chloride containing water. *Corrosion Science* 22:675-687.
- Bates, R.G. 1964. *Determination of pH: Theory and Practice*. New York, NY: J. Wiley & Sons.
- Batista, W., A.M.T. Louvisse, O.R. Mattos, and L. Sathler. 1988. The electrochemical behaviour of Incoloy 800 and AISI 304 stainless steel in solutions that are similar to those within occluded corrosion cells. *Corrosion Science* 28(8):759-768.
- Beavers, J.A., and N.G. Thompson. 1988. *Container Corrosion in High Level Nuclear Waste Repositories*. NRC Contract No. NRC-04-87-009. Year 1, First Semi-annual Report. Columbus, OH: Cortest Columbus Technologies, Inc.
- Beavers, J.A., N.G. Thompson, and C.L. Durr. 1992. *Pitting, Galvanic, and Long-Term Corrosion Studies on Candidate Container Alloys for the Tuff Repository*. NUREG/CR-5709. Columbus, OH: Cortest Columbus Technologies, Inc.
- Bianchi, G., G. Fiori, P. Longhi, and F. Mazza. 1978. "Horse Shoe" Corrosion of Copper Alloys in Flowing Sea Water: Mechanism, and Possibility of Cathodic Protection of Condenser Tubes in Power Stations. *Corrosion* 34:396-406.
- Bogaerts, W.F., and A.A. Van Haute. 1985. Chloride pitting and water chemistry control in cooling or boiler circuits. *Corrosion Science* 25:1149-1161.
- Box, G.E.P., W.G. Hunter, and J.S. Hunter. 1978. *Statistics for Experimenters*. New York, NY: John Wiley & Sons.
- Brookes, H.C., and F.J. Graham. 1989. Influence of the electrolyte and alloy composition on the pitting behavior of stainless steel alloys. *Corrosion* 45(4):287-293.
- Campbell, H.S. 1974. A Review: Pitting Corrosion of Copper and Its Alloys. R.W. Staehle et al., eds. *Localized Corrosion*. Houston, TX: National Association of Corrosion Engineers (NACE): 625-638.

- Covino, B.S. 1987. Fundamentals of Stainless Steel Acid Pickling Processes. *New Steelmaking Technology from the Bureau of Mines*. Bureau of Mines Information Circular 9195. Washington, DC: Bureau of Mines. Office of Technology Transfer.
- Cragolino, G.A., and N. Sridhar. 1990a. Integrated waste package experiments. *Report on Research Activities for the Quarter April 1 Through June 30, 1990*. W.C. Patrick, ed. CNWRA 90-02Q. San Antonio, TX: CNWRA.
- Cragolino, G.A., and N. Sridhar. 1990b. Integrated waste package experiments. *Report on Research Activities for the Quarter July 1 Through September 30, 1990*. W.C. Patrick, ed. CNWRA 90-03Q. San Antonio, TX: CNWRA.
- Cragolino, G.A., and N. Sridhar. 1991a. Integrated waste package experiments. *Report on Research Activities for Calendar Year 1990*. W.C. Patrick, ed. NUREG/CR-5817. CNWRA 91-01A. San Antonio, TX: CNWRA.
- Cragolino, G.A., and N. Sridhar. 1991b. Integrated waste package experiments. *Report on Research Activities for the Quarter January 1 Through March 31, 1991*. W.C. Patrick, ed. CNWRA 91-01Q. San Antonio, TX: CNWRA.
- Cragolino, G.A., and N. Sridhar. 1991c. Integrated waste package experiments. *Report on Research Activities for the Quarter April 1 Through June 30, 1991*. W.C. Patrick, ed. CNWRA 91-02Q. San Antonio, TX: CNWRA.
- Cragolino, G.A., and N. Sridhar. 1991d. Integrated waste package experiments. *Report on Research Activities for the Quarter July 1 Through September 30, 1991*. W.C. Patrick, ed. CNWRA 91-03Q. San Antonio, TX: CNWRA.
- Cragolino, G.A., and N. Sridhar. 1991e. *A Review of Localized Corrosion of High-Level Nuclear Waste Container Materials — I*. CNWRA 91-004. San Antonio, TX: CNWRA.
- Cragolino, G.A., and N. Sridhar. 1991f. Localized corrosion of a candidate container material for high-level nuclear waste disposal. *Corrosion* 47(6):464-472.
- Cragolino, G.A., and N. Sridhar. 1992a. Integrated waste package experiments. *Report on Research Activities for Calendar Year 1991*. W.C. Patrick, ed. NUREG/CR-5817. Vol. 2. CNWRA 91-01A. San Antonio, TX: CNWRA.
- Cragolino, G.A., and N. Sridhar. 1992b. Integrated waste package experiments. *Report on Research Activities for the Period January 1 Through June 30, 1992*. W.C. Patrick, ed. CNWRA 92-01S. San Antonio, TX: CNWRA.
- Crolet, J.L., L. Séraphin and R. Tricot. 1976. Influence de la teneur en chlorure sur le pH de dép passivation des aciers inoxydables. *Mémoires Scientifiques Revue Métallurgie*. 73(1):1-8.

- De Chialvo, M.R.G., R.C. Salvarezza, D. Vasquez Moll, and A.J. Arvia. 1985. Kinetics of passivation and pitting corrosion of polycrystalline copper in borate buffer solutions containing sodium chloride. *Electrochimica Acta* 30(11):1501-1511.
- DOE Site Characterization Plan. 1988. *Site Characterization Plan, Yucca Mountain Site, Nevada Research and Development Area*. DOE/RW-0199. U.S. Department of Energy. Office of Civilian Radioactive Waste Management. Volume III, Part A. Chapter 7: 19-105.
- Dong, S., Y. Xie, and G. Cheng. 1992. Cyclic voltammetric and spectroelectrochemical studies of copper in alkaline solution. *Electrochimica Acta* 37(1):17-22.
- Drogowska, M., L. Brossard, and H. Menard. 1992. Copper dissolution in  $\text{NaHCO}_3$  and  $\text{NaHCO}_3 + \text{NaCl}$  aqueous solutions at pH 8. *J. Electrochemical Society* 139(1):39-47.
- Efird, K.D., and E.D. Verink. 1977. The Crevice Protection Potential for 90-10 Copper Nickel. *Corrosion* 33:328-331.
- Fabis, P.M., and B.S. Covino. 1986. Near surface elemental concentration gradients in annealed 304 stainless steel as determined by analytic electron microscopy. *Oxidation of Metals* 25(5/6): 397-407.
- Farmer, J.C., R.A. van Konynenburg, R.D. McCright, and G.E. Gdowski. 1988. *Survey of Degradation Modes of Candidate Materials for High-Level Radioactive-Waste Disposal. Volume 5. Localized Corrosion of Copper-Based Alloys*. UCID-21362. Vol. 5. Livermore, CA: LLNL.
- Fukuda, T., and M. Akashi. 1992. The effect of chloride concentration for the crevice corrosion initiation of c.p.- titanium used for nuclear waste package. *Proceedings of the Annual Corrosion Conference. Corrosion/92*. Houston, TX: National Association of Corrosion Engineers (NACE). Paper No. 92.
- Galvele, J.R. 1976. Transport processes and the mechanism of pitting of metals. *J. Electrochemical Society* 123(4):464-474.
- Galvele, J.R. 1981. Transport processes in passivity breakdown — II. Full hydrolysis of the metal ions. *Corrosion Science* 21(8):551-579.
- Glass, R.S., G.E. Overturf, R.A. van Konynenburg, and R.D. McCright. 1986. Gamma radiation effects on corrosion—I. Electrochemical mechanisms for the aqueous corrosion processes of austenitic stainless steels relevant to nuclear waste disposal in tuff, *Corrosion Science* 26(8): 577-590.
- Glassley, W.E. 1986. Reference Waste Package Environment Report. UCRL-53726. Livermore, CA: LLNL.
- Glassley, W.E. 1990. Geochemical Interactions. Presentation to the Nuclear Waste Technical Review Board, January 18-19, 1990, Pleasanton, CA. Livermore, CA: LLNL.

- Gravano, S.M., and J.R. Galvele. 1984. Transport processes in passivity breakdown — III. Full hydrolysis plus ion migration plus buffers. *Corrosion Science* 24(6):517-534.
- Grubb, J.F. 1991. Pickling and Surface Chromium-Depletion of Corrosion Resistant Alloys. *Stainless Steels '91. Proceedings of International Conference on Stainless Steels*. China, Japan: The Iron and Steel Institute of Japan. 944-951.
- Hakkarainen, T. 1983. Repassivation of corrosion pits in stainless steel. M. Froment, ed. *Passivity of Metals and Semiconductors*. Elsevier Science Publishers B. V., Amsterdam, The Netherlands: 367.
- Hakkarainen, T. 1990. Electrochemical Conditions inside Growing Pits in Stainless Steel. *Advances in Localized Corrosion*. H. Isaacs et al. (eds.). Houston, TX: NACE: 277-282.
- Jallerat, N., F.L. Pari, F. Bourelier, and K. Vu Quang. 1984. Specific inhibition effect of carbonate and bicarbonate ions on pitting corrosion of stainless steels and Ni-base alloys. *Proc. 9th International Congress on Metallic Corrosion, Vol. 4*. Ottawa, Canada: National Research Council: 404-406.
- Kerrisk, J.F. 1987. Groundwater Chemistry at Yucca Mountain, Nevada, and Vicinity. LA-10929-MS. Los Alamos, NM: Los Alamos National Laboratory (LANL).
- Kim, Y.J., and R.A. Oriani. 1987. Corrosion properties of the oxide film formed on grade 12 titanium in brine under gamma radiation, *Corrosion* 43:(2):85-97.
- Knauss, K.G., W.J. Beiriger, and D.W. Peifer. 1985. Hydrothermal Interaction of Crushed Topopah Spring Tuff and J-13 Water at 90, 150, and 250°C Using Dickson-Type, Gold-bag Rocking Autoclaves. UCRL-53630. Livermore, CA: LLNL.
- Knauss, K.G., T.J. Wolery, and K.J. Jackson. 1990. A new approach to measuring pH in brines and other concentrated electrolytes. *Geochimica et Cosmochimica Acta* 54:1519-1523.
- Leckie, H.P., and H.H. Uhlig. 1966. Environmental factors affecting the critical potential for pitting in 18-8 stainless steel. *J. Electrochemical Society* 113(12):1262-1267.
- Lee, Y.D., Y.H. Lee, J.S. Lee, and J.K. Kim. 1991. Descaling Behavior of Types 304 and 430 Annealed Strips. *Stainless Steels '91. Proceedings of International Conference on Stainless Steels*. China, Japan: The Iron and Steel Institute of Japan: 952-958.
- Lott, S.E., and R.C. Alkire. 1989. The role of inclusions on initiation of crevice corrosion of stainless steel. *J. Electrochemical Society*. 136(11):3256-3262.
- Luo, J.L., Y.C. Lu, and M.B. Ives. 1992. The Use of Microelectrodes to Determine the Local Conditions Within Active Pits, Paper No. 233. CORROSION/92. Houston, TX: NACE.
- Macdonald, D.D., and M. Urquidi-Macdonald, 1990. Thin-Layer Mixed-Potential Model for Corrosion of High-Level Nuclear Waste Canisters. *Corrosion* 46(5):380-390.

- Macdonald, D.D., and M. Urquidi-Macdonald. 1992. Corrosion Damage Function—Interface Between Corrosion Science and Engineering. *Corrosion* 48(5):354-367.
- Marcus, Y. 1989. Determination of pH in highly saline waters. *Pure & Applied Chemistry* 61:1133-1138.
- Mason, R.L., R.F. Gunst, and J.L. Hess. 1989. *Statistical Design & Analysis of Experiments*. New York, NY: John Wiley & Sons.
- Mattsson, E., and A.M. Fredriksson. 1968. Pitting Corrosion in Copper Tubes — Cause of Corrosion and Counter Measures. *British Corrosion Journal* 3:246-257.
- Mayer, S.T., and R.H. Muller. 1992. An in-situ Raman spectroscopic study of the anodic oxidation of copper in alkaline media. *J. Electrochemical Society* 139(2):426-433.
- McCright, R.D. 1988. *An Annotated History of Container Candidate Materials Selection*. UCID-21472. Livermore, CA: LLNL
- McCright, R.D., W.G. Halsey, G.E. Gdowski, W.L. Clarke. 1991. Candidate Container Materials for Yucca Mountain Waste Package Designs. *Proceedings of the Topical Meeting on Nuclear Waste Packaging. Focus '91*. La Grange Park, IL: American Nuclear Society (ANS): 125-135.
- McGuire, G.E., A.L. Bacarella, J.C. Griess, R.E. Clausing, and L.D. Hulett. 1978. Analysis of protective oxide films on copper-nickel alloys by Auger spectroscopy. *J. Electrochemical Society* 125(11):1801-1804.
- Milosev, I., M. Metikos-Hukovic, M. Drogowska, H. Menard, and L. Brossard. 1992. Breakdown of passive film on copper in bicarbonate solutions containing sulfate ions. *J. Electrochemical Society* 139(9):2409-2418.
- Nakayama, T., and K. Sasa. 1976. Effect of ultrasonic waves on the pitting potentials of 18-8 stainless steel in sodium chloride solution. *Corrosion* 32:283-285.
- Nakayama, G. and Akashi, M. 1991. The critical condition for initiation of localized corrosion of mild steel used for nuclear waste package. T. Abrajano, and L.H. Johnson, eds. *Scientific Basis for Nuclear Waste Management XIV. Materials Research Society Symposium Proceedings. Vol. 212*. Pittsburgh, PA: Materials Research Society (MRS): 279-286.
- Newman, R.C. 1983. Protection potentials for pitting of stainless steel in neutral chloride solutions. *Corrosion Science* 23:1045-1046.
- Newman, R.C., and E.M. Franz. 1984. Growth and repassivation of single corrosion pits in stainless steel. *Corrosion* 40:325-330.
- Notoya, T. 1990. Ant Nest Corrosion in Copper Tubing. *Corrosion Engineering* 39:353-362.

- Okayama, S., Y. Uesugi, and S. Tsujikawa. 1987a. The effect of alloying elements on the repassivation potential for crevice corrosion of stainless steels in 3% NaCl solution. *Corrosion Engineering* 36:157-168.
- Okayama, S., S. Tsujikawa, and K. Kikuchi. 1987b. Effects of alloying elements on the stainless steels depassivation pH. *Corrosion Engineering* 36:631-638.
- Oldfield, J.W., and W.H. Sutton. 1978a. Crevice corrosion of stainless steels — I. A mathematical model. *British Corrosion Journal* 13(1):13-22.
- Oldfield, J.W., and W.H. Sutton. 1978b. Crevice corrosion of stainless steels — II. Experimental studies. *British Corrosion Journal* 13(3):104-111.
- Oversby, V.M. 1985. The Reaction of Topopah Spring Tuff with J-13 Water at 150°C—Samples from Drill Cores USW G-1, USW GU-3, USW G-4, and UE-25h#1. UCRL-53629. Livermore, CA: LLNL.
- Pabalan, R.T. 1989. Test of Technical Procedure for Preparing Simulated and Modified J-13 Well Water. Internal Memorandum. CNWRA. August 10, 1989.
- Pabalan, R.T. and W. Murphy. 1991. Geochemical Modeling. *Report on Research Activities for Calendar Year 1990*. W.C. Patrick, ed. NUREG/CR-5817. Washington, DC: U.S. NRC: 2-24 to 2-25.
- Pabalan, R.T., W.M. Murphy, and P. Bertetti. 1990. Unsaturated Mass Transport (Geochemistry). *Report on Research Activities for the Quarter July 1 through September 30, 1990*. CNWRA 90-03Q. San Antonio, TX: CNWRA.
- Patrick, W.C. 1986. *Spent Fuel Test — Climax: An Evaluation of the Technical Feasibility of Geologic Storage of Spent Nuclear Fuel in Granite*. Final Report, UCRL-53702. Livermore, CA: LLNL.
- Perez Sanchez, M., M. Barrera, S. Gonzalez, and R.M. Souto. 1990. Electrochemical behavior of copper in aqueous moderate alkaline media containing sodium carbonate and bicarbonate and sodium perchlorate. *Electrochimica Acta* 35(9):1337-1343.
- Peters, D.T., and K.J.A. Kundig. 1991. Copper and copper alloys as containers for radioactive waste disposal. Part 1: A critical review of the literature on corrosion in prospective repository environments. *Waste Management '91*. Tucson, AZ.
- Pickering, H.W. 1990. A Critical Review of IR Drops and Electrode Potentials Within Pits, Crevices, and Cracks. *Advances in Localized Corrosion*. H. Isaacs et al., eds. Houston, TX: NACE: 77-91.
- Place, M.C., P.R. Rhodes, and R.D. Mack. 1991. Qualification of Corrosion Resistant Alloys for Sour Service. Paper No. 91-1. CORROSION/91. Houston, TX: NACE.

- Pourbaix, M. 1974. The Electrochemical Basis for Localized Corrosion. *Localized Corrosion*. R.W. Staehle, B.F. Brown, J. Kruger, and A. Agrawal, eds. Houston, TX: NACE: 12-33.
- Ramirez, A.L., (ed.). 1991. *Prototype Engineered Barrier System Field Test (PEBSFT) Final Report*. UCRL-ID-106159. Livermore, CA: LLNL.
- Reed, D.T., and R.A. van Konynenburg. 1990. Progress in Evaluating the Corrosion of Candidate HLW Container Metals in Irradiated Air-Steam Mixtures. *Proceedings of the Topical Meeting on Nuclear Waste Packaging. Focus '91*. La Grange Park, IL: ANS: 185-192
- Reed, D.T., and R.A. van Konynenburg. 1991. Corrosion of Copper-Based Materials in Irradiated Moist-Air Systems, 317, Scientific Basis for Nuclear Waste Management XIV, T. A. Abrajano, Jr. and L. H. Johnson, eds. MRS Symposium Proceedings, Vol. 212. Pittsburgh, PA: MRS: 317.
- Reed, D.T., V. Swayambunathan, B.S. Tani, and R.A. van Konynenburg. 1990. Corrosion Product Identification and Relative Rates of Corrosion of Candidate Metals in an Irradiated Air-Steam Environment. Scientific Basis for Nuclear Waste Management XIII, V.M. Oversby and P.W. Brown, eds. MRS Symposium Proceedings, Vol. 176. Pittsburgh, PA: MRS: 517-524.
- Rosenfeld, I.L. and I.S. Danilov. 1967. Electrochemical aspects of pitting corrosion. *Corrosion Science* 7:129-142.
- Rosenfeld, I.L., I.S. Danilov, and R.N. Oranskaya. 1978. Breakdown of the passive state and repassivation of stainless steels. *J. Electrochemical Society* 125(11):1729-1735.
- Shalaby, H.M., F.M. Al-Kharafi, and V.K. Gouda. 1989. A Morphological Study of Pitting Corrosion of Copper in Soft Tap Water. *Corrosion* 45:536-547.
- Sharland, S.M. 1992. A mathematical model of the initiation of crevice corrosion in metals. *Corrosion Science* 33(2):183-201.
- Shoesmith, D.W., T.E. Rummery, D. Owen, and W. Lee. 1976. Anodic oxidation of copper in alkaline solutions. *J. Electrochemical Society* 123(6):790-799.
- Short, D.W., D.J. Ruffner, and L.J. Jardine. 1991. Engineered Barrier System and Waste Package Design Concepts for a Potential Geologic Repository at Yucca Mountain. *Proceedings of the Topical Meeting o Nuclear Waste Packaging Focus '91*. La Grange Park, IL: ANS: 113-124.
- Spinks, J.W.T., and R.J. Woods. 1990. Introduction to Radiation Chemistry, 3<sup>rd</sup> Edition, J. Wiley & Sons, Inc., New York, NY.
- Sridhar, N. 1987. Behavior of Nickel-Base Alloys in Corrosive Environments. *Metals Handbook. Volume 13. Corrosion*. Materials Park, OH: ASM International: 643-647.

- Sridhar, N., G.A. Cragnolino, and F.F. Lyle. 1990. Progress Report of Activities and Recommendations in the Integrated Waste Package Experimental Program. May 1988-April 1990. CNWRA Task Activity 20-3704-042-005-900. San Antonio: TX: CNWRA.
- Sridhar, N., G.A. Cragnolino, H. Pennick, and T.Y. Torng. 1991. Application of a Transient Crevice corrosion Model to the Prediction of Performance of High-level Nuclear Waste Container Materials. *International Symposium on Life Prediction of Corrodible Structures*. R.N. Parkins, ed. Houston, TX: NACE.
- Sridhar, N., and G.A. Cragnolino. 1992. The effect of environment on localized corrosion of copper based high-level nuclear waste container materials. *Corrosion/92*. Houston, TX: NACE. Paper No. 92-121.
- Sridhar, N., and G.A. Cragnolino. 1993. Long-term life prediction of localized corrosion of Fe-Ni-Cr-Mo high-level nuclear waste container materials. *Corrosion/93*. Houston, TX: NACE. Paper No. 93-197.
- Sridhar, N., G.A. Cragnolino, J.C. Walton, and D. Dunn. 1993a. Prediction of crevice corrosion using modeling and experimental techniques. *Application of Accelerated Corrosion Tests to Service Life Prediction of Materials*. G. Cragnolino and N. Sridhar, ed. ASTM STP-1194. Philadelphia, PA: ASTM.
- Sridhar, N., G.A. Cragnolino, and D. Dunn. 1993b. Integrated waste package experiments. *Report on Research Activities for the Period July 1 Through December 31, 1992*. W.C. Patrick, ed. CNWRA 92-02S. San Antonio, TX: CNWRA.
- Starr, K.K., E.D. Verink, Jr., and M. Pourbaix. 1976. The significance of the protection potential for Fe-Cr alloys at room temperature. *Corrosion* 32:47-51.
- Strehblow, H.-H., and B. Titze. 1980. The investigation of the passive behavior of copper in weakly acid and alkaline solutions and the examination of passive film by ESCA and ISS. *Electrochimica Acta*. 25:839-850.
- Strehblow, H.-H. 1984. Breakdown of passivity and localized corrosion: theoretical concepts and fundamental experimental results. *Werkstoffe und Korrosion* 35:437-448.
- Stumm, W., and J.J. Morgan. 1981. *Aquatic Chemistry*. 2nd. ed. New York, NY: John Wiley & Sons.
- Syrett, B.C., and S.S. Wing. 1980. Effect of Flow on Corrosion of Copper-Nickel Alloys in Aerated Sea Water and in Polluted Sea Water. *Corrosion* 36:73-85.
- Szklarska-Smialowska, Z. 1986. *Pitting Corrosion of Metals*. Houston, TX: NACE: 201-236.
- Tester, J.W. and H.S. Isaacs. 1975. Diffusional effects in simulated localized corrosion. *J. Electrochemical Society* 122(11):1438-1445.

- Thomas, J.G.N., and A.K. Tiller. 1972a. Formation and Breakdown of Surface Films on Copper in Sodium Hydrogen Carbonate and Sodium Chloride Solutions—Effects of Anion Concentrations. *British Corrosion Journal* 7:256-262.
- Thomas, J.G.N., and A.K. Tiller. 1972b. Formation and Breakdown of Surface Films on Copper in Sodium Hydrogen Carbonate and Sodium Chloride Solutions—Effects of Temperature and pH. *British Corrosion Journal* 7:263-267.
- Thompson, N. G., and B. C. Syrett. 1992. Relationship Between Conventional Pitting and Protection Potentials and a New, Unique Pitting Potential. *Corrosion* 48(8):649-659.
- Thompson, N. G., J.A. Beavers, and C. L. Durr. 1992. *Potentiodynamic Polarization Studies on Candidate Container Alloys for the Tuff Repositories*. NUREG/CR-5708. Columbus, OH: Cortest Columbus Technologies, Inc.
- Tromans, D., and R. Sun. 1992. Anodic behavior of copper in weakly alkaline solutions. *J. Electrochemical Society*. 139(7): 1945-1951.
- Tsujikawa, S., and Y. Hisamatsu. 1984. Repassivation potential as a crevice corrosion characteristic for austenitic and ferritic stainless steels. *Improvement of Corrosion Resistance of Structural Materials in Aggressive Media*. Ya. M. Kolotyркиn, ed. Moscow: Russia: Nauka Publishers.
- Tsujikawa, S., Y. Soné, and Y. Hisamatsu. 1987. Analysis of Mass Transfer in a Crevice Region for a Concept of the Repassivation Potential as a Crevice-Corrosion Characteristic. A. Turnbull, ed. *Corrosion Chemistry Within Pits, Crevices, and Cracks*. Her Majesty's Stationery Office. London: United Kingdom: 171-186.
- Turnbull, A. 1983. The solution composition and electrode potential in pits, crevices and cracks. *Corrosion Science* 23(8):833-870.
- Van Konynenburg, R.A. 1986. Radiation Chemical Effects in Experiments to Study the Reaction of Glass in an Environment of Gamma-Irradiated Air, Groundwater, and Tuff. UCRL-53719. Livermore, CA: LLNL.
- Walton, J.C., and S.K. Kalandros. 1992. *TWITCH — A Model for Transient Diffusion, Electromigration, and Chemical Reaction in One Dimension*. CNWRA 92-019. San Antonio, TX: CNWRA.
- Watson, M., and J. Postlethwaite. 1990. Numerical simulation of crevice corrosion of stainless steels and nickel alloys in chloride solutions *Corrosion* 46(7):522-530.
- Westerman, R.E., S.G. Pitman, and J.H. Haberman. 1987. Corrosion Testing of 304L Stainless Steel in Tuff Groundwater Environments. UCRL-21005. Livermore, CA: LLNL.
- Wilde, B.E., and E. Williams. 1971. The relevance of accelerated electrochemical pitting tests to the long-term pitting and crevice corrosion behavior of stainless steel in marine environments. *J. Electrochemical Society* 118:1057-1062.

- Wilde, B.E. 1974. On Pitting and Protection Potentials: Their use and possible misuses for predicting localized corrosion resistance of stainless alloys in halide media. *Localized Corrosion*. R.W. Staehle, B.F. Brown, J. Kruger, and A. Agrawal, eds. Houston, TX: NACE: 342-352.
- Yashiro, H., and K. Tanno. 1990. The effect of electrolyte composition on the pitting and repassivation behavior of AISI 304 stainless steel at high temperature. *Corrosion Science* 31:485-490.
- Yunker, W.H. 1990. Corrosion Behavior of Copper-base Materials in a Gamma-irradiated Environment, Final Report. WHC-EP-0188. Westinghouse Hanford Co., Richland, WA.
- Zimmerman, R.M., R.L. Schuch, D.S. Mason, M.L. Wilson, M.E. Hall, M.P. Board, R.P. Bellman, and M.P. Blanford. 1986. *Final Report: G-Tunnel Heated Block Experiment*. SAND84-2620. Albuquerque, NM: Sandia National Laboratories (SNL).

**APPENDIX A**

**CHARACTERIZATION OF PLATES OF ALLOYS  
TESTED IN THE IWPE PROGRAM**

## CHARACTERIZATION OF PLATES OF ALLOYS TESTED IN THE IWPE PROGRAM

The pedigree and chemical compositions of the alloys examined thus far in the IWPE program are shown in Tables A-1 through A-3. Generally, there was reasonable agreement between the analyses of the manufacturer and Charles Kawin Co., who performed the independent analyses for CNWRA. However, significant difference in carbon content was found for alloy C-22, with the Kawin analysis indicating a higher carbon concentration. The analysis supplied by the manufacturer is generally after primary melting operation but before secondary melting in the Electroslag Remelting (ESR) stage and subsequent processing. In contrast, the Kawin analysis was performed on the final plate. It is not unusual for some carbon pick-up to occur between primary melting and secondary melting operations. The mechanical properties supplied by the manufacturers are shown in Table A-4.

The microstructures of the as-received plates are shown in Figures A-1 through A-8. The microstructures of types 304L and 316L stainless steels (Figures A-1 and A-2) are typical of hot-rolled and annealed products. Elongated inclusions are visible in the microstructures of these alloys which are probably MnS inclusions. The microstructure of alloy 825 (Figure A-3) indicates a wide variation in grain size. This may be typical of hot-rolled and annealed product of this alloy. The dual grain size can result from a low annealing temperature where insufficient time is given for grain growth. It must be noted that this alloy, which is stabilized by the addition of Ti, is given a stabilizing treatment at temperatures lower than the solution annealing treatment to avoid sensitization. The higher magnification view (Figure A-4) does not show any grain boundary precipitation. Cuboidal particles of Ti(C,N) can be seen in the microstructure. The microstructure of alloy C-22 also appears free of grain boundary precipitates although primary carbides can be seen in the form of strings of dark particles (Figures A-5). The microstructure of CDA-102 (Figure A-6) represents a fully recrystallized structure, typical of this product. The inclusion content is low. The microstructure of CDA-715 (Figure A-7) indicates a hot-rolled and annealed microstructure. The bent annealing twins in this microstructure may represent either residual cold work or an artifact of the metallographic process such as excessive grinding. This was not examined further. The dark particles that are strung along the rolling direction may be iron-rich particles. The microstructure of CDA-613 (Figure A-8) indicates an as-hot worked state with a large number of inter- and intra-boundary precipitates. The dark particles were analyzed by SEM-EDX, and were found to be rich in Fe and Al. Hence, these particles may be a Fe, Al intermetallic that is common in this alloy system (Cragolino and Sridhar, 1990a). Reannealing this material at 815°C (1500°F) for 30 minutes followed by water quenching resulted in a more recrystallized microstructure, with relatively clean grain boundaries. However, this was not pursued further because CDA-613 was de-emphasized in the program.

**Table A-1. Heat numbers and suppliers of alloys examined in the IWPE Project. All alloys supplied as 12 mm (0.5 inch) plates.**

<b>Alloy</b>	<b>Manufacturer</b>	<b>Vendor</b>	<b>Heat No.</b>	<b>Specification</b>
Type 304L SS (UNS S30403)	G.O. Carlson	E.M. Jorgenson	TO954-A64B	ASTM A 240-87
Type 316L SS (UNS S31603)	Eastern Stainless	E.M. Jorgenson	P80746	ASTM A 240-87
Alloy 825 (UNS N08825)	Inco Alloys Intl.	Metal Goods	HH4371FG	ASTM B 424-84
Alloy C-22 (UNS N06022)	Haynes Intl.	Metal Goods	2277-8-3175	ASTM B 575-86
CDA-102 (UNS C10200)	Revere Copper	H.M. Hillman Brass & Copper	6681	ASTM B 152
CDA-715 (UNS C71500)	Revere Copper	H.M. Hillman Brass & Copper	7037 - 6132A	ASTM B 171
CDA 613 (UNS C61300)	Ampco Metal	Ampco Metal	M5459	ASTM B 169-85A

Table A-2. Chemical compositions of austenitic alloys tested in the IWPE program.

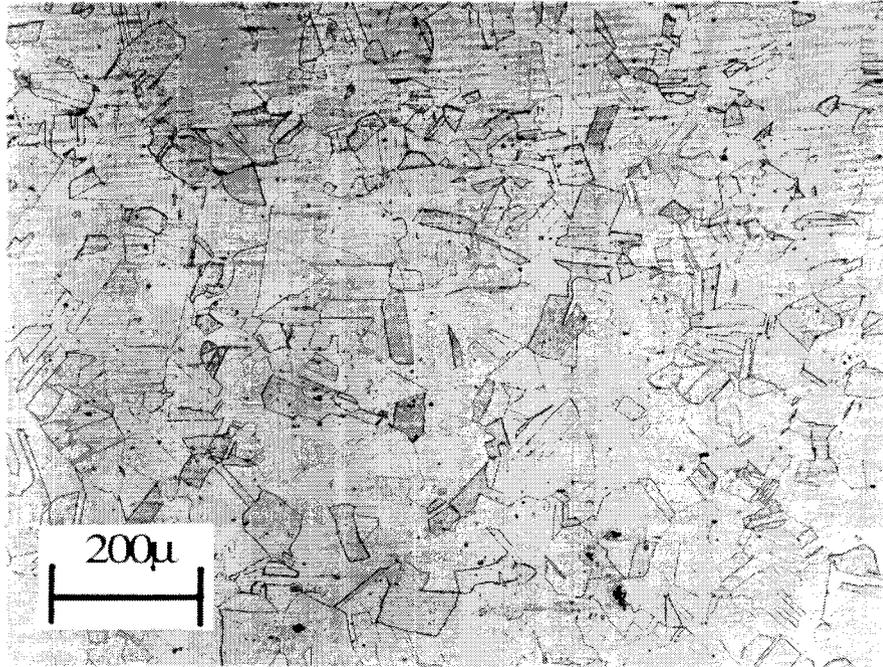
Alloy	Source of Analyses	Elemental Composition, wt. %										
		Al	C	Cr	Cu	Fe	Mn	Mo	Ni	P	S	Others
Type 304L SS	Manufacturer	—	0.022	18.3	—	Bal.	1.46	—	9.14	0.026	0.005	Si:0.47 N:0.07
	Kawin	—	0.029	18.44	0.19	Bal.	1.38	0.15	9.00	0.024	0.005	Si:0.44 N:0.07
Type 316L SS	Manufacturer	—	0.014	16.35	0.27	Bal.	1.58	2.07	10.04	0.026	0.018	Si:0.49 N:0.06
	Kawin	—	0.019	16.64	0.29	Bal.	1.56	2.16	10.43	0.025	0.014	Si:0.45 N:0.06
Alloy 825	Manufacturer	0.07	0.010	22.09	1.79	30.41	0.35	3.21	41.06	—	—	Si:0.19 Ti:0.82
	Kawin	0.05	0.013	22.98	1.80	28.09	0.33	3.56	41.76	0.008	0.003	Si:0.13 Ti:0.93
Alloy C-22	Manufacturer	—	0.004	21.40	—	3.80	0.12	13.60	Bal.	0.008	—	Si:0.03 W:3.00 V:0.15
	Kawin	0.18	0.015	21.97	—	4.42	0.13	14.25	Bal.	0.005	0.002	Si:0.06 W:2.98 V:0.16

Table A-3. Chemical compositions of copper-based alloys tested in the IWPE program.

Alloy	Source of Analyses	Elemental Composition, wt.%										
		Al	C	Cr	Cu	Fe	Mn	Mo	Ni	P	S	Others
CDA-102	Manufacturer	—	—	—	99.95	—	—	—	—	—	—	—
	Kawin	—	—	—	99.95	—	—	—	—	0.001	0.002	O:0.004
CDA-715	Manufacturer	—	0.013	—	69.20	0.54	0.57	—	29.57	0.004	0.006	Pb:0.010
	Kawin	—	0.019	—	68.95	0.55	0.62	—	29.85	0.001	0.011	Pb:0.004
CDA-613	Manufacturer	6.66	—	—	90.61	2.44	—	—	0.03	0.006	—	Sn:0.3
	Kawin	7.05	0.005	—	89.93	2.56	0.02	—	0.02	0.001	0.001	Sn:0.3

**Table A-4. Mechanical properties of the plates. Data supplied by the manufacturers.**

<b>Alloy</b>	<b>Yield Strength MPa (Ksi)</b>	<b>Tensile Strength MPa (Ksi)</b>	<b>% Elongation</b>	<b>% Reduction in Area</b>	<b>Hardness</b>
Type 304L SS	257.2 (37.3)	559.2 (81.1)	65	65	BHN 150
Type 316L SS	282.0 (40.9)	588.8 (85.4)	60	66	BHN 148
Alloy 825	291.7 (42.3)	664.0 (96.3)	48	71	R <sub>B</sub> 81
Alloy C-22	372.3 (54.0)	779.1 (113.0)	68	—	—
CDA-102	79.3 (11.5)	211.0 (30.6)	65	—	R <sub>F</sub> 44
CDA-715	362.7 (52.6)	468.9 (68.0)	30	—	—
CDA-613	272.7 (39.6)	525.7 (76.3)	47.5	—	—



**Figure A-1. Microstructure of the transverse section of type 304L stainless steel. Magnification 100X.**

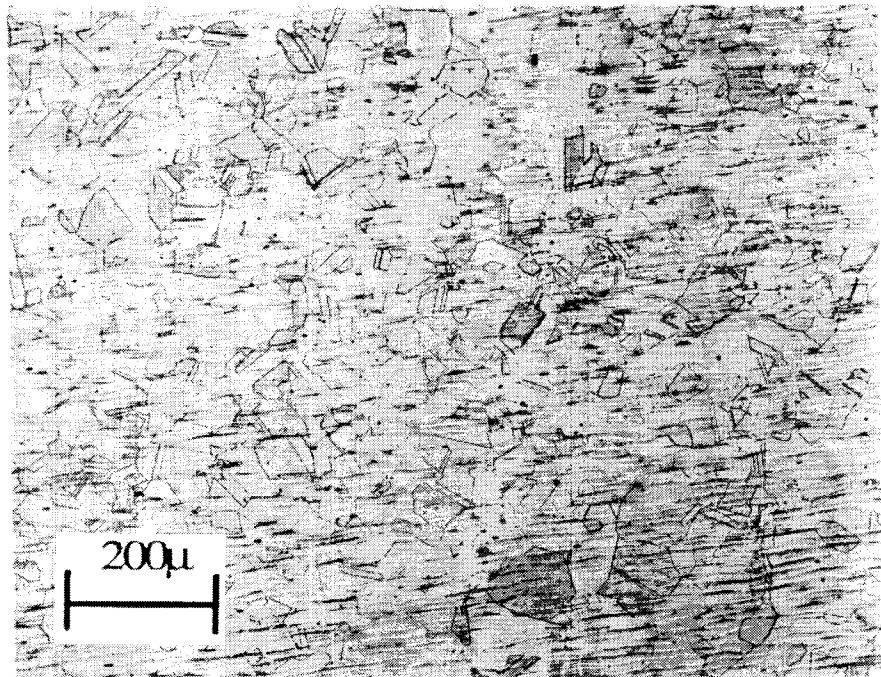


**Figure A-2. Microstructure of the transverse section of type 316L stainless steel. Magnification 100X.**

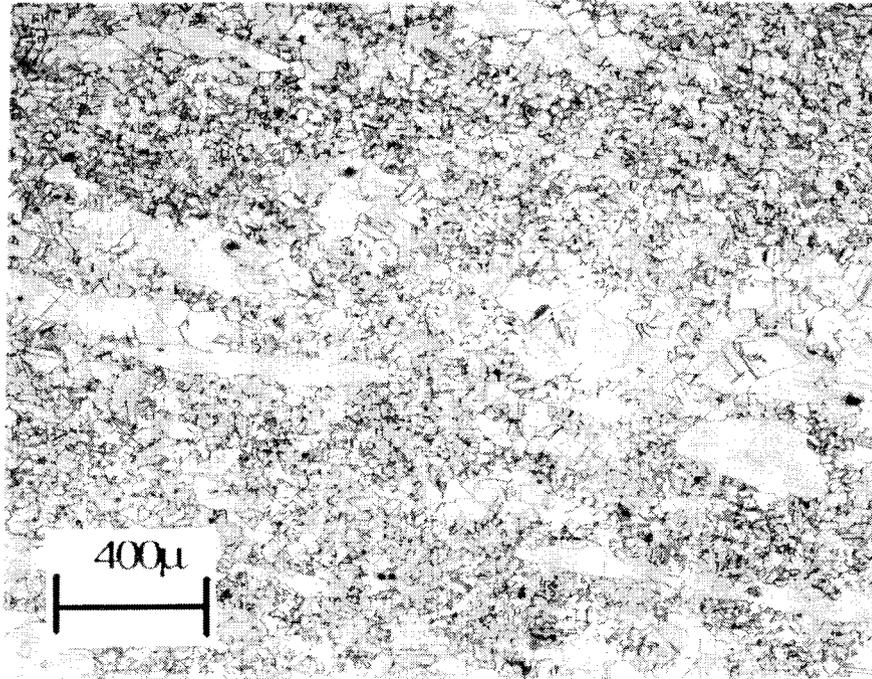


**Figure A-3. Microstructure of the transverse section of alloy 825 in the as-received condition. Magnification 50X.**

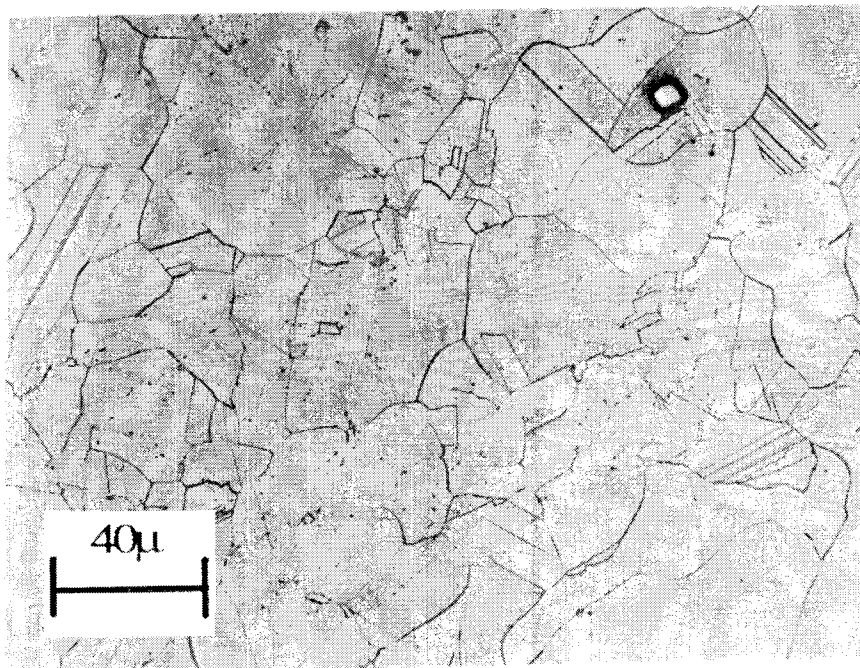


**Figure A-4. Microstructure of the transverse section of alloy 825 in the as-received condition. Magnification 500X.**

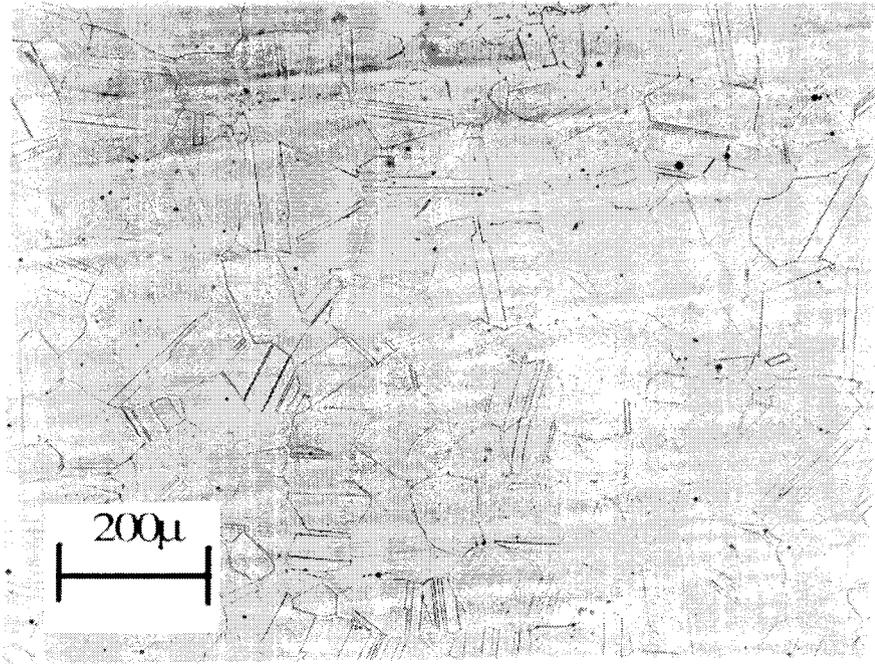


**Figure A-5. Microstructure of a section of alloy C-22 in the as-received condition. Magnification 100X.**

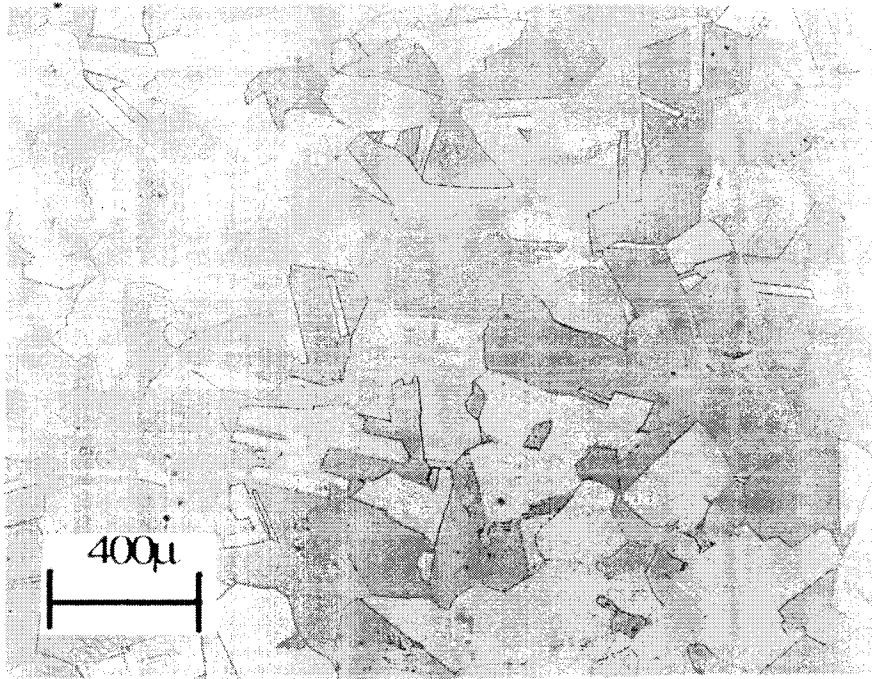


**Figure A-6. Microstructure of the transverse section of CDA-102. Magnification 50X.**

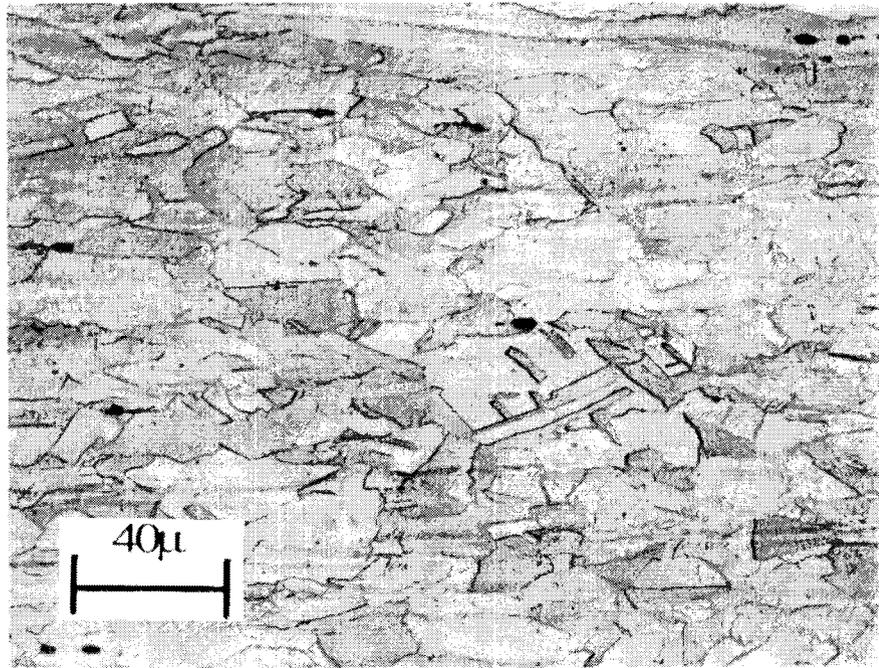


**Figure A-7. Microstructure of the longitudinal section of CDA-715. Magnification 500X.**

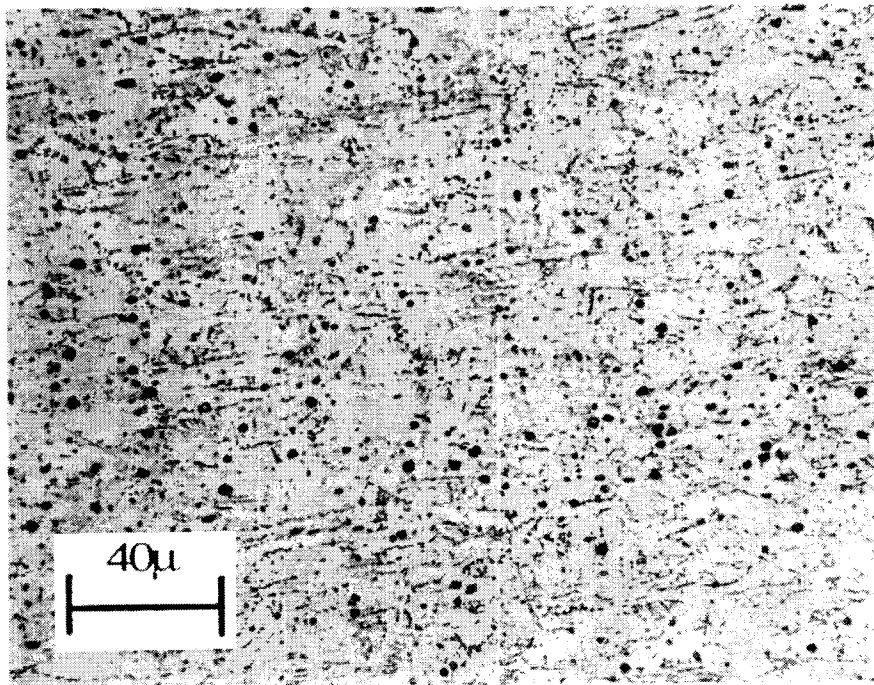


**Figure A-8. Microstructure of the longitudinal section of CDA-613. Magnification 500X.**

**APPENDIX B**

**SOLUTION PREPARATION FOR LOCALIZED  
CORROSION EXPERIMENTS**

# SOLUTION PREPARATION FOR LOCALIZED CORROSION EXPERIMENTS

## B.1 PREPARATION OF SIMULATED J-13 SOLUTIONS

Studies were conducted on simulated J-13 well water to test its stability as a function of time and to identify possible sources of error or uncertainties in the preparation procedure (Pabalan, 1989). Based on this study (Pabalan, 1989), the procedure for preparation of simulated J-13 water and its modifications was formulated (Sridhar et al. 1990). The CNWRA Technical Operating Procedure (TOP)-010, shown below, is followed in preparing these solutions.

- Preparation of Stock Solution A

Add 1.377 g of  $\text{CaSO}_4 \cdot 2\text{H}_2\text{O}$  to 900 mL of high purity water at room temperature and stir until dissolved. Then add 0.944 g of  $\text{Ca}(\text{NO}_3)_2 \cdot 4\text{H}_2\text{O}$ , 0.119 g of KCl, and 0.569 g of  $\text{MgCl}_2 \cdot 6\text{H}_2\text{O}$  to the solution and stir until dissolved completely. Care should be taken to add magnesium chloride quickly since it is hygroscopic. Pour into a 1000 mL flask and dilute to volume with water.

- Preparation of Stock Solution B

Add 6.720 g of  $\text{NaHCO}_3$ , and 0.376 g of  $\text{KF} \cdot 2\text{H}_2\text{O}$  to 900 mL of high purity water at room temperature and stir until dissolved. Care should be taken in adding KF since it is hygroscopic. Pour solution into a 1000 mL flask and dilute to volume with water.

- Preparation of Solution

Mix 25 mL of stock solution A and 25 mL of stock solution B with 925 mL of high purity water in a 1000 mL volumetric flask. Add more water to dilute to 1000 mL. Augmentation of chloride shall be accomplished by addition of appropriate amounts of KCl to stock solution A.

## B.2 MODEL SOLUTION PREPARATION AND ANALYSES

These solutions were primarily used to study the effect of anionic species and were prepared with only sodium salts. In the solutions with the initial room temperature pH of 8.2, the initial bicarbonate concentration was 85 ppm. However, during the heat-up and test periods, some of the bicarbonate was lost as  $\text{CO}_2$  and the resulting pH increased to 9.5. The simulated crevice solutions, containing high ionic concentrations (0.5 M to 4 M), were prepared without the addition of nitrate or fluoride salts. In solutions with pH lower than 6, HCl was added to adjust the pH. Bicarbonate was not added, since this is unstable and would have evolved as  $\text{CO}_2$ .

### B.2.1 Measurement of Bicarbonate Concentration in Aqueous Solutions

Most of the studies on localized corrosion of the candidate container materials included in this task involved aqueous solutions containing bicarbonate ions. Thus, an appropriate method must be

applied for the determination of the  $\text{HCO}_3^-$  concentration, particularly for long-term tests where this concentration may vary with time. A simple technique for this purpose is described in ASTM D 513-88: Standard for Total and Dissolved Carbon Dioxide in Water, Test Method A — Gas Sensing Electrode Test Method. The total concentration of dissolved carbonate species present as  $\text{CO}_2$ ,  $\text{H}_2\text{CO}_3$ ,  $\text{HCO}_3^-$ , and  $\text{CO}_3^{2-}$  in water are determined potentiometrically by using a carbon dioxide electrode. Volatile weak acids, such as  $\text{HNO}_2$ ,  $\text{H}_2\text{SO}_3$ , acetic acid, and formic acids, are known as potential interferences in this method. This is not a matter of concern because these anions are not included in the model solutions to be tested. By knowing the total concentration of dissolved carbonate species, the pH of the solution, and the partial pressure of  $\text{CO}_2$  in equilibrium with the solution, the concentration of each species can be calculated by using the thermodynamic constants for the various equilibria involved. These equilibria were briefly discussed in a previous report (Cragolino and Sridhar, 1991b).

In addition to bicarbonate, the model solutions may eventually contain other anions, such as chloride, sulfate, nitrate, and fluoride, which are the predominant anionic species in the groundwaters in the proximity of the proposed Yucca Mountain repository site. For this reason, a test matrix including 10 solutions (Table B-1) was designed to measure the  $\text{HCO}_3^-$  ion concentration in the presence of various concentrations of those anions to confirm whether interference by the various anions can be disregarded. Additionally, for each solution, the pH and the chloride concentration were measured. The measurements were conducted using a Model 95-02 Orion carbon dioxide electrode, a Model 94-17B Orion chloride electrode, and a Model 81-02 Orion pH combination electrode in conjunction with a Model 720 Orion pH-ion selective electrode meter.

**Table B-1. Nominal composition of the bicarbonate-containing solutions for  $\text{HCO}_3^-$ ,  $\text{Cl}^-$ , and pH measurements**

Solution	$\text{HCO}_3^-$ (ppm)	$\text{Cl}^-$ (ppm)	$\text{SO}_4^{2-}$ (ppm)	$\text{NO}_3^-$ (ppm)	$\text{F}^-$ (ppm)
1	88	6	20	10	2
2	88	10000	20	10	2
3	88	6	10000	10	2
4	88	6	20	10000	2
5	88	6	20	10	200
6	8800	6	20	10	2
7	8800	10000	20	10	2
8	8800	6	10000	10	2
9	8800	6	20	10000	2
10	8800	6	20	10	200

Following the procedure described in ASTM D 513-88, the carbon dioxide electrode was calibrated within the specified range of 0 to 400 ppm CO<sub>2</sub>. The CO<sub>2</sub> concentration was measured in all the solutions, but a dilution factor of 1:20 was used for solutions 5 to 10. For the measurement of the chloride concentration, a dilution factor of 1:100 was applied to solutions 2 and 7.

Results of the measurements of HCO<sub>3</sub><sup>-</sup> and Cl<sup>-</sup> concentrations for each solution as well as the corresponding pH values are summarized in Table B-2. Triplicate measurements were conducted for each solution, and the values reported are the mean of those measurements. In addition, triplicate samples were prepared in the specific case of solutions 1 and 5, as denoted by the suffixes -a, -b, and -c.

**Table B-2. Values of HCO<sub>3</sub><sup>-</sup> concentration, Cl<sup>-</sup> concentration, and pH for solutions included in Table B-1.**

Solution	HCO <sub>3</sub> <sup>-</sup> (ppm)	Cl <sup>-</sup> (ppm)	pH
1-a	93.3	10.6	8.17
1-b	94.0	9.3	8.35
1-c	95.2	10.1	8.41
2	101.0	11000	8.16
3	102.3	8.6	8.09
4	100.2	8.5	8.51
5	108.1	7.6	8.13
6-a	8263	7.5	8.21
6-b	8928	8.6	8.29
6-c	9372	8.6	8.28
7	9261	12500	8.05
8	9067	7.8	8.13
9	9400	8.1	8.14
10	10120	8.3	8.25

The mean value of the HCO<sub>3</sub><sup>-</sup> concentration for solutions 1-a to 1-c is 94.2 ppm with a standard deviation of 1.0 ppm. For solutions 2 to 4, the mean value is 101.2 ppm with a standard deviation of 1.1 ppm. Since the 95 percent confidence interval for solutions 1-a to 1-c is ± 2.4, it can be concluded that the addition of 10,000 ppm chloride, sulfate, or nitrate affects the determination of the bicarbonate concentration at the low bicarbonate concentration level, probably through their effect on the ionic strength of the solutions. On the other hand, for solutions 6 to 9, the mean value is 9048 ppm with

a standard deviation of 425 ppm. In this case the nominal bicarbonate composition of 8800 ppm lies within the 95 percent confidence interval for the measurements, which is 446 ppm. It can be concluded that the presence of chloride, sulfate, and nitrate at the high bicarbonate concentration level does not affect the determination of the bicarbonate concentration.

According to Table B-2, the measured values of the  $\text{HCO}_3^-$  concentration in the presence of 200 ppm fluoride (solutions 5 and 10) lie outside the 95 percent confidence limits for solutions 2 to 4 and 6 to 9, which are  $\pm 2.7$  and  $\pm 446$  ppm, respectively. These results seem to indicate that fluoride interferes with the determination of bicarbonate, presumably through an effect similar to that mentioned above for weak volatile acids. It should be noted that the pK of HF is 3.45, whereas that of  $\text{HNO}_2$  is 3.37, suggesting that both anions ( $\text{F}^-$  and  $\text{NO}_2^-$ ) may have a very similar effect if their volatility is comparable. For example, a 10 percent positive error in the determination of 61 ppm  $\text{HCO}_3^-$  ( $10^{-3}$  M) is caused by 160 ppm  $\text{NO}_2^-$  ( $3.5 \times 10^{-3}$  M) according to ASTM D-513. Additional work is needed to identify beyond doubts the nature of the interference and determine the possibility of using a correction term.

The mean pH values were found to be  $8.26 \pm 0.16$  and  $8.19 \pm 0.09$  for the nominal bicarbonate concentration of 88 and 8800 ppm, respectively. Obviously, under conditions of equilibrium of the solutions with the partial pressure of  $\text{CO}_2$  in the atmosphere, the  $\text{HCO}_3^-$  anion constitutes more than 99 percent of the total concentration of dissolved carbonate species. No variation of pH should be expected in that concentration range. The reason is that the pH value should be practically equal to the arithmetic mean of the pK values for the two successive dissociation or acidity constants of dissolved carbon dioxide, which are 6.35 and 10.33 at 25°C (Stumm and Morgan, 1981). Therefore, by assuming infinite dilution conditions, a pH of 8.34 should be expected, which is very close to that measured.

The mean value of the chloride concentration for all the solutions, with the exception of solutions 2 and 7, was 8.6 ppm with a standard deviation of 1 ppm. No statistical significance can be attributed to the difference in the mean values between both sets of solutions containing 88 and 8800 ppm bicarbonate. It is apparent that higher values than the nominal chloride concentration were measured in all solutions, including those containing 10000 ppm chloride.

## B.2.2 Evolution of pH with Time in Model Solutions

As mentioned previously, the pH in near-neutral solutions evolved from about 8 to about 9. This was modeled (Pabalan et al., 1990) in terms of the exsolution of  $\text{CO}_2$ . The time evolution of pH was monitored in a test solution containing 8500 ppm  $\text{HCO}_3^-$ , 1000 ppm  $\text{Cl}^-$ , 1000 ppm  $\text{SO}_4^{2-}$ , 10 ppm  $\text{NO}_3^-$ , and 2 ppm  $\text{F}^-$ . In one series of experiments, two batches of the solution (approximately 900 mL) were placed in polypropylene bottles and loosely covered. The bottles were then placed in a shaker bath at 25°C at 30 rpm. The pH readings (three readings per sample) were taken on samples that were withdrawn at periodic intervals for up to 20 days. The experiments were repeated for two other solutions, the first containing 85 ppm  $\text{HCO}_3^-$  and other anions at the same concentration as above, and the second containing only 8500 ppm  $\text{HCO}_3^-$ . The results are shown in Figure B-1. In both the 8500 ppm  $\text{HCO}_3^-$  solutions, the pH increased slowly from 8.1 to 9.1 over 480 hours (20 days). Correspondingly, the total carbonate (in terms of the bicarbonate equivalent) decreased (Table B-3). For the 85 ppm  $\text{HCO}_3^-$  solution, there was a maximum in pH after about 100 hours (5 days). Correspondingly, the total carbonate concentration measured by the electrode increased slightly (Table B-3). It can also be seen from Table B-3 that nitrogen purging accelerated the decrease in bicarbonate concentration.

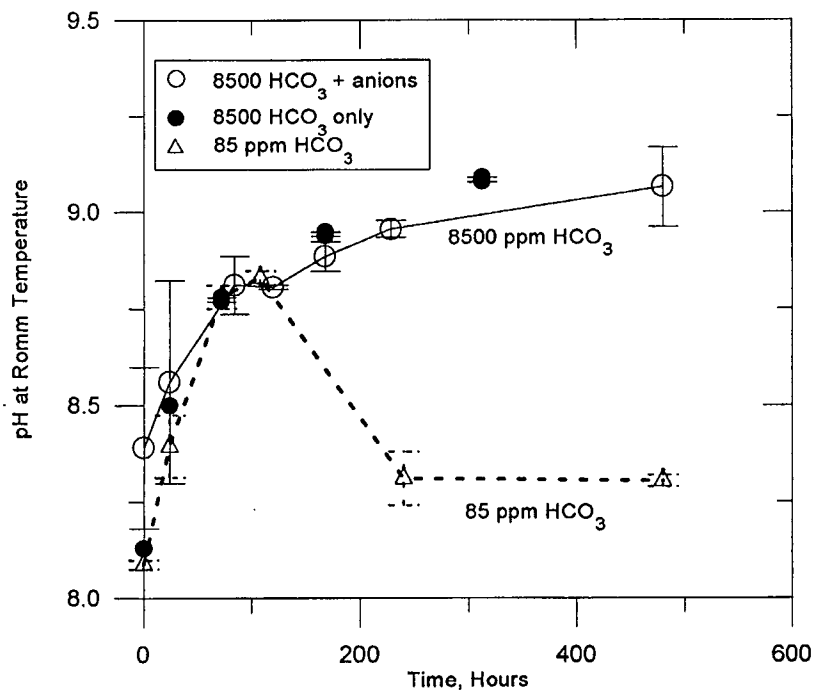


**Figure B-1.** Change in pH measure at room temperature as a function of time. Solution maintained at 25°C in a loosely covered polypropylene bottle in a shaker bath.

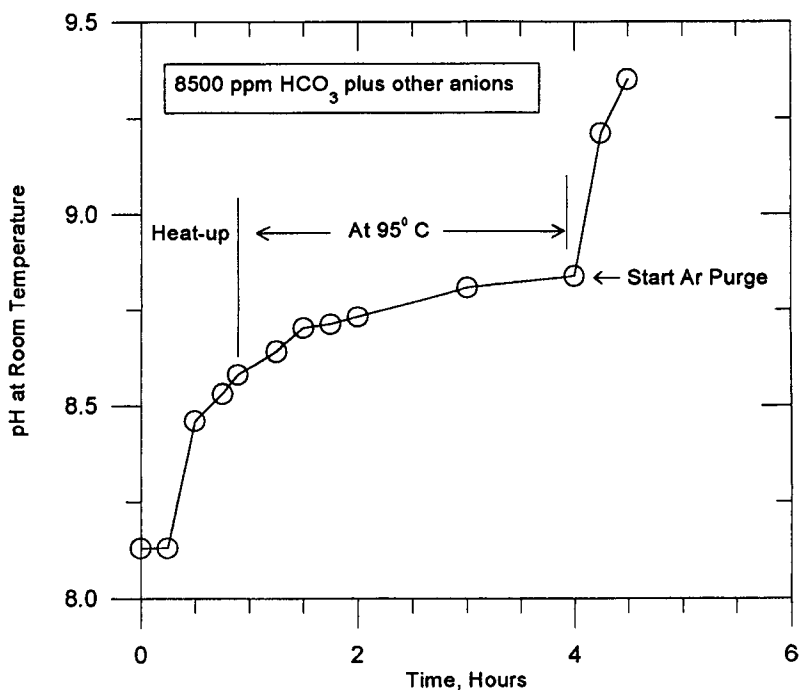


**Figure B-2.** Change in pH of a solution heated to 95°C from room temperature. All pH measured at room temperature from solutions withdrawn from glass test cell.

**Table B-3. Measured bicarbonate concentration before and after the 20-day exposure to ambient conditions. Temperature: 25°C. Solutions were diluted 20:1 for analysis unless otherwise specified.**

Solution	HCO <sub>3</sub> <sup>-</sup> Concentration, ppm	
	Initial	Final
8500 ppm HCO <sub>3</sub> <sup>-</sup> , 1000 ppm Cl <sup>-</sup> , 20 ppm SO <sub>4</sub> <sup>2-</sup> , 10 ppm NO <sub>3</sub> <sup>-</sup> , 2 ppm F <sup>-</sup> (20 days)	8013 8207	7458 7348
8500 ppm HCO <sub>3</sub> <sup>-</sup> only (20 days); 200:1 dilution for analysis	9316	7237
85 ppm HCO <sub>3</sub> <sup>-</sup> , 1000 ppm Cl <sup>-</sup> , 20 ppm SO <sub>4</sub> <sup>2-</sup> , 10 ppm NO <sub>3</sub> <sup>-</sup> , 2 ppm F <sup>-</sup> (20 days)	91	113
8500 ppm HCO <sub>3</sub> <sup>-</sup> , 1000 ppm Cl <sup>-</sup> , 20 ppm SO <sub>4</sub> <sup>2-</sup> , 10 ppm NO <sub>3</sub> <sup>-</sup> , 2 ppm F <sup>-</sup> , (24 hours); 200:1 dilution for analysis	8873	7126
8500 ppm HCO <sub>3</sub> <sup>-</sup> , 1000 ppm Cl <sup>-</sup> , 20 ppm SO <sub>4</sub> <sup>2-</sup> , 10 ppm NO <sub>3</sub> <sup>-</sup> , 2 ppm F <sup>-</sup> , (24 hours); Nitrogen purge	7985	5129

The effect of heating and purging on the change in pH can be seen in Figure B-2. The change in pH is more rapid due to the faster exsolution of CO<sub>2</sub> and the resulting pH is higher due to the lower solubility of CO<sub>2</sub> at the higher temperature. In the localized corrosion experiments conducted at 95°C, the pH of the solution can be assumed to be essentially 9.2 since the rise in pH is rapid. For the localized corrosion tests at room temperature, the pH evolves more slowly. However, purging with argon/nitrogen is expected to result in a more rapid increase in pH than shown in Figure B-1.

**APPENDIX C**

**CYCLIC POLARIZATION EXPERIMENTS ON THE  
AUSTENITIC ALLOYS — DATA TABLES**

**Table C-1. Results of cyclic polarization tests on alloy 825 in simulated J-13 solutions modified to various chloride levels**

Test No.	Chloride (ppm)	$E_p$ (mV <sub>SCE</sub> )	$E_{peak}$ (mV <sub>SCE</sub> )	$E_{rp}$ (mV <sub>SCE</sub> )	$E_{corr}$ (mV <sub>SCE</sub> )	$(E_p - E_{rp})$ (mV)	Initial pH	Final pH
34	0	783	382	741	-579	42	8.31	9.73
27	6	767	377	717	-480	50	8.23	9.78
30	6	768	355	706	-522	62	8.31	9.69
32	6	760	351	698	-534	62	8.30	9.76
33	6	743	322	685	-547	58	8.21	9.85
29	6	769	356	705	-557	64	8.30	9.61
31	6	747	322	681	-527	66	8.32	9.89
24	20	736	327	675	-570	61	8.31	9.86
8	20	773	380	707	-565	66	8.28	9.61
14	20	735	339	687	-470	48	8.30	9.85
22	20	739	335	683	-506	56	8.34	9.72
21	20	738	349	682	-588	56	8.28	9.56
23	20	761	352	697	-573	64	8.29	9.50
12	20	646	374	121	-543	525	8.27	9.48
16	100	740	323	366	-542	374	8.30	9.65
19	100	729	316	669	-637	60	8.25	9.72
9	100	754	361	688	-576	66	8.05	9.59
18	100	742	341	656	-592	86	8.32	9.64
17	100	726	329	672	-520	54	8.23	9.71
15	100	739	350	417	-563	322	8.30	9.66
20	100	739	334	309	-571	430	8.26	9.56
26	200	728	315	415	-526	313	8.40	9.85
10	200	746	353	152	-600	594	8.05	9.52
13	200	723	334	377	-579	346	8.27	9.67
25	200	740	335	335	-546	405	8.28	9.70
11	300	579	347	34	-566	545	8.05	9.52
47	300	628	316	103	-589	525	8.32	9.52
48	300	729	320	51	-585	678	8.38	9.41
5	1000	691	282	-35	-655	726	8.08	—
3	1000	699	294	-46	-647	745	8.12	9.50
4	1000	679	298	-63	-631	742	8.11	9.49
6	1000	467	291	-26	-610	493	8.10	9.48
2	1000	669	284	135	-657	534	8.09	9.71
1	1000	682	277	-48	-668	730	8.14	9.66
7	1000	699	306	-42	-643	741	8.11	9.65

Table C-2. Summary of results of cyclic polarization tests on alloy 825 using a two-level full factorial experimental design

Trial	Cl <sup>-</sup> (ppm)	T (°C)	F <sup>-</sup> (ppm)	NO <sub>3</sub> <sup>-</sup> (ppm)	SO <sub>4</sub> <sup>2-</sup> (ppm)	E <sub>corr</sub> (mV <sub>SCE</sub> )	E <sub>p</sub> (mV <sub>SCE</sub> )	E <sub>rp</sub> (mV <sub>SCE</sub> )	E <sub>p</sub> -E <sub>rp</sub> (mV)	Visual Rating	LCI
1	6	60	2	10	20	-413	820	756	64	2	15.6
2	1000	60	2	10	20	-343	678	38	640	4	377.6
3	6	95	2	10	20	-447	782	758	24	0	0.0
4	1000	95	2	10	20	-555	626	82	544	4	347.6
5	6	60	200	10	20	-372	807	577	230	0	0.0
6	1000	60	200	10	20	-541	709	187	522	4	294.5
7	6	95	200	10	20	-432	737	610	127	0	0.0
8	1000	95	200	10	20	-460	593	-87	680	3	344.0
9	6	60	2	1000	20	-429	812	679	133	2	49.1
10	1000	60	2	1000	20	-453	1061	889	172	2	32.4
11	6	95	2	1000	20	-602	736	662	74	2	30.2
12	1000	95	2	1000	20	-509	712	672	40	0	0.0
13	6	60	200	1000	20	-461	776	612	164	0	0.0
14	1000	60	200	1000	20	-443	778	566	212	0	0.0
15	6	95	200	1000	20	-590	716	535	181	0	0.0

Table C-2. Summary of results of cyclic polarization tests on alloy 825 using a two-level full factorial experimental design (cont'd)

Trial	Cl <sup>-</sup> (ppm)	T (°C)	F <sup>-</sup> (ppm)	NO <sub>3</sub> <sup>-</sup> (ppm)	SO <sub>4</sub> <sup>2-</sup> (ppm)	E <sub>corr</sub> (mV <sub>SCE</sub> )	E <sub>p</sub> (mV <sub>SCE</sub> )	E <sub>rp</sub> (mV <sub>SCE</sub> )	E <sub>p</sub> -E <sub>rp</sub> (mV)	Visual Rating	LCI
16	1000	95	200	1000	20	-593	717	560	157	0	0.0
17	6	60	2	10	1000	-428	769	644	125	2	32.5
18	1000	60	2	10	1000	-449	764	108	656	4	343.5
19	6	95	2	10	1000	-647	715	715	0	0	0.0
20	1000	95	2	10	1000	-492	713	-3	716	4	401.7
21	6	60	200	10	1000	-609	765	568	197	0	0.0
22	1000	60	200	10	1000	-450	743	179	564	4	303.6
23	6	95	200	10	1000	-419	730	574	156	1	21.4
24	1000	95	200	10	1000	-523	698	-2	700	4	401.2
25	6	60	2	1000	1000	-471	895	815	80	2	26.8
26	1000	60	2	1000	1000	-474	759	631	128	2	33.7
27	6	95	2	1000	1000	-478	723	707	16	0	0.0
28	1000	95	2	1000	1000	-555	703	662	41	0	0.0
29	6	60	200	1000	1000	-437	776	548	228	0	0.0

Table C-2. Summary of results of cyclic polarization tests on alloy 825 using a two-level full factorial experimental design (cont'd)

Trial	Cl <sup>-</sup> (ppm)	T (°C)	F <sup>-</sup> (ppm)	NO <sub>3</sub> <sup>-</sup> (ppm)	SO <sub>4</sub> <sup>2-</sup> (ppm)	E <sub>corr</sub> (mV <sub>SCE</sub> )	E <sub>p</sub> (mV <sub>SCE</sub> )	E <sub>rp</sub> (mV <sub>SCE</sub> )	E <sub>p</sub> -E <sub>rp</sub> (mV)	Visual Rating	LCI
30	1000	60	200	1000	1000	-419	666	567	99	0	0.0
31	6	95	200	1000	1000	-617	721	560	161	0	0.0
32	1000	95	200	1000	1000	-554	691	583	108	0	0.0
33	300	95	2	10	1000	-509	728	55	673	4	369.8
34	1000	80	2	10	20	-503	686	-10	696	4	405.8
35	1000	95	2	10	200	-470	751	-17	768	4	409.1
36	1000	95	100	10	20	-545	725	-101	826	4	455.7
37	1000	95	2	100	20	-488	709	-20	729	4	411.3

Initial pH of Solutions:  $8.15 \pm 0.08$  ( $1\sigma$ ). Final pH:  $9.34 \pm 0.27$  ( $1\sigma$ )

C4

Table C-3. Results of two-level, full factorial experiments on type 316L stainless steel

Trial Number	Chloride (ppm)	Nitrate (ppm)	Fluoride (ppm)	Sulfate (ppm)	$E_{corr}$ (mV <sub>SCE</sub> )	$E_p$ (mV <sub>SCE</sub> )	$E_{rp}$ (mV <sub>SCE</sub> )	Visual Rating	LCI
1	6	10	2	20	-739	510	62	4	351.4
2	1000	10	2	20	-680	97	-171	4	1105.2
3	6	1000	2	20	-602	740	740	0	0.0
4	1000	1000	2	20	-721	204	-136	4	666.7
5	6	10	200	20	-513	749	680	0	0.0
6	1000	10	200	20	-666	179	-242	4	940.8
7	6	1000	200	20	-637	705	633	0	0.0
8	1000	1000	200	20	-454	283	-61	3	364.7
9	6	10	2	1000	-642	728	728	0	0.0
10	1000	10	2	1000	-701	176	-224	3	681.8
11	6	1000	2	1000	-682	700	700	0	0.0
12	1000	1000	2	1000	-596	333	-11	3	309.9
13	6	10	200	1000	-683	711	647	0	0.0
14	1000	10	200	1000	-502	187	-286	4	1011.8
15	6	1000	200	1000	-626	732	676	0	0.0
16	1000	1000	200	1000	-663	266	-83	3	393.6

Table C-3. Results of two-level, full factorial experiments on type 316L stainless steel (cont'd)

Trial Number	Chloride (ppm)	Nitrate (ppm)	Fluoride (ppm)	Sulfate (ppm)	$E_{corr}$ (mV <sub>SCE</sub> )	$E_p$ (mV <sub>SCE</sub> )	$E_{rp}$ (mV <sub>SCE</sub> )	Visual Rating	LCI
REPEAT RUNS									
17	6	10	2	20	-705	577	12	4	391.7
18	3.6	10	2	20	-454	787	755	0	0.0
19	3.6	10	2	20	-625	785	785	0	0.0
20	20	10	2	20	-647	771	771	0	0.0
21	20	10	2	20	-652	746	746	0	0.0
22	20	10	2	20	-622	764	—	2	—
23	100	10	2	20	-656	313	-63	4	480.5
24	100	10	2	20	-657	340	-68	4	480.0
25	100	10	2	20	-638	435	-49	4	445.1
26	300	10	2	20	-661	188	-68	4	544.7
27	300	10	2	20	-607	282	-46	4	465.2
28	300	10	2	20	-578	231	-85	4	547.2

$HCO_3 = 85.5$  ppm ( $NaHCO_3 = 122$  ppm)  
 Temperature = 95°C

Table C-4. Analysis of variance (anova) table for the factorial experiments on alloy 825 for LCI (blocking was not considered)

Factor	Effect	Coefficient	Std. Error	95% C.I.	p-value
Average	95.5	95.5	2.49	—	—
Cl	169.0	84.5	4.99	12.2	0.00
T	2.3	1.1	4.99	12.2	0.67
F	-20.4	-10.2	4.99	12.2	0.01
NO <sub>3</sub>	-169.4	-84.7	4.99	12.2	0.00
SO <sub>4</sub>	4.6	2.3	4.99	12.2	0.40
Cl*T	11.4	5.7	4.99	12.2	0.06
Cl*F	-3.8	-1.9	4.99	12.2	0.49
Cl*NO <sub>3</sub>	-174.0	-87.0	4.99	12.2	0.00
Cl*SO <sub>4</sub>	6.4	3.2	4.99	12.2	0.25
T*F	18.8	9.4	4.99	12.2	0.01
T*NO <sub>3</sub>	-16.3	-8.1	4.99	12.2	0.02
T*SO <sub>4</sub>	8.2	4.1	4.99	12.2	0.15
F*NO <sub>3</sub>	-1.2	-0.6	4.99	12.2	0.83
F*SO <sub>4</sub>	6.4	3.2	4.99	12.2	0.25
NO <sub>3</sub> *SO <sub>4</sub>	-11.0	-5.5	4.99	12.2	0.07
Cl*T*F	4.4	2.2	4.99	12.2	0.43
Cl*T*NO <sub>3</sub>	-14.0	-7.0	4.99	12.2	0.03
Cl*T*SO <sub>4</sub>	8.6	4.3	4.99	12.2	0.13
Cl*F*NO <sub>3</sub>	8.8	4.4	4.99	12.2	0.13
Cl*F*SO <sub>4</sub>	-0.8	-0.4	4.99	12.2	0.89
Cl*F*NO <sub>3</sub> *SO <sub>4</sub>	0.4	0.2	4.99	12.2	0.95
T*F*NO <sub>3</sub>	-4.8	-2.4	4.99	12.2	0.39
T*F*SO <sub>4</sub>	0.5	0.2	4.99	12.2	0.93
T*NO <sub>3</sub> *SO <sub>4</sub>	-9.4	-4.7	4.99	12.2	0.11

$R^2 = 0.998$

Adjusted  $R^2 = 0.991$

Table C-5. Analysis of variance (anova) table for the factorial experiments on type 316L stainless steels for LCI (blocking was not considered)

Factor	Effect	Coefficient	Std. Error	95% C.I.	p-value
F*NO <sub>3</sub> *SO <sub>4</sub>	0.03	0.013	4.99	12.2	1.00
Average	364.12	364.12	15.17	—	—
Cl	640.39	320.20	30.34	385.6	0.03
NO <sub>3</sub>	-294.51	-147.26	30.34	385.6	0.06
F	-50.51	-25.26	30.34	385.6	0.34
SO <sub>4</sub>	128.96	-64.48	30.34	385.6	0.15
Cl*NO <sub>3</sub>	-206.66	-103.33	30.34	385.6	0.09
Cl*F	37.34	18.67	30.34	385.6	0.43
Cl*SO <sub>4</sub>	-41.11	-20.56	30.34	385.6	0.40
NO <sub>3</sub> *F	-4.06	-2.03	30.34	385.6	0.92
NO <sub>3</sub> *SO <sub>4</sub>	46.99	23.50	30.34	385.6	0.36
F*SO <sub>4</sub>	153.94	76.97	30.34	385.6	0.12
Cl*NO <sub>3</sub> *F	-91.91	-45.96	30.34	385.6	0.20
Cl*NO <sub>3</sub> *SO <sub>4</sub>	-40.86	-20.43	30.34	385.6	0.40
Cl*F*SO <sub>4</sub>	66.09	33.05	30.34	385.6	0.27
NO <sub>3</sub> *F*SO <sub>4</sub>	-57.51	-28.76	30.34	385.6	0.30

$R^2 = 0.998$

Adjusted  $R^2 = 0.977$

Table C-6. Effect of other anions on cyclic polarization behavior of alloy 825. The ph values reported are final room temperature ph unless otherwise noted.

Environment	Temp. °C	E <sub>CORR</sub> (mV <sub>SCE</sub> )	E <sub>p</sub> (mV <sub>SCE</sub> )	E <sub>rp</sub> (mV <sub>SCE</sub> )
1000 ppm Cl + 85 ppm HCO <sub>3</sub> + 20 ppm SO <sub>4</sub> + 10 ppm NO <sub>3</sub> + 2 ppm F, pH 8.9	30	-416	817	165
1000 ppm Cl + 85 ppm HCO <sub>3</sub> + 20 ppm SO <sub>4</sub> + 10 ppm NO <sub>3</sub> + 2 ppm F, pH 8.2	95	-555	626	82
10,000 ppm Cl + 85 ppm HCO <sub>3</sub> + 20 ppm SO <sub>4</sub> + 10 ppm NO <sub>3</sub> + 2 ppm F, pH 8.9	30	-533	864,387	-20, -1
10,000 ppm Cl + 85 ppm HCO <sub>3</sub> + 20 ppm SO <sub>4</sub> + 10 ppm NO <sub>3</sub> + 2 ppm F, pH 9.1	50	-495	606	46
10,000 ppm Cl + 85 ppm HCO <sub>3</sub> + 20 ppm SO <sub>4</sub> + 10 ppm NO <sub>3</sub> + 2 ppm F, pH 9.32	95	-477	418	-77 *
SJ-13 water + 0.0232g/l sodium metasilicate	95	-565, -555	773, 763	729, 719
SJ-13 water + 300 ppm Cl + 0.023g/l sodium metasilicate	95	-545, -518	713, 731	40, 31
1000 ppm Cl, added as MgCl <sub>2</sub> · 6H <sub>2</sub> O + 85 ppm HCO <sub>3</sub> + 20 ppm SO <sub>4</sub> + 10 ppm NO <sub>3</sub> + 2 ppm F, pH 8.1	95	-644, -659	605, 546	-4, -75
10,000 ppm Cl + 85 ppm HCO <sub>3</sub> + 20 ppm SO <sub>4</sub> + 1000 ppm NO <sub>2</sub> + 2 ppm F, pH 8.9	95	-432	577	577

6-9

Table C-6. Effect of other anions on cyclic polarization behavior of alloy 825. The ph values reported are final room temperature ph unless otherwise noted. (cont'd)

Environment	Temp. °C	$E_{CORR}$ (mV <sub>SCE</sub> )	$E_p$ (mV <sub>SCE</sub> )	$E_{rp}$ (mV <sub>SCE</sub> )
1000 ppm Cl + 85 ppm HCO <sub>3</sub> + 20 ppm SO <sub>4</sub> + <b>1000 ppm NO<sub>3</sub></b> + 2 ppm F, pH 8.9, Nitrate added at +979 mV <sub>SCE</sub>	95	-521	733	188
1000 ppm Cl + 85 ppm HCO <sub>3</sub> + 20 ppm SO <sub>4</sub> + <b>1000 ppm NO<sub>3</sub></b> + 2 ppm F, pH 8.9, Nitrate added at +592 mV <sub>SCE</sub>	95	-493	728	676
1000 ppm Cl + <b>1000 ppm HCO<sub>3</sub></b> + 20 ppm SO <sub>4</sub> + 10 ppm NO <sub>3</sub> + 2 ppm F, pH 10.2	95	-512, -498	657, 673	-167, -303
1000 ppm Cl + <b>2000 ppm HCO<sub>3</sub></b> + 20 ppm SO <sub>4</sub> + 10 ppm NO <sub>3</sub> + 2 ppm F, pH 10.1	95	-537, -532	660, 673	-29, 9
1000 ppm Cl + 85 ppm HCO <sub>3</sub> + <b>20,000 ppm SO<sub>4</sub></b> + 10 ppm NO <sub>3</sub> + 2 ppm F, pH 9.5	95	-445	672	400
<b>3.6 ppm Cl</b> + 85 ppm HCO <sub>3</sub> + 20 ppm SO <sub>4</sub> + 10 ppm NO <sub>3</sub> + 2 ppm F, 1 atm. CO <sub>2</sub> , pH 5.3	95	-472	926	878
1000 ppm Cl + 85 ppm HCO <sub>3</sub> + 20 ppm SO <sub>4</sub> + 10 ppm NO <sub>3</sub> + 2 ppm F, 1 atm. CO <sub>2</sub> , pH 5.3	95	-507	586	-315

\* This value was chosen instead of a lower value derived from the intersection of forward and backward scan because of the heavy crevice corrosion.

Bold characters indicate the species factor that was changed with respect to the reference environment of 1000 ppm Cl<sup>-</sup> + 20 ppm SO<sub>4</sub><sup>2-</sup> + 10 ppm NO<sub>3</sub><sup>-</sup> + 2 ppm F<sup>-</sup> + 85 ppm HCO<sub>3</sub><sup>-</sup> at 95°C.

Table C-7. Effect of other anions on cyclic polarization behavior of alloy type 316L stainless steel. The pH values are final room temperature values unless otherwise noted.

Environment	Temp. °C	$E_{CORR}$ (mV <sub>SCE</sub> )	$E_p$ (mV <sub>SCE</sub> )	$E_{rp}$ (mV <sub>SCE</sub> )
1000 ppm Cl + 85 ppm HCO <sub>3</sub> + 20 ppm SO <sub>4</sub> + 10 ppm NO <sub>3</sub> + 2 ppm F	95	-680	97	-171
1000 ppm Cl + 85 ppm HCO <sub>3</sub> + 20 ppm SO <sub>4</sub> + <b>10,000 ppm NO<sub>3</sub></b> + 2 ppm F, pH 9.7	95	-652	746	746
1000 ppm Cl + 85 ppm HCO <sub>3</sub> + 20 ppm SO <sub>4</sub> + <b>1000 ppm NO<sub>3</sub></b> + 2 ppm F, pH 9.5	60	-425	—	96
1000 ppm Cl + <b>2000 ppm HCO<sub>3</sub></b> + 20 ppm SO <sub>4</sub> + 10 ppm NO <sub>3</sub> + 2 ppm F	95	-536	433	-16
1000 ppm Cl + 85 ppm HCO <sub>3</sub> + <b>20,000 ppm SO<sub>4</sub></b> + 10 ppm NO <sub>3</sub> + 2 ppm F, pH 7.99 (initial)	60	-341	836	-137
1000 ppm Cl + 85 ppm HCO <sub>3</sub> + <b>20,000 ppm SO<sub>4</sub></b> + 10 ppm NO <sub>3</sub> + 2 ppm F, pH 7.94 (initial)	95	-420	417	-163
<b>3.6 ppm Cl</b> + 85 ppm HCO <sub>3</sub> + 20 ppm SO <sub>4</sub> + 10 ppm NO <sub>3</sub> + 2 ppm F, 1 atm. CO <sub>2</sub> , pH 5.4	95	-560	926	926
1000 ppm Cl + 85 ppm HCO <sub>3</sub> + 20 ppm SO <sub>4</sub> + 10 ppm NO <sub>3</sub> + 2 ppm F, 1 atm. CO <sub>2</sub> , pH 5.5	95	-510	-13	-358
1000 ppm Cl + 85 ppm HCO <sub>3</sub> + 20 ppm SO <sub>4</sub> + 10 ppm NO <sub>3</sub> + 2 ppm F, 1 atm. CO <sub>2</sub> , pH 5.5	60	-321	263	-64

Bold characters indicate the species factor that was changed with respect to the reference environment of 1000 ppm Cl<sup>-</sup> + 20 ppm SO<sub>4</sub><sup>2-</sup> + 10 ppm NO<sub>3</sub><sup>-</sup> + 2 ppm F<sup>-</sup> + 85 ppm HCO<sub>3</sub><sup>-</sup> at 95°C.

Table C-8. Electrochemical parameters from cyclic polarization curves of alloy 825 in simulated crevice solutions

Test	Environment	Temp. °C	$E_{corr}$ (mV <sub>SCE</sub> )	$E_p$ (mV <sub>SCE</sub> )	$E_{rp}$ (mV <sub>SCE</sub> )	$i_{pass}$ A/cm <sup>2</sup>	$i_{peak}$ A/cm <sup>2</sup>
38	4M Cl <sup>-</sup> , pH 8.17	95	-624	-7	-200	$7 \times 10^{-7}$	$1.5 \times 10^{-6}$
37	4M Cl <sup>-</sup> , pH 2.54	95	-321	-40	-141	$1 \times 10^{-6}$	$1 \times 10^{-6}$
37R	4M Cl <sup>-</sup> , pH 3.10	95	-365	-44	-137	$1 \times 10^{-6}$	$1 \times 10^{-6}$
17	4M Cl <sup>-</sup> , pH 1.1	95	-340	-39	-120	$2 \times 10^{-5}$	$4 \times 10^{-3}$
18	4M Cl <sup>-</sup> , pH 0.03	95	-282	Active Corrosion			
18R	4M Cl <sup>-</sup> , pH 0.06	95	-288	Active Corrosion			
39	4M Cl <sup>-</sup> , pH 2.91	60	-337	56	-61	$8 \times 10^{-7}$	$8 \times 10^{-7}$
40	4M Cl <sup>-</sup> , pH 1.13	60	-332	73	-24	$4 \times 10^{-6}$	$3 \times 10^{-4}$
41	4M Cl <sup>-</sup> , pH 0.0	60	-291	-47	-51	$2.5 \times 10^{-4}$	$3 \times 10^{-2}$
22	4M Cl <sup>-</sup> , pH 2.0	30	-323	770	757	$1 \times 10^{-6}$	$6 \times 10^{-6}$
19	4M Cl <sup>-</sup> , pH 0.01	30	-284	913	913	$2 \times 10^{-5}$	$1.5 \times 10^{-3}$
21	4M Cl <sup>-</sup> , pH -0.36	30	-287	Active Corrosion			
42	0.5M Cl <sup>-</sup> , pH 6.08	95	-448	269	12	$1.5 \times 10^{-6}$	$5 \times 10^{-6}$
23	0.5M Cl <sup>-</sup> , pH 1.0	95	-301	248	19	$8 \times 10^{-6}$	$5 \times 10^{-4}$
25	0.5M Cl <sup>-</sup> , pH 0.1	95	-292	Active Corrosion			
27	0.5M Cl <sup>-</sup> , pH 1.02	30	-269	816	791	$1 \times 10^{-6}$	$4 \times 10^{-6}$
29	0.5M Cl <sup>-</sup> , pH 0.17	30	-284	869	864	$4 \times 10^{-6}$	$3 \times 10^{-4}$

Table C-8. Electrochemical parameters from cyclic polarization curves of alloy 825 in simulated crevice solutions (cont'd)

Test	Environment	Temp. (°C)	$E_{\text{corr}}$ (mV <sub>SCE</sub> )	$E_p$ (mV <sub>SCE</sub> )	$E_{\text{rp}}$ (mV <sub>SCE</sub> )	$i_{\text{pass}}$ A/cm <sup>2</sup>	$i_{\text{peak}}$ A/cm <sup>2</sup>
43	3 M Cl <sup>-</sup> , pH 3.08	95	-349	32	-85	1.5 x 10 <sup>-6</sup>	1.5 x 10 <sup>-6</sup>
31	3M Cl <sup>-</sup> + 0.25M SO <sub>4</sub> <sup>2-</sup> , pH 1.1	95	-277	96	-77	2 x 10 <sup>-6</sup>	2 x 10 <sup>-6</sup>
33	3M Cl <sup>-</sup> + 0.25M SO <sub>4</sub> <sup>2-</sup> , pH 0.03	95	-289	Active Corrosion			
35	3M Cl <sup>-</sup> + 0.25M SO <sub>4</sub> <sup>2-</sup> , pH 1.1	30	-290	835	835	1 x 10 <sup>-6</sup>	1 x 10 <sup>-6</sup>

Table C-9. Electrochemical parameters from cyclic polarization curves of types 304L stainless steel in simulated crevice solutions

Test	Environment	Temp. (°C)	$E_{corr}$ (mV <sub>SCE</sub> )	$E_p$ (mV <sub>SCE</sub> )	$E_{rp}$ (mV <sub>SCE</sub> )	$i_{pass}$ (A/cm <sup>2</sup> )	$i_{peak}$ (A/cm <sup>2</sup> )
6R	4M Cl <sup>-</sup> , pH 8.9	95	-745	-286	-529	$1 \times 10^{-6}$	$2 \times 10^{-6}$
9	4M Cl <sup>-</sup> , pH 3.0	95	-405	-353	-400	$2 \times 10^{-6}$	$2 \times 10^{-6}$
14	4M Cl <sup>-</sup> , pH 1.3	95	-434	Active Corrosion			
5	4M Cl <sup>-</sup> , pH 9.27	30	-488	-51	-216	$4 \times 10^{-7}$	$4 \times 10^{-7}$
10	4M Cl <sup>-</sup> , pH 3.0	30	-459	-219	-235	$4 \times 10^{-6}$	$8 \times 10^{-5}$
13	4M Cl <sup>-</sup> , pH 1.1	30	-461	-184	-213	$7 \times 10^{-5}$	$2.5 \times 10^{-3}$
20	4M Cl <sup>-</sup> , pH 0.03	30	-426	Active Corrosion			
24	0.5M Cl <sup>-</sup> , pH 1.05	95	-406	-130	-145	$5 \times 10^{-4}$	$5 \times 10^{-2}$
26	0.5M Cl <sup>-</sup> , pH 0.11	95	-382	Active Corrosion			
28	0.5M Cl <sup>-</sup> , pH 1.09	30	-432	-43	-16	$7 \times 10^{-6}$	$5 \times 10^{-4}$
30	0.5M Cl <sup>-</sup> , pH 0.11	30	-428	Active Corrosion			

Table C-10. Electrochemical parameters from cyclic polarization curves of types 316L stainless steel in simulated crevice solutions

Test	Environment	Temp. (°C)	$E_{\text{corr}}$ (mV <sub>SCE</sub> )	$E_p$ (mV <sub>SCE</sub> )	$E_{\text{rp}}$ (mV <sub>SCE</sub> )	$i_{\text{pass}}$ (A/cm <sup>2</sup> )	$i_{\text{peak}_2}$ (A/cm <sup>2</sup> )
8	4M Cl <sup>-</sup> , pH 8.8	95	-708	-187	-348	$1 \times 10^{-6}$	$2 \times 10^{-6}$
12	4M Cl <sup>-</sup> , pH 3.0	95	-345	-297	-325	$2 \times 10^{-5}$	$2 \times 10^{-5}$
14	4M Cl <sup>-</sup> , pH 1.4	95	-392	-288	-240	$1.5 \times 10^{-2}$	$4 \times 10^{-2}$
7	4M Cl <sup>-</sup> , pH 9.29	30	-685	-48	-237	$6 \times 10^{-7}$	$1.5 \times 10^{-6}$
11	4M Cl <sup>-</sup> , pH 3.0	30	-436	-147	-288	$2.5 \times 10^{-6}$	$1.2 \times 10^{-5}$
15	4M Cl <sup>-</sup> , pH 1.04	30	-400	-176	-152	$3 \times 10^{-5}$	$3.5 \times 10^{-4}$

**APPENDIX D**

**RESULTS OF CYCLIC POLARIZATION EXPERIMENTS  
ON COPPER-BASED ALLOYS**

Table D-1. Results of full-factorial experiments on alloy CDA-715

Trial	HCO <sub>3</sub> <sup>-</sup> (ppm)	Cl <sup>-</sup> (ppm)	SO <sub>4</sub> <sup>2-</sup> (ppm)	T (°C)	pH, 25°C		E <sub>corr</sub> (mV <sub>SCE</sub> )	E <sub>break</sub> (mV <sub>SCE</sub> )	E <sub>rp</sub> (mV <sub>SCE</sub> )	Comments
					Initial	Final				
1	85	6	20	30	8.04	9.46	-229	56	56	Uniform corrosion, brown film
2	8500	6	20	30	8.29	9.08	-230	831	799	Uniform corrosion, Ni-color
3	85	1000	20	30	8.49	9.18	-261	NA*	NA	Uniform corrosion, Ni-color
4	8500	1000	20	30	8.52	9.17	-280	845	13	Pits, green deposit
5	85	6	1000	30	8.54	9.24	-232	NA	NA	Uniform corrosion, red film
6	8500	6	1000	30	8.34	9.25	-249	820	56	Pits, green deposit
7	85	1000	1000	30	8.05	9.24	-283	NA	NA	Uniform corrosion, red film
8	8500	1000	1000	30	8.52	9.42	-259	506	26	Pits, green deposits
8R	8500	1000	1000	30	8.25	9.13	-237	678	54	Shallow pits, green deposits
9	85	6	20	95	8.5	9.78	-299	198	-18	Uniform corrosion, red film
10	8500	6	20	95	8.42	10.16	-427	602	530	No pitting, dark brown stain
11	85	1000	20	95	8.15	9.78	-338	-29	-242	Uniform corrosion, red film
12	8500	1000	20	95	8.41	9.87	-365	628	552	No pitting, tarnished
13	85	6	1000	95	8.26	9.99	-343	74	-162	A few shallow pits
14	8500	6	1000	95	8.43	—	-350	611	551	Shallow pits at crevice
15	85	1000	1000	95	—	10.02	-293	-24	-241	Uniform corrosion, red film
16	8500	1000	1000	95	8.38	10.08	-425	612	525	No pits, Ni-color

\* NA — Not Applicable

Table D-2. Effect of temperature and bicarbonate on electrochemical parameters of alloy CDA-715

T (°C)	HCO <sub>3</sub> <sup>-</sup> (ppm)	E <sub>corr</sub> (mV <sub>SCE</sub> )	E <sub>break</sub> (mV <sub>SCE</sub> )	E <sub>rp</sub> (mV <sub>SCE</sub> )	Comments
30	8500	-259	506	26	Pits, green deposit
40	8500	-266	499	38	Pits, green deposit
60	8500	-279	718	49	Few pits, green deposit
80	8500	-331	602	58	One or two shallow pits
60	6000	-309	376	12	Shallow pits, green deposit
60	4000	-305	276	-20	Pits, green deposit
60	2000	-305	76	-77	Shallow pits, brown scale
60	1000	-293	24	79	Uniform corrosion, red film
60	122	-287	-51	-19	Uniform corrosion, red film
95	8500	-425	612	525	No pits

Cl<sup>-</sup>: 1000 ppm; SO<sub>4</sub><sup>2-</sup>: 1000 ppm; NO<sub>3</sub><sup>-</sup>: 10 ppm; F<sup>-</sup>: 2 ppm

Table D-3. Results of full-factorial experiments on alloy CDA-102

Trial	HCO <sub>3</sub> <sup>-</sup> (ppm)	Cl <sup>-</sup> (ppm)	SO <sub>4</sub> <sup>2-</sup> (ppm)	T (°C)	pH, 25°C		E <sub>corr</sub> (mV <sub>SCE</sub> )	E <sub>break</sub> (mV <sub>SCE</sub> )	E <sub>rp</sub> (mV <sub>SCE</sub> )	Comments
					Initial	Final				
1	85	6	20	30	8.18	9.67	-245	NA*	NA	Uniform corrosion, brown film
2	8500	6	20	30	8.41	9.28	-221	864	839	Pits, green deposit
3	85	1000	20	30	8.18	8.96	-231	-62	-62	Uniform corrosion, brown film
4	8500	1000	20	30	8.39	9.22	-210	855	367	Pits, green deposit
5	85	6	1000	30	8.64	9.24	-143	82	109	Uniform corrosion, brown film
6	8500	6	1000	30	8.45	9.25	-212	329	73	Pits, green deposit
7	85	1000	1000	30	8.01	9.21	-245	-36	-36	Uniform corrosion, dark film
8	8500	1000	1000	30	8.46	9.09	-201	312	72	Pits, green deposits
9	85	6	20	95	8.20	10.37	-288	325	421	Pits, dark green film
10	8500	6	20	95	8.35	9.69	-231	630	630	No pitting, thick black film
11	85	1000	20	95	9.08	9.96	-345	-64	-64	Uniform corrosion, red film
12	8500	1000	20	95	8.36	9.86	-406	591	591	No pitting, thick black film
13	85	6	1000	95	8.28	10.22	-355	102	-50	No pitting, dark brown film
14	8500	6	1000	95	8.51	9.78	-284	617	617	No pitting, thick black film
15	85	1000	1000	95	8.13	10.35	-348	-47	24	Uniform corrosion, red film
16	8500	1000	1000	95	8.29	9.65	-404	633	633	No pits, thick black film

NO<sub>3</sub><sup>-</sup>: 10 ppm; F<sup>-</sup>: 2 ppm

\* NA — Not Applicable

Table D-4. Preliminary analysis of x-ray diffraction on corrosion product scraped from CDA-102 pitted in a 8500 ppm  $\text{HCO}_3^-$  solution at room temperature to which  $\text{Cl}^-$  and  $\text{SO}_4^{2-}$  were added. The d values are given in order of decreasing intensity. The powder specimens were mixed with aluminum as a reference. Letters indicate possible origins of the peaks.

d — Spacing in Angstroms	
1000 ppm $\text{Cl}^-$ Added	1000 ppm $\text{SO}_4^{2-}$ Added
5.47 (Atacamite)	6.81*
2.78 (Atacamite)	2.84 (Malachite)
2.83 (Atacamite)	3.44 (Azurite)
2.86 (Malachite)	2.50 (Brochantite, Azurite)
5.01 (Atacamite)	3.66 (Malachite, Azurite)
2.08 (Aluminum reference)	4.98 (Malachite)
3.68 (Malachite)	2.46 (Cuprite)
1.81 (Atacamite)	2.40*
2.51 (Atacamite?, Cuprite)	2.75 (Brochantite)
1.71 (Atacamite)	2.33 (Aluminum reference)
4.70 (Malachite)	5.91 (Malachite)
—	2.12 (Cuprite)

\* — Peak unaccounted for

Atacamite:  $\text{CuCl} \cdot \text{Cu}(\text{OH})_2$   
 Azurite:  $2\text{Cu}(\text{CO}_3) \cdot \text{Cu}(\text{OH})_2$   
 Brochantite:  $\text{CuSO}_4 \cdot 3\text{Cu}(\text{OH})_2$   
 Cuprite:  $\text{Cu}_2\text{O}$   
 Malachite:  $\text{CuCO}_3 \cdot \text{Cu}(\text{OH})_2$